THE STRUCTURAL EVOLUTION OF THE BUMBENI COMPLEX AND BUMBENI RIDGE AND ITS RELATIONSHIP WITH GONDWANA BREAK-UP: INSIGHTS FROM HIGH RESOLUTION AEROMAGNETIC DATA AND FIELD MAPPING.

by

MAWANDE NCUME

A thesis submitted in fulfilment of the academic

requirements for the degree of Master of Science in the

Discipline of Geological Sciences

in the School of Agricultural, Earth and Environmental Sciences,

College of Agriculture, Engineering and Science

University of KwaZulu-Natal,

Durban, South Africa

2021

As the candidate's supervisors, we have approved this dissertation for submission.

Signed: [redacted] Name: ...Lauren Hoyer..... Date: ...19 February 2021.....

Signed: ...[redacted] Name: ...Nigel Hicks..... Date: ...19 February 2021

DECLARATION: PLAGIARISM

I, Mawande Ncume, declare that:

1. The research reported in this thesis, except where otherwise indicated or acknowledged, is my original research.

2. This thesis has not been submitted in full or in part for any degree or examination to any other university.

3. This thesis does not contain other persons' data, pictures, graphs or other information, unless specifically acknowledged as being sourced from other persons.

4. This thesis does not contain other persons' writing, unless specifically acknowledged as being sourced from other researchers. Where other written sources have been quoted, then:

    - Their words have been re-written but the general information attributed to them has been referenced.

5. This thesis is primarily a collection of material, prepared by myself presented as a poster and oral presentations at conferences.

6. This thesis does not contain text, graphics or tables copied and pasted from the Internet, unless specifically acknowledged, and the source being detailed in the thesis and in the References sections.

_____

Signed: Mawande Ncume

Date:

Acknowledgements

1. First and foremost, I would like to acknowledge the Almighty God for affording me the time to start and finish this research.

2. Special appreciation to my lovely wife, Mrs Olwethu Ncume, for her firm love, prayers, support and sacrifices during the start till the end of this research. During the extensive period that you were ill you still encouraged me to focus on my research. You always reminded me that seeing me productive will make you get better soon. I love you so much 'We will grow old together'.

3. A big thank you to my lovely mother (Ms Kholeka Ncume), brother (Mr Lwando Ncume) and grandmother (Mrs Mavies Matyani Ncume) because without their love and support I would not be the person I am.

4. My deepest gratitude is extended to my supervisor's Dr Lauren Hoyer and Dr Nigel Hicks. I appreciate your encouragement, patience and mentorship throughout this research. I did not only learn geological research from you guys but the importance of spending time with family and striving for excellence at all times. As well as being organised in travelling and food arrangements and also finding joy in the food one eats in the field. This includes home-made rusks (by Dr Hoyer) and banana bread (from Dr Hicks and the Mrs). I also learnt what 'proper coffee' is.

5. I greatly acknowledge the Council for Geoscience for funding this research.

6. I sincerely thank the Council for Geoscience, Pietermaritzburg office family (Dr G.A., Botha, Mrs R. Singh, Ms P. Dlamini, Mr S. Ngubelanga, Mr S. Chiliza. Ms E. Ngcobo and Ms N Dunga) for their sharing their research expertise and willingness to help and thank you for making the office environment conducive for work, fun and memorable moments (cake sessions).

7. I extend my appreciation to my senior colleagues at the Council for Geoscience, Pretoria office, for their personal advices and assistance with geological and geophysical data processing. Thank you (leadership); Mr E. Chirenje, Mr Z. Nxantsiya, Mr C. Craill, Mr L. Ledwaba, Dr T. Dhansay, Mrs Z. Sibewu and Mr N. Moabi.

Abstract

The Bumbeni Complex is the remnant of a Cretaceous volcanic centre (~133 Ma) that is now exposed along the southern end of the Lebombo Mountain Range, adjacent to the cover sequences that infill the Zululand Basin in northern KwaZulu-Natal, South Africa. The Bumbeni Complex forms the western limit of the north-east trending Bumbeni Ridge and postdates the rocks of the Karoo Large Igneous Province. The comparison of field relationships, structural data, high-resolution aeromagnetic data and borehole logs are used to determine the formation and structural evolution of the Bumbeni Complex and Bumbeni Ridge by understanding the tectonic regimes responsible for the development of the brittle deformation structures in the study area. These events are then correlated with the regional tectonic events related to Gondwana break-up, thus further constraining the timing of deformation and possible formation mechanisms of the Bumbeni volcanism.

The rhyolites of the Jozini Formation (Lebombo Group) provide a basement to the rocks of the Bumbeni Complex. These rhyolites are characterised by a N-S oriented eastward dipping normal and dextral strike-slip faults and associated planar systematic joint sets. These fractures are representative of a dextral strike-slip regime, interpretable on a dextral Riedel shear system. The presence of these dextral strike-slip faults suggests that a rotation in the paleo-stress regime from a vertical σ_1 to a horizontal NE-SW oriented σ_1 have occurred during deformation, which may be related to the second deformation event (175–155 Ma) attributed here to stage two of Gondwana break-up. These structural deformation patterns developed in the Jozini Formation are absent in the rocks of the Bumbeni Complex, suggesting the deformation in the Lebombo Group occurred prior and/or during the eruption and intrusion of the Bumbeni Complex.

The aeromagnetic data defines four distinct magnetic domains (Domains 1–4), which are separated by distinct regional magnetic discontinuities and are defined by their structural framework. Domain 1 occurs in the SW of the study area and is characterised by N-S oriented wide lineaments (low frequency, deep seated), and correlate with the Lebombo Group and are likely related to the N-S oriented faults occurring in the Jozini Formation rhyolites. The formation of these structures is here associated with the E-W orientated spreading attributed to the initial stages of Gondwana break-up (~180–175 Ma). Domains 2, 3 and 4 mainly display E-W and NE-SW oriented high frequency shallow structures, which cross-cut each other suggesting that the shallow structures occurred at different times and post-date the occurrence of the deep structures. These structures are related to the second deformation event which is constrained between stages 2 and 3 (175–135 Ma).

The field evidence reveals that the Bumbeni Complex comprises basaltic and rhyolitic rocks of the Mpilo and Fenda Formations, respectively, indicating bimodal volcanism typical of rift related extension. The bimodal volcanism is most likely related to local extension associated with the upwelling of the continental lithospheric mantle. The position of the Zululand Basin boreholes (ZD and ZG) in relation to the aeromagnetic anomalies and the geomagnetic timescale, reveal that the Bumbeni Complex comprise NE-striking remanent and non-remanently magnetised plutonic bodies. These NE-striking plutonic bodies, which are a result of ascended magma occur in the southeast and northeast of the study area, delineated from the aeromagnetic data, and are indicative of emplacement during positive and negative polarity periods which prevailed during the Cretaceous. The position of the Bumbeni Complex and extension of the volcanism along the Bumbeni Ridge is correlated with a once-active E-W trending spreading centre located in the Northern Natal Valley at ~133–125.3 Ma, based on its paleo-position. Thus, the Bumbeni event is attributed to a combination of these processes. This event is likely a volcanic centre that formed along a failed rift system.

Table of Contents

List of Figures

List of Tables

1. Introduction

The 133±5 Ma (Isochron age) Bumbeni Complex is a predominantly felsic volcanic complex that is exposed in the Zululand Basin, KwaZulu-Natal, South Africa (Allsopp et al., 1984). The Bumbeni Complex postdates the basalts and rhyolites of the Lebombo Group of the Karoo Large Igneous Province, which form the basement of the study region. The complex is partially covered by younger sedimentary deposits of the Maputaland Group. It has been proposed by Bristow and Duncan (1983) that the felsic rocks of the Bumbeni Complex are primarily a product of a plinian-type eruption associated with cyclic rhyolitic dome building and collapse. Plinian eruptions are characterised by the release of copious amounts of coarse ejecta, including pumice and ash, at rapid rates with sustained open vent discharge (Walker, 1981). Hence, plinian eruptions are generally accompanied by pyroclastic flow deposits that occur during collapse of the eruption column, lava flows (Walker, 1981; Mothes et al., 2008), and the summit area can eventually collapse forming a caldera (Deino et al., 2004).

The exposed Bumbeni Complex forms the western limit of the Bumbeni Ridge, which extends north-eastwards below Cretaceous and Cenozoic cover sequences, that has been identified through drilling and from regional airborne gravity and aeromagnetic data (Barkhuizen, 1989; Shone, 2006). The origin of the Bumbeni Complex and Bumbeni Ridge has been investigated based on the geology, geochemistry and regional geophysics and formation models presented (Stratten, 1964; Wolmarans and Saggerson, 1988; Barkhuizen, 1989). However, there is currently no published scientific information on the detailed structural evolution of the Bumbeni Complex and Bumbeni Ridge. Furthermore, previous research does not investigate the tectonic framework and orientation of the Bumbeni Complex and Bumbeni Ridge, particularly the interpretation of high-resolution aeromagnetic data in conjunction with brittle deformation structures. There is also no comparison between the structural framework of the basement geology and that of the Bumbeni Complex and Bumbeni Ridge.

The interpretation of lineaments from the high-resolution aeromagnetic data, and how these are related to the brittle structures in the region, is important in defining deformation structures and the difference in the tectonic framework between the disparate geological units. It is possible to interpret these lineaments as structural boundaries or faults, based on the nature and offset of similar magnetic anomalies. The understanding of the tectonic framework assists in determining whether the lithostratigraphic units have been affected by a regional tectonic event or not (or multiple episodes) and also if the study region is associated with either strike-slip, compressional or extensional tectonic events. The deformation associated with the study area could, therefore, be interpreted in relation to known regional paleo-tectonic event(s). The timing and sequence of the structural evolution of the

region should also be deducible based on the sequence of the regional deformation event(s). Thus, this study focuses on understanding the relationship between the basement rocks of the Lebombo Group and the geological units of the Bumbeni Complex and Bumbeni Ridge, and the associated paleo-stress regimes that will allow the sequence of deformation events to be inferred. The tectonic framework of the basement geology will correspond to that of the Bumbeni Complex and Bumbeni Ridge only if they have been deformed during the same tectonic episode. Thus, if the regions corresponding to the basement geology and the Bumbeni Complex and Bumbeni Ridge reveal contrasting tectonic frameworks, it would imply that the structures in these regions originated during time periods and different paleo-stress regimes.

The tectonic events related to Gondwana break-up, which commenced in the Early Jurassic, are the most recent known protracted regional tectonic events that have led to the formation of continents and the opening of the Atlantic and Indian Oceans (Cox, 1992; Hawkesworth et al., 1999; Mueller and Jokat, 2019). An in-depth knowledge of the tectonic framework of the offshore east coast and the adjacent onshore region of South Africa is therefore important as it would help contribute towards the understanding of the development of the east coast continental margin, which coincides with the break-up of Gondwana (Cox, 1992; Watkeys and Sokoutis, 1998; Jokat et al., 2003). The Bumbeni Complex falls in this region and thus, the extensional tectonics related to this well-studied break-up event may have affected its structure (Martin and Hartnady, 1986; Watkeys and Sokoutis, 1998). This break-up event forms part of how we can now understand the development of the continental margin and the Bumbeni Complex in relation to Gondwana break-up (Martin and Hartnady, 1986; Watkeys and Sokoutis, 1998). Therefore, understanding the relationship between the tectonic framework of the study region and the Gondwana break-up related events is critical in determining the paleo-stress regimes that affected the study region. Furthermore, the deformation in the onshore and offshore regions is correlated and also scrutinised in relation to Gondwana break-up.

1.1. Aim and Objectives

The principal aim of this study is to unravel the structural evolution of the Bumbeni Complex and the Bumbeni Ridge using field evidence, structural and high-resolution aeromagnetic data analyses. This involves the comparison of the deformation structures occurring in the Lebombo Group with those in the Bumbeni Complex and Bumbeni Ridge so as to provide a clear understanding of the paleo-stress regimes responsible for their formation. The paleo-stress regimes will then be interpreted in relation to the deformation events related to the break-up of Gondwana.

The aim of the study will be met by undertaking the following objectives:

(i) To understand the classification, formation and deformation history of the geological units, including the classification of the fractures and associated orientations revealed by the various lithostratigraphic units. This will be achieved through the description of geological units, analyses of the geological field relationships, geochemical, borehole and structural data of the lithostratigraphic units in the onshore study region.

(ii) To identify the paleo-stress regimes responsible for the brittle deformation structures based on their orientations.

(iii) To identify distinct differences or similarities in the structural framework of the basement and the Bumbeni Complex and Bumbeni Ridge by undertaking lineament analyses and interpretation of the high-resolution aeromagnetic data in relation to the geology and brittle deformation structures in the onshore and the offshore region adjacent to the study area

(iv) Classifying the structural framework of the region into domains and deduce the tectonic regimes that were most likely responsible for the formation of the associated deformation structures so as to deduce the timing of occurrence of these structures with regards to the regional tectonic events.

(v) Correlating the tectonic framework of the onshore study area and the offshore region adjacent to the study area in order to understand the origin and location of Bumbeni Complex and Bumbeni Ridge.

To correlate the tectonic framework of the onshore and offshore regions in order to examine the relationship between the structural evolution of the Bumbeni Complex and Bumbeni Ridge and the regional tectonic events related to Gondwana break-up.

1.2. Geological Setting

The study area is located in northern KwaZulu-Natal, South Africa, within the Mesozoic Zululand Basin (Fig. 1.1). The Zululand Basin is developed above the Late Carboniferous to Jurassic sedimentary and volcanic basement of the Karoo Supergroup (Smith, 1990; Smith et al., 1993; Shone, 2006). Post-dating the sedimentary succession of the Karoo Supergroup are the volcanic successions and intrusive rocks of the Karoo Large Igneous Province (Karoo Supergroup) (Fig. 1.1) (Marsh et al., 1997; Le Gall et

al., 2002; Duncan and Marsh, 2006). The volcanic successions of the Karoo Large Igneous Province (Karoo LIP) represent Continental Flood Basalts and are divided into the lower Lebombo and upper Drakensberg Groups (Encarnación et al., 1996; Hawkesworth et al., 1999; Duncan and Marsh, 2006). The Lebombo Group forms the thick volcanic basement to the study area (Figs. 1.1 and 1.2).

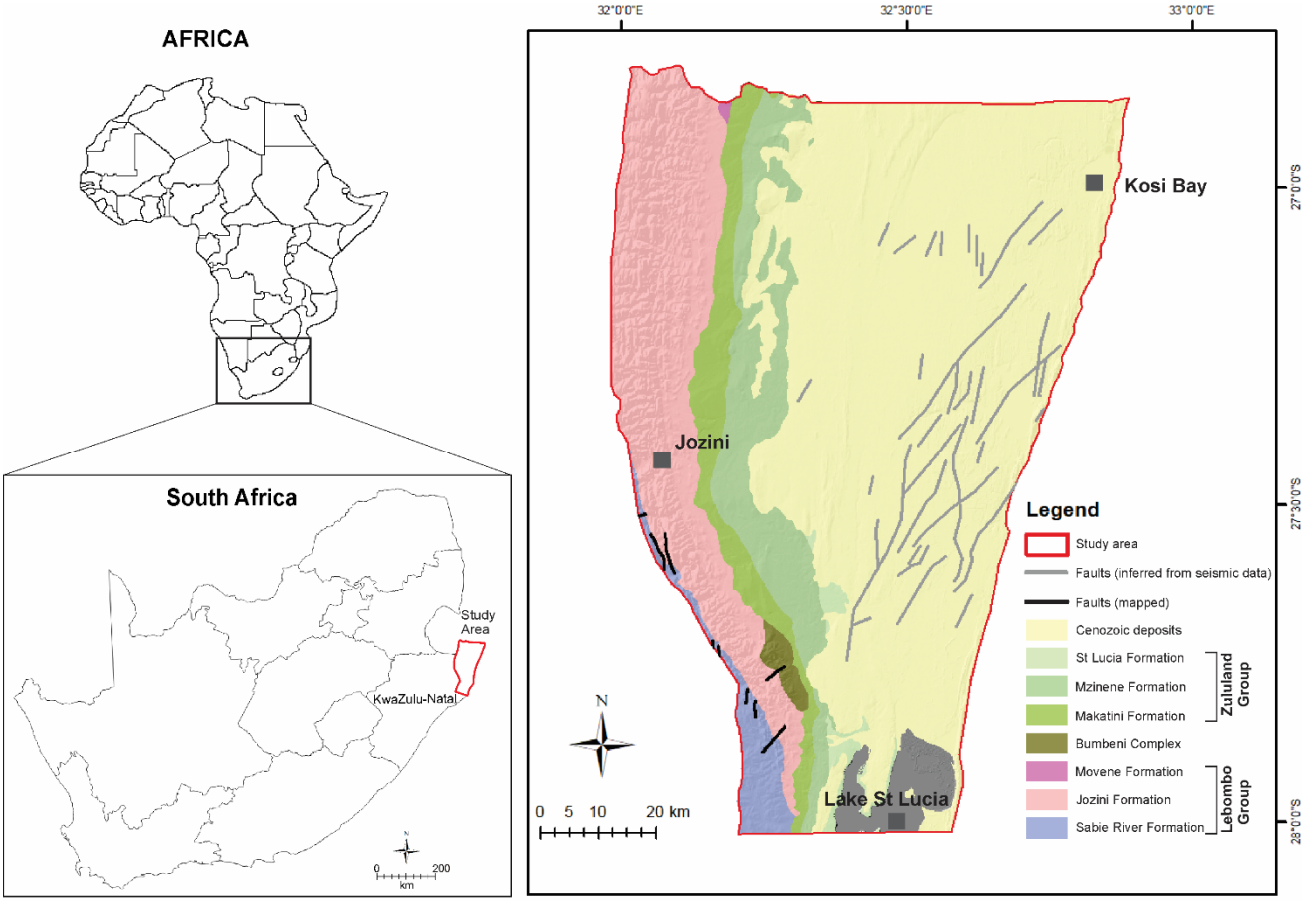

Figure 1.1: The geographical location of South Africa in the continent of Africa and the locality of the study area in the northern KwaZulu-Natal. A geological map, overlain on the hillshade map created in ArcGIS®, summarising the lithostratigraphy and faults of the study area (modified after the 1: 1 000 000-scale geological map of South Africa, Council for Geoscience, 2019). The Lebombo Group (Sabie River, Jozini and Movene Formations) is shown, however, not all the formations outcrop in the study area. The Bumbeni Complex and the sedimentary infill of the Zululand Basin including the Makatini, Mzinene and St Lucia Formations (Zululand Group) and the Cenozoic deposits are also shown.

1.2.1. The Karoo Large Igneous Province

The sedimentary succession of the Karoo Supergroup, reaching a maximum thickness of ~6 km in the main Karoo Basin of South Africa, comprises from base to top, the Dwyka, Ecca, Beaufort and Stormberg Groups with the latter comprised of the Molteno, Elliot and Clarens Formations (Smith et al., 1993; Catuneanu et al., 1998; Johnson et al., 2006; Bordy and Head, 2018). The sedimentary sequence is capped by volcanic rocks of the Karoo LIP which comprises a voluminous succession of

volcanic and intrusive rocks, that cover an estimated area of ~3 000 000 km^2 (Fig. 1.2) (Eales et al., 1984; Le Gall et al., 2002).

The 700-km-long Lebombo mountain range, extending from Empangeni (South Africa) in the south to Zimbabwe in the north, forms the eastern-most region of the Karoo volcanism (Fig. 1.2) (Eales et al., 1984; Marsh et al., 1997). This prominent mountain range is made up of the Lebombo Group volcanics which are subdivided into the Mashikiri, Letaba, Sabie River, Jozini, Mbuluzi and Movene Formations, respectively. The basal 182.1±1.6 Ma Mashikiri Formation comprises nephelinites (Watkeys, 2002; Riley et al., 2004). The 182.7±0.8 Ma Letaba Formation picritic lavas overlie the Mashikiri Formation in the northern Lebombo area and in the Tuli and Save regions of Zimbabwe (Riley et al., 2004; Duncan and Marsh, 2006; Hastie et al., 2013). The overlying, 184.2±1.0 to 181.2±1.0 Ma, Sabie River Formation comprises voluminous eruptions of continental flood basalts which cover most of southern Africa including the southern Lebombo region (Duncan et al., 1997; Riley et al., 2004; Duncan and Marsh, 2006). The Sabie River Formation basalts are overlain by rhyodacites and rhyolites of the 177.8±0.7 Ma Jozini Formation (Riley et al., 2004), and the Mbuluzi Formation which are largely confined to Eswatini (previously known as Swaziland) (Riley et al., 2004; Duncan and Marsh, 2006; Hastie et al., 2013). These rhyodacites and rhyolites are more resistant to erosion than the underlying mafic lavas and therefore characterise the Lebombo mountain range, the top of which is a well-preserved erosion level (Eales et al., 1984; Duncan and Marsh, 2006). The 137 Ma Movene Formation overlies the Mbuluzi Formation and comprises interlayered rhyolites and basalts, which form a small occurrence extending from northern KwaZulu-Natal into southern Mozambique (Bristow and Cleverly, 1983; Eales et al., 1984; Duncan and Marsh 2006).

The volcanic rocks that constitute the Drakensberg Group occur along the western border of KwaZulu-Natal and cover the northern areas of the Eastern Cape and most regions of Lesotho (Fig. 1.2) (Marsh et al., 1997; Duncan and Marsh, 2006). This group comprises basaltic rocks ranging from tholeiitic to basaltic andesites (Duncan and Marsh, 2006; Svensen et al., 2014). These rocks are subdivided into the lower Barkley East and upper Lesotho Formations, based on variations in the trace and minor element compositions of the lavas, with the upper geological units characterised by a dominance of low Ti/Zr ratios (titanium-Ti; zirconium-Zr) in contrast to the lower geological units.

The intrusive/sub-volcanic rocks of the Karoo LIP occur as a network of dolerite sills, dykes and saucer-shaped sheets which are best developed in the main Karoo Basin (Chevallier and Woodford, 1999; Duncan and Marsh, 2006; Jourdan et al., 2008). The sills and sheets vary in thickness ranging from a few metres to >200 m and are predominantly tholeiitic in composition (Marsh and Eales 1984; Marsh et al., 1997; Jourdan et al., 2008; Svensen et al., 2014).

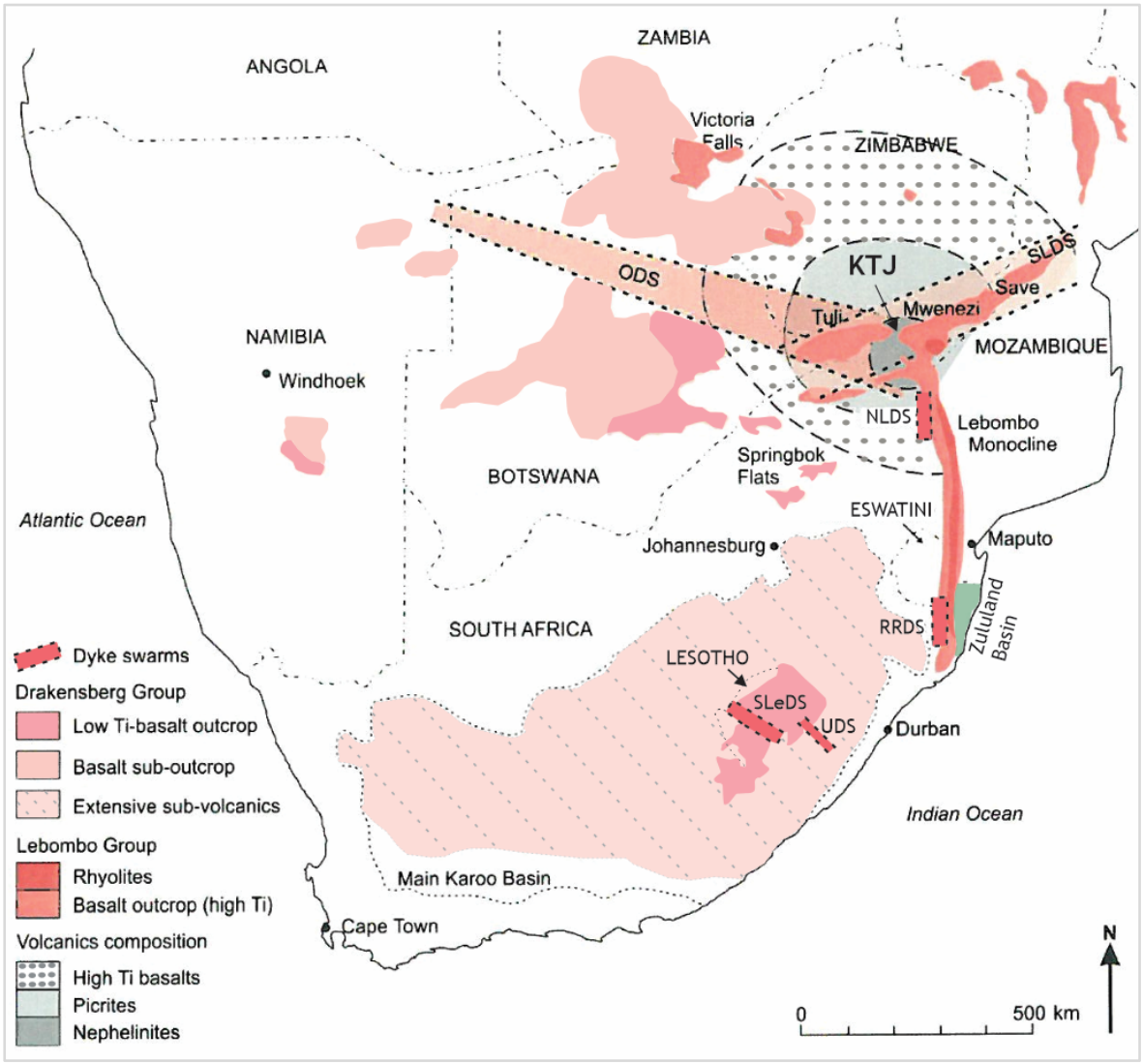

Figure 1.2: Regional outcrop map of the remnant lavas belonging to the KIP in southern Africa. The map further illustrates the extent of the rocks of the Drakensberg and Lebombo Groups. The dolerite intrusions of the sub-volcanic complex of the KIP are widespread in the region but occur extensively in the main Karoo Basin. ODS: Okavango Dyke Swarm, SLDS: Save-Limpopo Dyke Swarm, NLDS: Northern Lebombo Dyke Swarm, KTJ: Karoo triple junction, RRDS: Rooi Rand Dyke Swarm, SLeDS: Southern Lesotho Dyke Swarm, UDS: Underberg Dyke Swarm. Eswatini: Swaziland. (Adapted and modified from Hoyer, 2015 after Duncan and Marsh, 2006; Jourdan et al., 2008; Klausen, 2009; Hastie et al., 2014). The current study was undertaken in the Zululand Basin, which is coloured green, adjacent the Lebombo mountains.

1.2.1.1. Dyke Swarms associated with the Karoo LIP

The dyke swarms of the Karoo LIP include the Okavango Dyke Swarm (ODS) (Reeves, 1978; Elburg and Goldberg, 2000, Jordan et al., 2004, Klausen, 2009), the Save-Limpopo Dyke Swarm (SLDS), the Northern Lebombo Dyke Swarm (NLDS) (Jourdan et al., 2006; Klausen 2009; Hastie et al., 2011a) and the Rooi Rand Dyke Swarm (RRDS) (Fig. 1.2) (Meth, 1996; Hastie et al., 2014). The ODS, SLDS and NLDS converge at Mwenezi, forming the well-known Karoo triple junction (Campbell and Griffiths, 1990;

Watkeys, 2002; Jourdan et al., 2004). The 181.4±0.7 and 182.3±1.7 Ma NLDS (Jourdan et al., 2005; Jourdan et al., 2007a) comprises sub-parallel, north-south oriented dykes that cross-cut the Lebombo Group and the Clarens Formation in the northern portion of the Lebombo mountain range (Saggerson and Bristow, 1983; Armstrong et al., 1984; Klausen, 2009; Hastie et al., 2011b).

The RRDS has a MORB-like composition (the only such known composition in the Karoo LIP), dated at 173±0.7 Ma (Jourdan et al., 2008), intruded into the southern portion of the Lebombo mountains (Watkeys, 2002; Hastie et al., 2013). The RRDS forms a ~200-km-long north-south trending dyke swarm extending from the KwaZulu-Natal Province in the south into east-central Swaziland in the north (Armstrong et al., 1984; Meth, 1996). It is suggested that this dyke swarm was developed from the melting of the asthenosphere with crustal contamination (Saggerson and Bristow, 1983; Armstrong et al., 1984; Meth, 1996). It also appears that the RRDS was emplaced during the main stages of faulting, tilting and warping of the Lebombo mountains caused by extensional events related to the initial stages of Gondwana break-up (Armstrong et al., 1984; Meth, 1996; Hastie et al., 2014).

1.3. Regional Tectonic Setting

Gondwana is subdivided into East (Africa and South America) and West Gondwana (Antarctica, India, Madagascar, Australia), which separated during the break-up of the supercontinent (Shackleton, 1996; Mueller and Jokat, 2019). The regional tectonic framework relevant to the study area includes the onshore and offshore events related to Gondwana break-up, which commenced in the Early Jurassic (Hawkesworth et al., 1999; Watkeys, 2002). The Gondwana break-up event is thought to have been accompanied by the Early Jurassic closure of the Paleo-Tethys Ocean, which was located between the ancient continents of Gondwana and Laurasia, and the development of oceans of the southern hemisphere including Atlantic and Indian Oceans (Watkeys, 2006; Mueller and Jokat, 2019). The causes of continental break-up are not well understood and the available models favour lithospheric extension in response to subduction and the emplacement of a deep-seated mantle plume (Hawkesworth et al., 1999). It is suggested by Martin and Hartnady (1986), based on Duncan's (1984) Jurassic position of the Bouvet hot-spot relative to Africa, that the hot spot may have been a cause of separation of Africa and Antarctica (prior to ~145 Ma) and the separation of the Falkland Plateau and the Natal Valley (~125 Ma). Although the cause of the Gondwana break-up is contentious, this event is a major geological occurrence that has affected the southern hemisphere and has shaped the existing continents (Watkeys, 2006; Mueller and Jokat, 2019). This event, which also led to the emplacement of oceanic crust in parts of the Africa-Antarctica Corridor, commenced in the Early

Jurassic and is still active today with geological evidence preserved in the offshore basins on the continental shelf around southern Africa (Watkeys, 2002; Mueller and Jokat, 2019).

1.3.1. The development of the southern African Margin and Gondwana break-up

The development of a continental margin as a product of continental break-up is attributed to either stretching normal to the margin or strike-slip movement parallel to the coastline (Watkeys and Sokoutis, 1998). According to Watkeys and Sokoutis (1998) not all continental margins conform to these two end-member situations but these scenarios may occur in conjunction with one another.

The development of the southern African margin, a region where Africa, South America and Antarctica where once linked, was not solely caused by Karoo volcanism (although contemporaneous) or the extraction of the Falkland Plateau but is a product of prolonged tectonic history related to the Gondwana break-up event (Cox, 1992; Watkeys and Sokoutis, 1998; Jokat et al., 2003). This event has received consideration with studies paying particular attention to the early stages of break-up in plate reconstructions (i.e., Martin and Hartnady, 1986; Cox, 1992; Hanyu et al., 2017) and implications to the present location of the continents (i.e., Hawkesworth et al., 1999; Eagles and König, 2008; Leinweber and Jokat, 2012).

The Gondwana break-up event, from a southern African perspective, took place in stages (Fig. 1.3) (Smith and Hallam, 1970; Shackleton, 1996; Watkeys and Sokoutis, 1998). The first stage (180–175 Ma) involved faulting and rifting along the Lebombo mountains (Watkeys and Sokoutis, 1998), supposedly related to Karoo volcanism (Fig. 1.3a and b) (Storey, 1995; Watkeys and Sokoutis, 1998; Hawkesworth et al., 1999). During this stage no continental separation is proposed by Watkeys and Sokoutis (1998), in accordance with Cox's (1992) stage one, in the Early Jurassic break-up of Gondwana. This was followed by stage two (175–155 Ma), the linking of the Gastre Fault System-Agulhas Falklands Fracture Zone from the proto-Pacific Ocean to the Lebombo mountains with dextral strike-slip movement along this system resulting in rotation of microplates, for example the Falkland Islands (Fig. 1.3c) (Storey and Kyle, 1997; Watkeys, 2002). The third stage (155–135 Ma) involved the linking of the Davie Fracture Zone from the Tethys Ocean in the north to the proto-Pacific Ocean in the south where strike-slip movement separated Gondwana into East and West Gondwana (Fig. 1.3d) (Encarnación, 1996; Watkeys and Sokoutis, 1998; Boger et al., 2001). The fourth stage (135–115 Ma) is marked by the initiation of seafloor spreading attributed to the arrival of the Tristan da Cunha plume beneath a proto-South Atlantic rift and the separation of South America and Africa (Fig. 1.3e) (Watkeys and Sokoutis, 1998; Watkeys, 2002). The fifth and final stage of break-up (115–90 Ma) involved the final separation of South America and Africa by sea-floor spreading (Fig. 1.3f) (Watkeys, 2002).

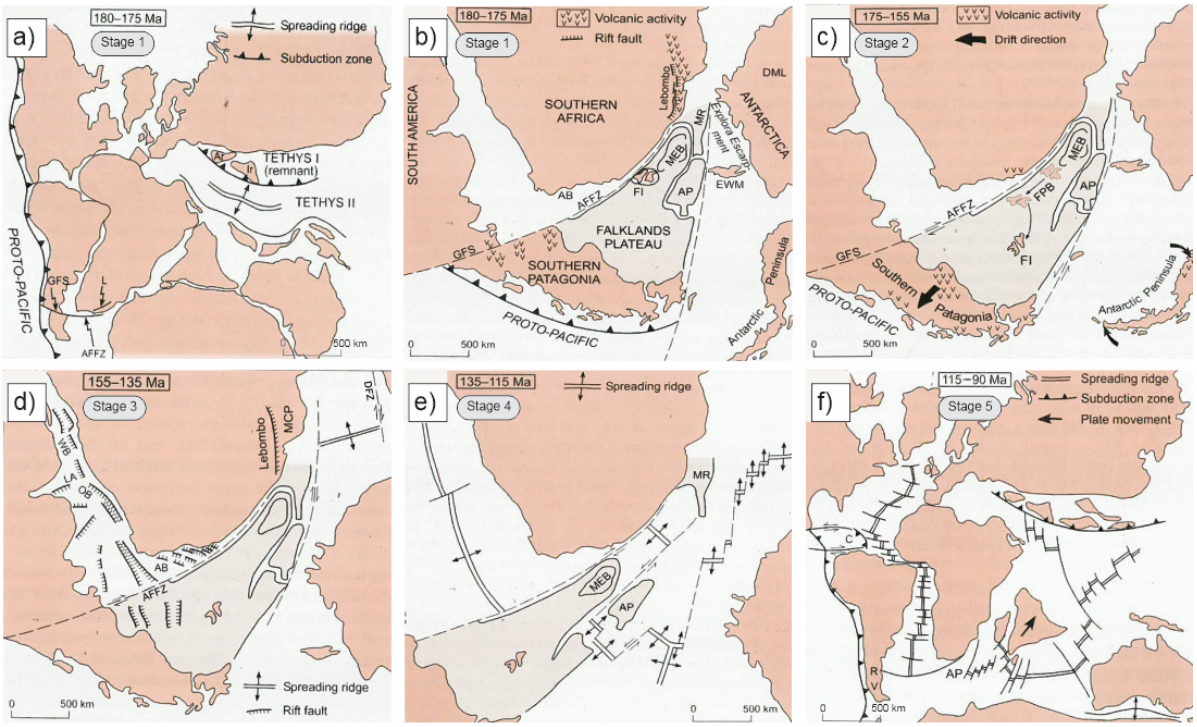

Figure 1.3: The stages of Gondwana break-up from 180 to 90 Ma are presented (modified after Watkeys and Sokoutis, 1998; Watkeys, 2006; Hicks, 2017). (a) Gondwana was attached to the supercontinent Pangaea during stage 1 (180–175 Ma). Gondwana was bounded by two oceans, Tethys I and II, in the northeast and the proto-Pacific Ocean in the west. (b) During the first stage (180–175 Ma) there was some rifting without continent separation. The northern end of the Agulhas-Falklands Fracture Zone at this stage was in close proximity to the southern termination of the Lebombo mountains. (c) South America moved away from Africa by sea-floor spreading during this stage (stage 2) at about 175–155 Ma. This stage also involved the extension of the Maurice Ewing Bank (MEB) and rotation of the Falkland Islands (FI). Plate rotation was caused by strike-slip movement along the Gastre Fault System (GFS)–Agulhas-Falklands Fracture Zone (AFFZ). (d) The third stage (155–135 Ma) was characterised by strike-slip movement along the Davie Fracture Zone (DFZ), now located on the east coast of Tanzania and Mozambique, which caused the separation of East and West Gondwana. (e) At about 135–115 Ma (stage 4) West Gondwana was split and this event involved the extraction of the MEB and the Agulhas Plateau (AP) to create the Natal Valley. (f) The last stage (stage 5; 115–90 Ma) involved the separation of Antarctica and Australia and also any link between South America and Africa. This stage resulted in the present day plate configuration. Key: (Ar) Armenian microplate, (Ir) Iranian microplate, (L) Lebombo mountains, (AB) Agulhas Bank, (FPB) Falkland Plateau Basin, (EWM) Ellsworth Island, (DML) Drönning Maud Land, (FPB) Falkland Plateau Basin, (WB) Walvis Basin, (LA) Luderitz Arch, (OB) Orange River Basin, (MCP) Mozambique Coastal Plain, Mozambique Ridge (MR), (C) Caribbean.

1.3.1.1. The Mozambique Coastal Plain and the Northern Natal Valley

The origin of the Mozambique Coastal Plain is uncertain; understanding the nature of the onshore and offshore crust underlying the Mozambique Coastal Plain and the Northern Natal Valley is important when determining the tectonic framework of the study region. This regional basement has previously been interpreted as; oceanic crust (e.g., Martin and Hartnady, 1986; Leinweber and Jokat, 2012; Mueller and Jokat, 2019), continental crust (e.g., Dingle and Scruton, 1974; Moulin et al., 2020) or a

mixture of the two (Cox, 1992) with Hanyu et al. (2017) suggesting that the basement here comprises mafic volcanic intrusions. The Mozambique Coastal Plain and the Northern Natal Valley are thought to have originated because of stage two of Gondwana break-up (Fig. 1.3b) (Watkeys and Sokoutis, 1998). The Mozambique Coastal Plain is assumed to extend immediately south of the Mateke-Sabi monocline and in close proximity to the Lebombo monocline (composed of the Lebombo Group) (Fig. 1.4) (Cox, 1992; Mueller and Jokat, 2019).

Leinweber and Jokat (2011) associated the Mozambique Coastal Plain with thickened oceanic crust and an extinct spreading centre in the southern coast of the plain. It is suggested by Leinweber and Jokat (2012) that the Northern Natal Valley developed as result of the southwestern departure of Antarctica relative to Africa at about 159.1 Ma. Acccording to Leinweber and Jokat (2011) the Northern Natal Valley is a region dominated by complicated patterns of magnetic anomalies; however, it is mainly charaterised by SW–NE oriented anomalies. In this region no magnetic or gravity anomalies have been interpreted as delineating the Continental Oceanic Boundary (Leinweber and Jokat, 2012). The position of the Continental Oceanic Boundary, although contentious, has been associated with Mozambique channel, in the Mozambique coast, which is also an area where the oldest sea-floor spreading anomalies (167 Ma) were identified (Leinweber et al., 2013). It has also been associated with both the Mozambique Coastal Plain and the Northern Natal Valley, which form part of the Africa-Antarctica Corridor (Fig. 1.4) (Hanyu et al., 2017; Mueller and Jokat, 2019).

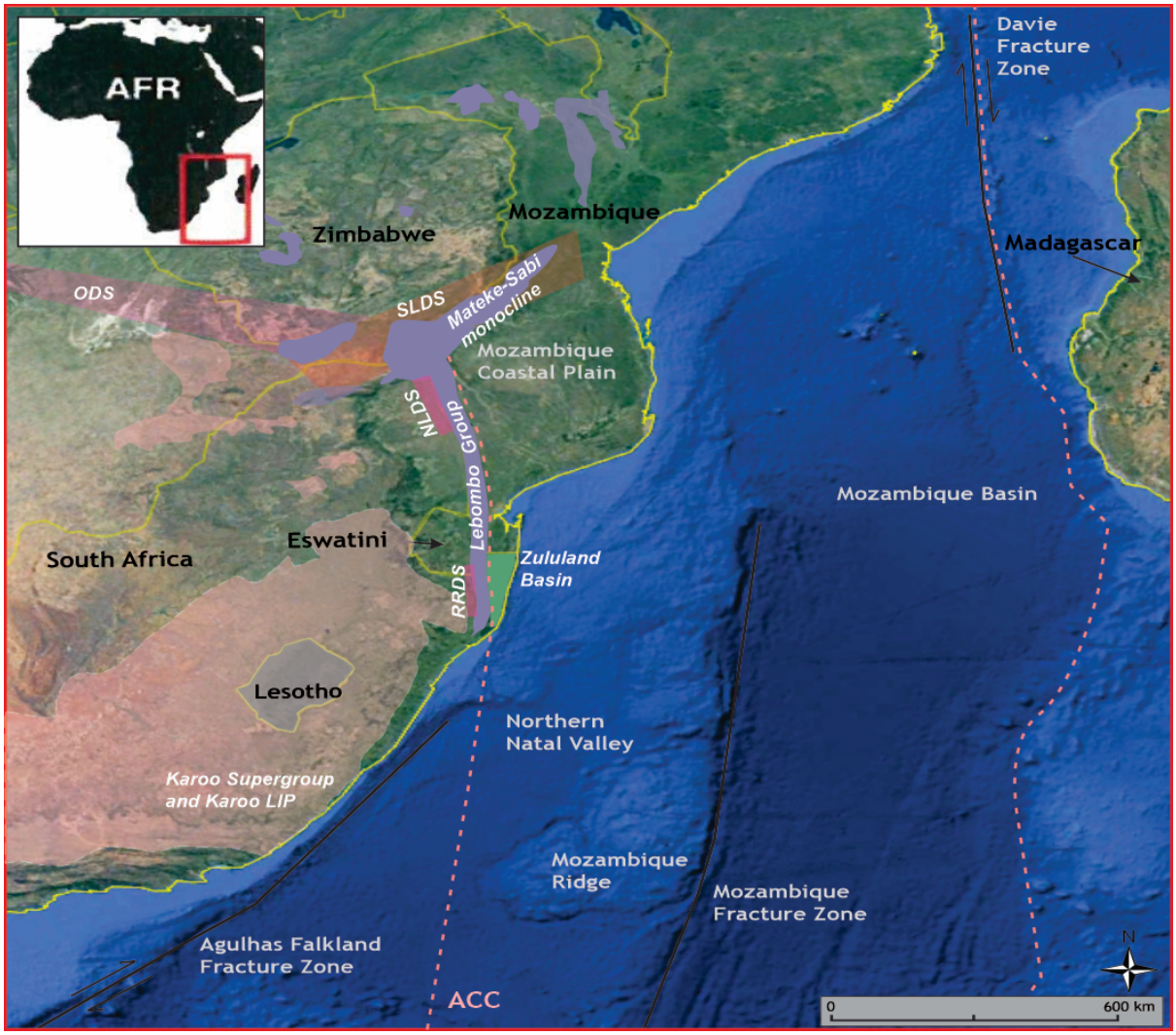

Figure 1.4: The position of the Africa (AFR)-Antarctica Corridor (ACC) (highlighted by the dashed pink line) with respect to the east coast of South Africa, Mozambique, Madagascar and the Agulhas Falklands and Davie Fracture Zone. The generalised satellite map shows regions that comprise the Africa-Antarctica Corridor, namely the Mozambique Coastal Zone, Northern Natal Valley, Mozambique Ridge, Mozambique Basin and Mozambique Fracture Zone. (Modified after Mueller and Jokat, 2019). The generalised geology of the Karoo Supergroup, the Karro LIP and the Zululand Basin is also shown (modified after Cox et al., 1965; 1: 1 000 000-scale geological map of South Africa, Council for Geoscience, 2019).

1.3.1.2. The KwaZulu-Natal–Maputaland Margin

The KwaZulu-Natal–Maputaland Margin extends from Richards Bay, in the south to the Maputo area in the north and the basement geology comprises volcanic rocks of the Lebombo Group (Fig. 1.5) (Cleverly and Bristow, 1979; Baby et al., 2018). The exposed Lebombo Group along the Lebombo mountains forms the western limit of this margin (Baby et al., 2018). Graben structures have been identified through 2D seismic data underneath this margin (McMillan, 2003; Baby et al., 2018). The Bumbeni Ridge, a NE-SW trending basement ridge, extends from the southern margin of the Lebombo mountains and beneath Cretaceous and Cenozoic cover sequences (Fig. 1.5). The Bumbeni Ridge divides the Cretaceous Zululand Basin into two sub-basins, namely the Kosi and St Lucia troughs, which comprise eastward tilted sedimentary infill (Fig. 1.5.) (Shone 2006; Baby et al., 2018).

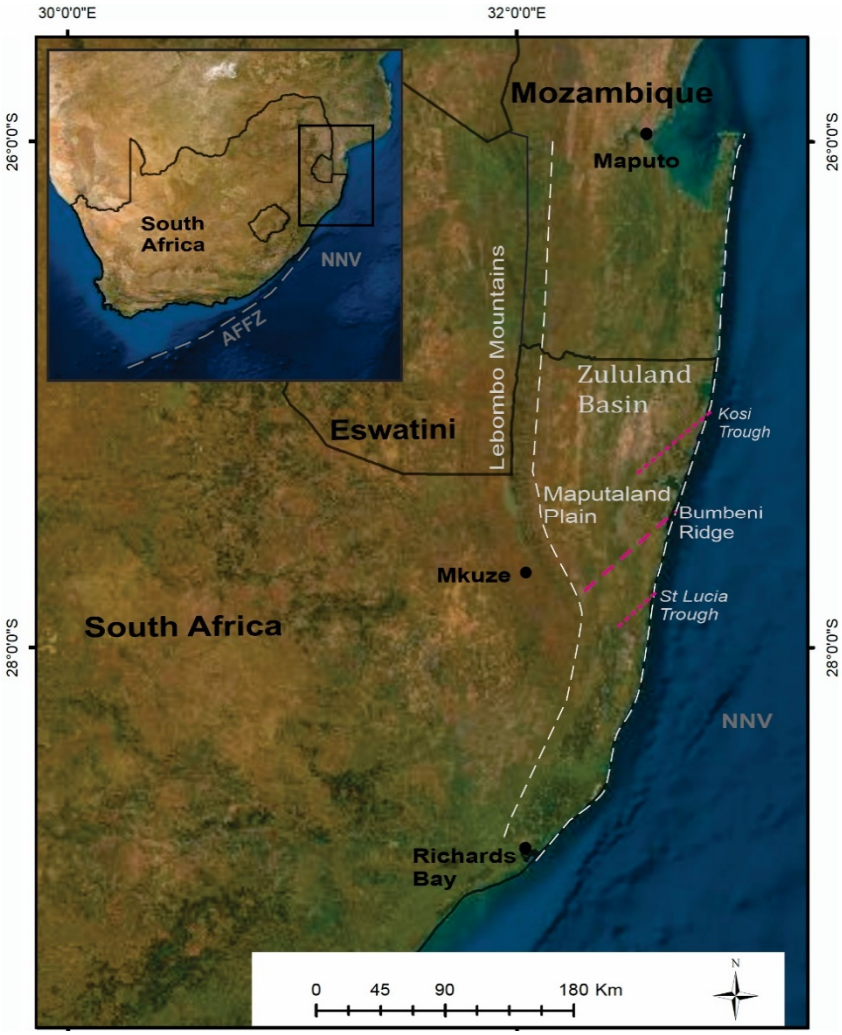

Figure 1.5: The extent of the KwaZulu-Natal-Maputaland margin is shown (on the ArcGIS satellite image) with dashed white lines (modified after Baby et al., 2018). The Lebombo mountains, Zululand Basin and Maputaland Plain are highlighted. The locations of the Kosi trough, the NE trending Bumbeni Ridge and the St Lucia Trough are shown with dashed pink lines (adapted from Broad et al., 2006). The Northern Natal Valley located in the Indian Ocean, east coast South Africa is also shown.

1.4. Local Geological Setting

The Mesozoic Zululand Basin is developed beneath the Maputaland Plain in northern KwaZulu-Natal (Fig. 1.6), and its western limit is marked by the eastward-tilted Lebombo mountain range representing the eastern-most extent of the Jurassic-age Karoo LIP (Fig. 1.6) (Saggerson and Bristow, 1983; Duncan et al., 1997; Marsh et al., 1997). The southern portion of the Lebombo mountains comprises the basal 184.2 ± 1.0 to 181.2 ± 1.0 Ma Sabie River Formation basalt, which is overlain by the 177.8 ± 0.7 Ma erosion resistant, ~2000-m-thick rhyodacites and rhyolites of the Jozini Formation (Saggerson and Bristow, 1983; Duncan et al., 1997; Jourdan et al., 2004; Jourdan et al., 2007a). The upper suite is represented by the 137 Ma interbedded rhyolites and basalts of the Movene Formation extending from northern KwaZulu-Natal into Mozambique (Bristow and Cleverly, 1983; Cox and Bristow, 1984; Duncan and Marsh 2006; Klausen, 2009).

Intruding the Jozini Formation are the rhyolite plugs, dome-like lava flows and dykes of the Ntabankosi Suite, which are generally grey, brown and reddish brown in fresh colour (Saggerson and Bristow, 1983; Watkeys, 2002). These rocks are typically porphyritic with a cryptocrystalline to glassy groundmass and commonly show contorted flow lines (Saggerson and Bristow, 1983; Wolmarans and Du Preez, 1986). The rhyolitic domes generally form hills, whereas the dykes occur as irregular north-south trending ridges which pinch and swell along strike and can be up to 100-m-wide (Saggerson and Bristow, 1983).

The youngest volcanic event in the study area is the 133±5 Ma Bumbeni Complex, which comprises mafic to felsic volcanic rocks that crop out near the southern end of the Lebombo mountains (Fig. 1.6a) (Saggerson and Bristow, 1983; Allsopp et al., 1984; Wolmarans and Saggerson, 1988). The Bumbeni Complex comprises the mafic volcanics of the Mpilo Formation and felsic lava flows and pyroclastic deposits of the Fenda Formation and Nxwala Member, respectively (Fig. 1.6b) (Bristow and Duncan, 1983; Saggerson and Bristow, 1983; Wolmarans and Saggerson, 1988). According to Bristow and Duncan (1983) the air-fall and flow-tuff deposits of the Nxwala Member could represent products of plinian eruption associated with rhyolitic dome building and collapse.

Post-dating the intrusion of the Cretaceous Bumbeni Complex is a rift-drift sedimentary sequence of the Zululand Group which is a ~2000-m-thick succession of detrital material (Shone, 2006; Green, 2011). The Zululand Group is compartmentalized into two sub-basins, the Kosi and St Lucia troughs, by the Bumbeni Ridge, and is subdivided into the Makatini, Mzinene and St Lucia Formations (Shone, 2006; Green, 2011; Baby et al., 2018). The eastern region of the study area, extending from the Mozambique-South Africa border in northeastern Kwazulu-Natal Province, to the St Lucia estuary in the south, is dominated by the Maputaland Plain (Watkeys et al., 1993; Porat and Botha, 2008). The

Maputaland Plain is composed of Cenozoic sedimentary deposits of the Maputaland Group, which overlie the Zululand Group and basement rocks in the study area (Watkeys et al., 1993; Botha and Porat, 2007; Porat and Botha, 2008).

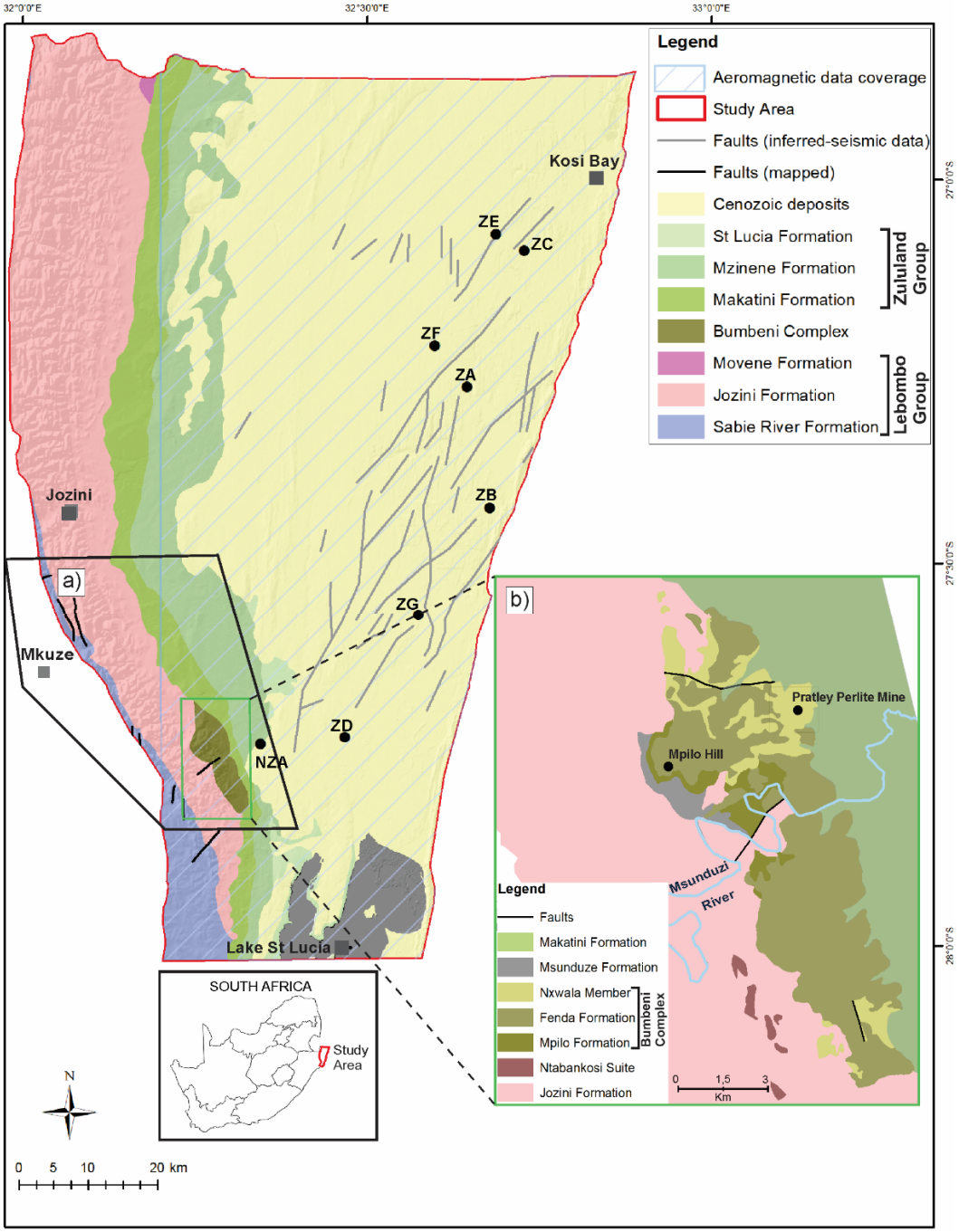

Figure 1.6: Location of the study area and geological map summarising the lithostratigraphy of the region. The Lebombo mountains in the west comprise the eastward tilted mafic and felsic volcanics of the Sabie River and Jozini Formations (Lebombo Group). The Lebombo Group which is intruded by the Bumbeni Complex to the south is overlain by sedimentary rocks of the Zululand Group and subsequently by the Cenozoic deposits in the east (modified after the 1: 1 000 000-scale geological map of South Africa, Council for Geoscience, 2019). Selected exploration boreholes drilled as part of the hydrocarbon exploration programme, conducted by the Zululand Oil Prospecting Company, Anglo Vaal and the Southern Oil Exploration Corporation (now PetroSA) between 1964 and 1978, are shown as black circles with borehole names. The area

in which the aeromagnetic data was acquired is shown with a blue hatching. (a) The field area outline in which the geological and structural observations and data were collected during field work. (b) The insert is a close-up view of a simplified field map showing the Ntabankosi Rhyolite Suite, the extent of the Bumbeni Complex (Mpilo and Fenda Formations and Nxwala Member) and the Msunduzi Formation (modified after Bristow and Cleverly, 1983; Wolmarans and Saggerson, 1988).

1.4.1. Lithostratigraphy of the Bumbeni Complex, Msunduze Formation and Zululand Group

1.4.1.1. Bumbeni Complex

The Bumbeni Complex comprises a variable suite of basaltic and rhyolitic lavas, ash-fall-tuffs and flow-tuffs (Cleverly and Bristow, 1979; Bristow and Duncan, 1983; Wolmarans and Saggerson, 1988). The complex is exposed in the Mkuze Game Reserve and extends southwards beyond the Msunduzi River where it has a total approximate thickness of 225 m (Cleverly and Bristow, 1979; Bristow 1980; Wolmarans and Saggerson, 1988).

The separation of the lithostratigraphic units comprising the Bumbeni Complex is controversial and it has been subdivided into the basal Mpilo, Fenda and Nxwala Formations (SACS, 1980; Bristow and Cleverly, 1983). Subsequently, Wolmarans and Saggerson (1988) subdivided the Complex into the lower Mpilo Formation and the upper, most-extensive Fenda Formation, which comprises the Nxwala Member; pyroclastic rocks and perlite horizons that are intercalated with the Fenda Formation (Wolmarans and Saggerson, 1988).

(i) Mpilo Formation

The Mpilo Formation is a succession of fine-grained, greyish-green and brownish-grey amygdaloidal alkali-basalts, that are predominantly vesicular (Wolmarans and Du Preez, 1986; Wolmarans and Saggerson, 1988). According to Bristow (1980) the Mpilo Formation forms the basal unit of the Bumbeni Complex and overlies the rhyolites of the Jozini Formation with a disconformable contact. This formation is best exposed on the lower flanks of Mpilo Hill north of the Msunduzi River, where it has a maximum thickness of 65 m (Fig. 1.6b) (Bristow, 1980; Wolmarans and Saggerson, 1988).

(ii) Fenda Formation

The Fenda Formation comprises rhyolitic lavas and pyroclastic deposits (SACS, 1980; Wolmarans and Saggerson, 1988) that form the bulk of the Bumbeni Complex and unconformably overlies the Mpilo Formation and where the latter is not developed, it unconformably overlies the Jozini Formation (Wolmarans and Saggerson, 1988). The lava flows are of limited lateral extent and generally consist of finely banded and contorted rhyolite lavas with lens-shaped zones of lithophysae (high crystallisation

domains) and locally developed autobreccias (SACS, 1980; Wolmarans and Saggerson, 1988). The pyroclastic deposits occur as localised breccias and highly welded tuffs (SACS, 1980; Wolmarans and Saggerson, 1988). Joubert and Johnson (1998) proposed a thickness of >100 m for the Fenda Formation.

(iii) Nxwala Member

The Nxwala Member comprises non-welded ash-flows and air-fall tuffs, perlite and perlitic pitchstone (derived from obsidian flows), coarse breccias consisting of pumice and perlitic pitchstone blocks and flow banded rhyolite (SACS, 1980; Bristow and Duncan, 1983). The tuffs of the Nxwala Member are generally light-coloured and are characterised by alternating thin (1 to 4-cm-thick) ash bands and thicker (20 to 40-cm-thick) coarser zones comprising unsorted fragments of rhyolitic pumice, rhyolite, pitchstone and basalt (SACS, 1980; Wolmarans and Du Preez, 1986).

1.4.1.2. Msunduze Formation

The Msunduze Formation crops out at the base of the Mpilo Hill to the north of the Msunduzi River and mainly comprises a locally-developed fluviatile conglomerate with subordinate sandstone and siltstone (Stratten, 1964; Bristow and Cleverly, 1983; Cooper, 2018). The origin of the conglomerate is controversial and it is thought to belong to the Lebombo Group (Bristow and Cleverly, 1983; Bristow and Duncan, 1983), whereas a connection with the Bumbeni Complex has been suggested (Wolmarans and Du Preez, 1986; Wolmarans and Saggerson, 1988).

The conglomerate comprises waterworn, poorly-sorted, well-rounded to sub-rounded pebbles and boulders of red-grey rhyodacite and soft grey-green andesite with subordinate occurrences of dolerite and basalt embedded in a green-coloured (chloritized) matrix (Hemans, 1976; Bristow and Cleverly, 1983). The matrix is fine-grained and comprises calcite and smaller fragments of the same rock types (Hemans, 1976). Large boulders are present at the base of the conglomerate unit and can be up to 1 m in diameter and mainly rhyodacitic in composition (Hemans, 1976). Towards the top it becomes uniform and finer with andesitic clasts being common with minor carbonaceous fossil wood fragments present in outcrop (Hemans, 1976). The thickness of the Msunduze Formation has been estimated at 150 m (Wolmarans and Saggerson, 1988) with a dip of 10° to the northeast (SACS, 1980; Bristow and Cleverly, 1983).

1.4.1.3. Zululand Group

The Zululand Basin is a rift-drift sedimentary basin that is developed along the northernmost section of KwaZulu-Natal and the sedimentary infill of this basin constitutes the Zululand Group (Fig. 1.6) (Broad et al., 2006; Green, 2011). The Zululand Group is subdivided into the lowermost Makatini Formation, the Mzinene Formation and the upper St. Lucia Formation (Shone, 2006; Green, 2011; Baby et al., 2018).

(i) Makatini Formation

The basal Makatini Formation comprises small-pebble conglomerate, sandstone, siltstone and limestone units which nonconformably overlie the Lebombo Group volcanic rocks (Shone, 2006). This formation was deposited during the Barremian to early Aptian (Kennedy and Klinger, 1975). The conglomerates likely represent longitudinal-bar gravels which would have been covered by bar-top sands during periods of weakening flood conditions (Tarkard et al., 1982; Shone, 2006), whilst the siltstone and marine mudrocks likely represent estuarine, tidal-flat and shallow-marine settings (Shone, 2006). The sedimentary environment where these geological units are inferred to have formed is a system of braided rivers flowing eastwards from steep mountains onto coastal plains, where they merged with tidal flats (Tankard et al., 1982).

(ii) Mzinene Formation

The Mzinene Formation comprises shallow-marine, fossiliferous, glauconitic siltstones and fine-grained sandstones that were deposited in the early Albian to late Cenomanian (Kennedy and Klinger, 1975; Shone, 2006). In some areas the Mzinene Formation directly overlies lavas of the Lebombo Group but typically overlies the Makatini Formation (Shone, 2006). Where it is found to overlie the Makatini Formation it is separated by a hardground which is a well indurated concretionary horizon subsequently bored by Lithophaga, a rock-boring gastropod (Kennedy and Klinger, 1975; Shone, 2006). This bored hardground is encrusted with the remnants of oysters and suggests a long period of non-deposition (Shone, 2006).

(iii) St Lucia Formation

The upper Coniacian to Maastrichtian St Lucia Formation, which is lithologically similar to the underlying Mzinene Formation, is characterised by buff and greenish grey, richly fossiliferous

glauconitic siltstones and bioturbated sandstone with interbedded large calcareous concretions (Kennedy and Klinger, 1975; Shone 2006). It is more fossil-rich than the Mzinene Formation, comprising echinoid, bivalve, gastropod, reptile bones, cephalopod remains, and fossil logs as well as plant remains and at least 62 ostracod species, and is separated from the underlying Mzinene Formation by an angular unconformity (Shone, 2006). An outcrop thickness of 7 m south of Lake St Lucia has been reported, however based on borehole data the St Lucia Formation has an approximate thickness of 900 m in northern Zululand (Shone, 2006).

2. Theoretical Background and Methods

2.1. Field Mapping

Geological field mapping of the Bumbeni Complex and Lebombo Group lithologies was undertaken in parts of the onshore Zululand Basin, northern KwaZulu-Natal. Field work comprised the description of lithological units and the recording of structural measurements of lineations, faults, systematic joint surfaces and associated kinematic indicators.

The lineations, slickenside-steps and fault drag features were used to determine the sense of movement along planar surfaces. The orientation of fault planes (strike and dip azimuth) and joint planes were measured utilising the dip and strike (right-hand rule) methodology and the results of the measurements are presented in stereonets and rose diagrams. Linear structures were measured as plunge and plunge direction. Measurements of planar and linear features were taken using a Silva Ranger compass and Midland Valley FieldMove Clino© digital mapping tool (a digital compass-clinometer for recording geological data using a smartphone). The FieldMove Clino© measurements were verified for accuracy by taking measurements with the Silva Ranger compass of identical planes and comparing the results. After a repeat in measurements, the observed degree of variation in measurements was insignificant. Therefore, FieldMove Clino© and Silva Ranger compass were used interchangeably. The magnetic declination (23°W) was adjusted accordingly and the right-hand rule method was applied for measuring strike on both tools. The field data was then exported as a .csv file for use in the program GeoRose and in GIS software.

2.2. Paleo-stress analysis

Paleo-stress analysis is the branch of structural geology that characterises principal stress orientations and ratios acting in the past from fault planes and their corresponding slip direction indicators (Žalohar and Vrabec, 2007; Simón, 2018). The understanding of the tectonic history of faulted and fractured geological regions has been achieved by relating both the slip and orientation of faults to the state of the stress at the time of displacement (e.g., Anderson, 1905; Price, 1966; Angelier, 1989; Abul Khair et al., 2015). Previous studies have revealed that qualitative and quantitative analyses of brittle fractures (e.g., faults, systematic joints) provide a key to the understanding of the evolution of paleo-stress fields through a series of tectonic events (e.g., Anderson, 1905; Angelier, 1989; Weinberger et al., 2010; Abul Khair et al., 2015).

Faulting is the brittle response of rocks to tectonic stresses (Orife et al., 2002). Faults reveal evidence of differential movement of the rock mass on either side of the fault plane (Price, 1966). The movement along the fault plane is classified as dip-slip when slip is in the vertical plane (e.g., normal or reverse faults), strike-slip when slip is horizontal or oblique-slip when there is a combination of vertical and horizontal displacement (Price, 1966). Strike-slip faults are further described as dextral (or clockwise) and sinistral (or anticlockwise) (Price, 1966). The geometrical properties and orientations of faults are controlled by the nature of the principal stress axes, where σ_1 is the maiximum stress direction, σ_2 is the intermediate stress direction, and σ_3 is the minimum stress direction (Anderson, 1905; Morris et al., 1996; Orife et al., 2002). Faults are produced in response to these principal stress directions, therefore the orientation information collected from faults in the field can be used to characterise the palaeo-stress regime (e.g., Angelier, 1984; Locombe et al., 1990; Orife et al., 2002). For example, the paleo-stress regime is defined by the nature of the vertical stress axes: (1) normal faulting occurs when σ_1 is vertical and σ_2 is the maximum horizontal stress axis, (2) strike-slip faulting occurs when σ_2 is vertical and σ_1 is the maximum horizontal stress axis, and (3) thrust faulting occurs when σ_3 is vertical and σ_1 is the maximum horizontal stress axis (Anderson, 1905; Delvaux et al., 1995). The changes in the orientation of the stress axes over time can cause new fault formation or the reactivation of older ones (Angelier, 1989; Orife et al., 2002). Pre-existing planes of weakness are more favourable zones of fault formation as compared to the creation of new faults (Orife et al., 2002).

Joints are geological structures formed in the brittle upper crust, which do not show evidence of displacement (Bates and Jackson, 1987; Bai et al., 2002; Weinberger et al., 2010). Joints usually develop as opening-mode fractures perpendicular to σ_3 and parallel to the σ_1-σ_2 plane (Hancock and Engelder, 1989; Arlegui and Simón, 2001; Fossen, 2010; Weinberger et al., 2010). Joints form due to the effect of a regional or local stress field (e.g., tectonic joints), hydro-fracturing, stress relaxation due to rock uplift and thermal contraction (e.g., columnar joints in basalts) (Engelder, 1985; Rogers et al., 1996; Bahat et al., 2005; Weinberger et al., 2010). These mechanisms are all different manifestations of the brittle deformation of cold rocks under low lithostatic pressure (Weinberger et al., 2010).

Joints formed in volcanic rocks such as those that occur in the study area, may be classified based on their origin and/or geometry as cooling related joints (e.g., columnar joints) and tectonic joints (Engelder, 1985; Rogers et al., 1996; Bahat et al., 2005). Differentiating columnar joints from the tectonic joints is straightforward, and is based on the geometry and mode of origin of the fractures.

Differentiating between non-columnar, planar cooling joints and tectonic joints in outcrop can be challenging, especially if the cooling joints intersect other joints (Rogers et al., 1996). However, the distinction between these joints is crucial for paleo-stress analysis (Khalifa, 2012). In general, tectonic joints occur as systematic, planar and sub-parallel joint sets whereas cooling joints are non-systematic and are usually curved, or conchoidal (Price, 1966; Dyer, 1988; Rogers et al., 1996; Weinberger et al., 2010) and cooling joints generally terminate against other joints (Rogers et al., 1996).

Systematic joints have been used extensively as indicators of paleo-stress regimes because they are (1) consistent in orientation over wide areas, (2) form perpendicular to σ_3, (3) occur pervasively in shallow tectonic environments, and (4) where several joint sets co-exist in one site, geometrical and chronological relationships supply information about fracture development (e.g., Dyer, 1988; Hancock, 1991; Arlegui and Simón, 2001). Regional systematic joints reflect the principal directions of the regional stress field that formed the joints (Engelder and Geiser, 1980). Thus, each set of joints is interpreted to represent a distinct event of jointing and associated stress regime and the occurrence of multiple joint sets reflects a change in the orientation of regional stresses over time (Engelder and Geiser, 1980). Hence, by compiling systematic joint results from a large number of outcrops, paleo-stress fields can be reconstructed (Arlegui and Simón, 2001). This is based on the assumptions that (1) the systematic joint sets formed in the same homogeneous stress field (i.e. related to the same deformational event), (2) the rocks themselves are fairly homogeneous, (3) the fractures do not significantly displace the stress field, and (4) that the structures have not rotated significantly since their initiation (Ramsay and Lisle, 2000; Igwe and Okonkwo, 2016).

2.2.1. Strike-slip deformation and the Riedel shear system

Strike-slip deformation occurs when one crustal or lithospheric block moves laterally relative to an adjacent block (Christie-Blick and Biddle, 1985). The occurrence, pattern and orientation of strike-slip faults can be influenced by the presence of pre-existing fractures including the reactivation of normal faults as strike-slip faults (Christie-Blick and Biddle, 1985). Strike-slip faults are generally characterised by the presence of en echelon faults and folds within and adjacent to the principal displacement zone (Christie-Blick and Biddle, 1985; Davis et al., 2000; Ahlgren, 2001). Although the magnitude of strike-slip displacement and width of the fault zones vary extensively, there are associated structures common to most strike-slip fault zones that help to define the style of deformation (Barlett et al., 1981). These structures include shear zones of en echelon conjugate strike-slip faults, zones of en echelon anticlines, low angle thrusts, and basins with systematic arrays of high angle normal and

reverse faults (Barlett et al., 1981; Christie-Blick and Biddle, 1985). These features are both compressional and extensional (with respect to the horizontal) (Barlett et al., 1981).

The term Riedel shears refers to a geometric fracture pattern generally associated with strike-slip fault systems, which was first observed from clay-cake deformation experiments (Barlett et al., 1981; Christie-Blick and Biddle, 1985; Davis et al., 2000; Katz et al., 2004). The basic geometry of Riedel structures consists of five sets of fractures oriented at specific angles to the trend of the principal displacement zone (Fig. 2.1) (Barlett et al., 1981; Christie-Blick and Biddle, 1985; Davis et al., 2000; Ahlgren, 2001). These commonly observed sets of fractures include (1) synthetic strike-slip faults or Riedel (R) shears, (2) antithetic strike-slip faults or conjugate Riedel (R') shears, (3) secondary synthetic faults or P-shears, (4) tension fractures (T), and (5) faults parallel to the principal displacement zone (PDZ), or Y-shears (Barlett et al., 1981; Christie-Blick and Biddle, 1985; Davis et al., 2000; Ahlgren, 2001). One of the prominent characteristics of a Riedel shear system is an overstepping, en echelon array of the R-shears oriented ~015° clockwise in a dextral Riedel system. In addition to the R-shears, in a dextral Riedel system, the fractures reveal different orientation relative to the PDZ, namely (1) R'-shears (oriented ~075°), (2) P-shears (oriented ~345°), (3) T-fractures (oriented ~045°) and (4) Y-shears strike parallel to the PDZ (Barlett et al., 1981; Davis et al., 2000; Ahlgren, 2001). Geological examples however, are usually more complex and the observed arrangements of structures do not necessarily conform to those predicted by models or experiments (Christie-Blick and Biddle, 1985). This is because rocks are heterogeneous, structures develop sequentially rather than instantaneously, and some early-formed structures tend to be rotated during protracted deformation (Christie-Blick and Biddle, 1985). It is therefore not vital for all the shears to exist but the presence of R-shears is mandatory for faults to be interpreted in a Riedel shear system (Davis et al., 2000). Systematic joints sets which are related to strike-slip regimes can be interpreted in a Riedel system and are a useful tool that can be used to deduce the principal directions of the regional paleo-stress fields which formed these fractures (Dyer, 1988).

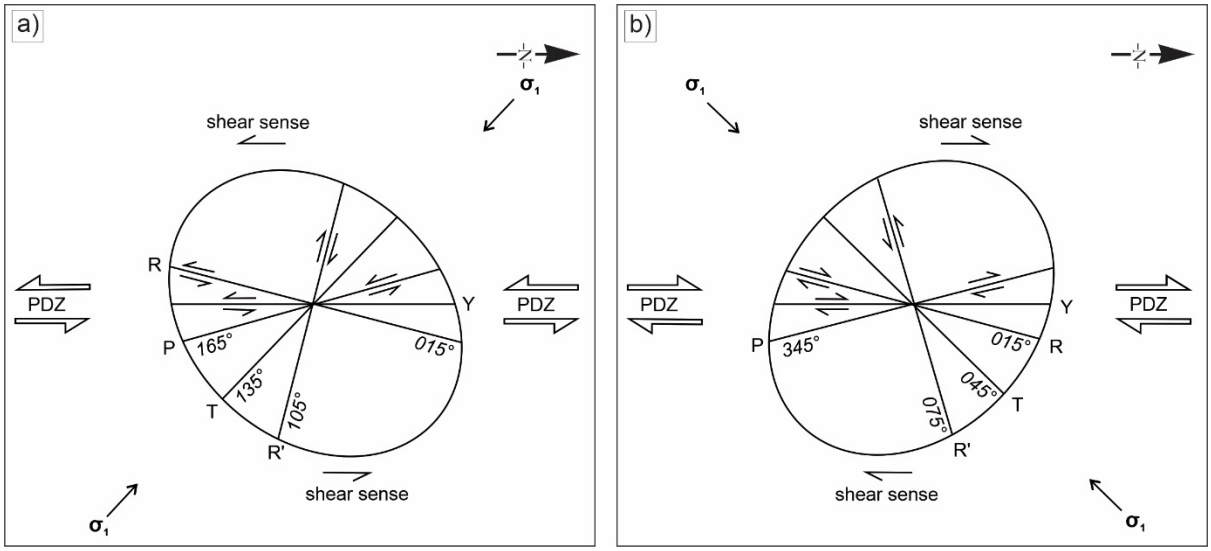

Figure 2.1. Top-view diagram showing the commonly observed fractures in an idealised Riedel shear system. (a) Fractures forming in an ideal sinistral strike-slip system. (b) Fractures forming in an ideal dextral strike-slip system. PDZ: principal displacement zone, Y: shears (oriented parallel to the PDZ), R: synthetic shears, R': antithetic shears, P: shears (secondary synthetic faults), T: tension fractures. Modified after Bartlett et al. (1981), Christie-Blick and Biddle (1985), Woodcock and Fischer (1986) and Davis et al. (2000).

Field data from seven faults and two associated lineations and eight hundred and fifty systematic joints were obtained in various outcrops within the study area (Fig. 1.6). Analyses of fault and lineation data obtained were done on stereonets and the joint surface measurements on rose diagrams using GeoRose 0.5.1 software and modified in Corel Draw 2019. Each stereonet plot presented in this study is in a lower hemisphere projection on equal angle nets. This was done in order to classify and compare the different structures and also to aid with the determination of the orientation of these structures.

The collected field data from the Jozini Formation rhyolites in three localities (JF Loc a–c) were grouped into a 10° interval from either side of the shear fracture directions of a Riedel shear system (Fig. 2.1). This was done to quantify the dominant directions associated with the major shear fracture orientations of a Riedel shear system.

2.3. Core logging

The Zululand Basin has been the focus of hydrocarbon exploration between 1964 and 1978 with the basin traversed by 2D seismic profiles and exploration boreholes (Viljoen et al., 2011; Chabangu et al., 2014). The earliest investigation was conducted between 1964–1965 by the Zululand Oil Prospecting Company and Anglo Vaal to test the oil and gas potential of the Zululand Group subsurface sandstones

(Viljoen et al., 2011; Chabangu et al., 2014). Subsequently, a basin-wide evaluation of the Zululand Basin was conducted by the Southern Oil Exploration Corporation (now PetroSA) between 1971–1978.

The drill core from three historical boreholes drilled in the Zululand Basin, namely NZA, ZD and ZB, were logged in detail, as these boreholes intersect the volcanic units of the Bumbeni Complex and the mafic and felsic units closest to the Bumbeni Complex and Bumbeni Ridge (Fig. 1.6). A borehole completion report of the ZG borehole, also in close proximity to the Bumbeni Ridge, drilled by the Southern Oil Exploration Corporation noted that this borehole intersects mafic volcanic rocks (Toschek, 1972). The nomenclature and classification of the pyroclastic rocks is based on the size and proportion of their pyroclasts (Fig. 2.2) (Le Maitre, 2002).

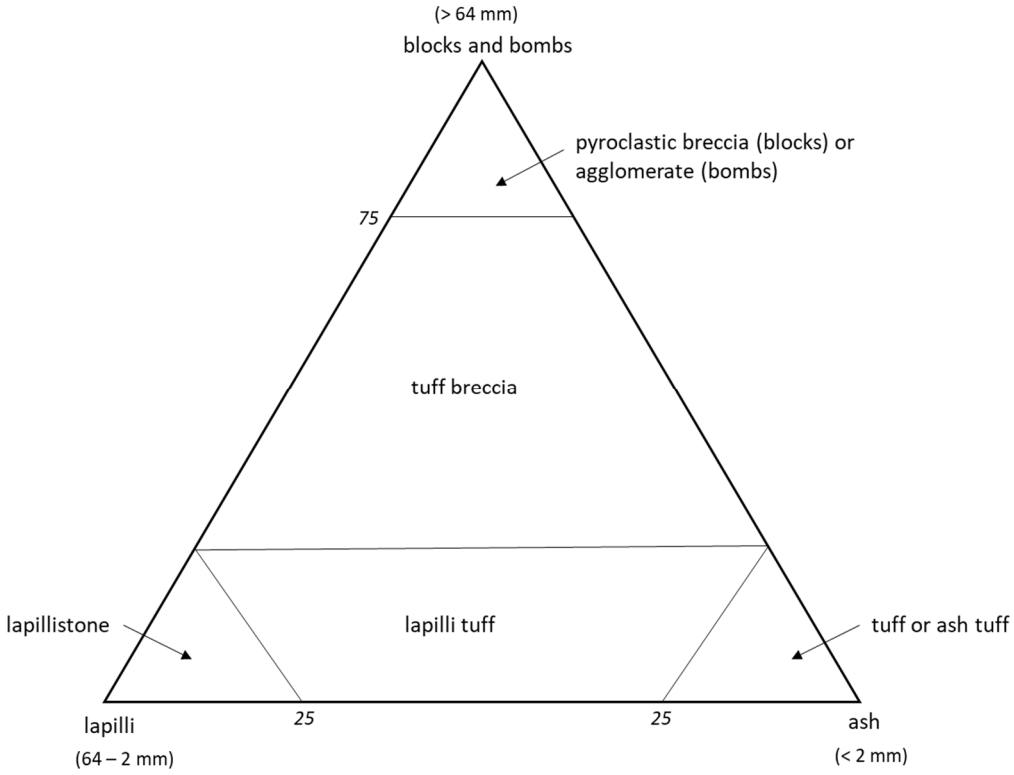

Figure 2.2: Classification of pyroclastic rocks of boreholes NZA, ZB and ZD based on size and proportions of blocks/bombs, lapilli and ash (modified after Le Maitre, 2002).

2.4. The aeromagnetic technique and related methodology

Geophysical survey techniques (i.e., gravitational, magnetic, electromagnetic) are used to measure the properties of the subsurface media (e.g., rock) based on their physical parameters (Kearey et al., 2002; Reynolds, 2011; Hinze et al., 2013). For the magnetic technique (ground and airborne), magnetic susceptibility of a material is an important parameter (Hunt, 1995; Kearey et al., 2002). This technique utilises the Earth's magnetic field, in search for local differences/anomalies that may be caused by

concealed geological features (Gunn, 1997; Kearey et al., 2002). Geological information that may be extracted or inferred from geophysical observations include lithology, deformation structures, hydrothermal alteration, weathering and depth to bedrock (Gunn, 1997; De Castro et al., 2014).

2.4.1. Magnetisation and Magnetic Susceptibility

The Earth is composed of three parts, the core (inner and outer core), mantle and crust where thermal convection processes within the outer core generates dipolar magnetic fields (Reeves, 2005; Opdyke and Mejia, 2004). The Earth's magnetic field is complex in structure and can be represented by means of a dipole field like that of a magnet (Reynolds, 2011). The main component of the geomagnetic field behaves like a dipolar electromagnet located at the centre of the Earth but inclined at 11.5° to the Earth's rotational axis (Reeves, 2005; Reynolds, 2011).

Magnetisation of a body is directly related to the concentration of the magnetic minerals, however this relationship varies according to the volume of magnetic minerals present (Gunn and Dentith, 1997). Minerals that cause magnetic anomalies include, for example, magnetite, pyrrhotite, hematite and ilmenite (Gunn and Dentith, 1997; Reeves, 2005). There are two forms of magnetisation associated with rocks, namely induced and remanent magnetisation (Telford, 1990; Gunn and Dentith, 1997; Reynolds, 2011). Induced magnetisation has the same direction as the Earth's present field and is proportional to the susceptibility of the material being magnetised, which is induced by an external magnetic field (Hill et al., 1997; McEnroe et al., 2009). Remanent magnetisation is permanent and can be in any direction, which in igneous rocks is typically locked in during magma cooling (Hill et al., 1997; McEnroe et al., 2009; Reynolds International, 2011). Basic and ultrabasic rocks have the highest susceptibilities whereas acidic igneous and metamorphic rocks have intermediate to low susceptibilities and sedimentary rocks have very low susceptibilities (Reynolds, 2011).

2.4.2. Units of Magnetic Field Measurements

The magnetic field (or geomagnetic field intensity) is measured with magnetometers (Kearey et al., 2002; Reeves, 2005). The magnetic flux lines between two poles per unit area is the flux density B measured in Tesla=weber/meter^2 (T=Wb/m^2) (Kearey et al., 2002; Hinze et al., 2012). The unit of Tesla is regarded as being too large to measure magnetic anomalies as a result the SI unit of measurement nanoTesla (nT=10^{-9}T, 1 billionth of a Tesla) was introduced as an appropriate subunit (Kearey et al., 2002; Reynolds, 2011; Reynolds International, 2011).

2.4.3. Application of the Aeromagnetic Technique

The magnetic survey method, which is the most widely employed geophysical technique for exploring the Earth's surface (Paterson and Reeves, 1985; Hinze et al., 2012), is relatively easy to apply in a wide variety of subsurface mapping, it acquires data over large areas in a short time and it is an inexpensive technique when compared to other geophysical methods (Paterson and Reeves, 1985; Elliot and Laharia, 2008; Hinze et al., 2012). Regional scale aeromagnetic surveys can be employed in delineating volcanosedimentary belts, concealed geological bodies and post-tectonic intrusive rocks (Paterson and Reeves, 1985; Gunn and Dentith, 1997). High-resolution aeromagnetic data can be used to delineate basement structures and to possibly deduce tectonic events in offshore and onshore basins (Gunn, 1997; Blakely et al., 2002; Al Kadasi 2014). The high-resolution aeromagnetic data is significant in the current study because it aids the identification, interpretation and extrapolation of geological bodies and linear structures (e.g., fractures).

2.4.4. Aeromagnetic Survey Method in the study area

The airborne magnetic data was acquired during the seasonally drier months (from May to August 2018) using a Cessna 210 aircraft. The flight lines were oriented in an east-west direction from the coastline to the western portions of the survey area. The survey specifications were:

(i) a line direction of 270°–090°
(ii) control line direction of 090° (to the line direction)
(iii) line spacing of 200 m
(iv) control line/tie-line spacing of 2000 m directed north to south
(v) a ground clearance of 80 m.

Compensation flights, which were undertaken before data acquisition to correct for the magnetic effects associated with the aircraft, involved pitch, roll and yaw at high-altitude over an area of low magnetic field gradient (Aerophysx, 2018). A figure-of-merit (FOM) was derived at the start and at the end of the survey as well as after any alteration to the aircraft and on-board instrumentation (Aerophysx, 2018). A FOM of less than 1 nT was regarded acceptable in this survey (Aerophysx, 2018).

Monitoring of the aircraft altitude was achieved by using a three axis flux-gate magnetometer (an Applied Physics Systems, Model 539) (Aerophysx, 2018). The aircraft carrying the magnetometer and spectrometer systems was flown at a constant altitude of 80 m (±15 m) to cover an area of approximately 35 720 line kilometres (Aerophysx, 2018). The ground clearance was monitored using the Freeflight Radar altimeter with a sensitivity of 10 cm and accuracy within a 5 cm region. Navigation

and positioning of the aircraft was done through a Pico PGU Guidance System, which utilises an L1 and L2 global positioning system (GPS) (Aerophysx, 2018). The total magnetic intensity measurements were obtained using the Scintrex CS-3 Caesium Vapour, fixed in wing-tip pods, with a dynamic range of 15 000–105 000 nT and a sensitivity of 0.0006 nT /$Hz^{1/2}$. The measurements were recorded at a sampling rate of 10 Hz and the monitoring of temporal variations in the Earth's magnetic field was achieved using a Geometrics G859 Cesium vapour magnetometer (Aerophysx, 2018).

During the process of data acquisition, data were exported from the data acquisition systems for field processing and quality control where Geometrics MagComp™ software was utilised for raw magnetic data compensation (Aerophysx, 2018). The corrections that were applied to the magnetic data in the field included compensations and the utilisation of the base station data to remove diurnal variations (Aerophysx, 2018). Final processing of the raw data was undertaken at the AEROPHYSX's office using Intrepid and Geosoft. Intrepid was used for data correction and gridding, whereas Geosoft was used to apply the vertical, horizontal and the Reduced-to-Pole filters.

2.4.5. Data Processing and Enhancement

The Earth's magnetic field is variable over time and can be mathematically modelled through the International Geomagnetic Reference Field (IGRF) (Maus et al., 2005). The IGRF, which provides the magnetic intensity, declination and inclination of the magnetic field for a certain time and location, is removed from the Total Magnetic Intensity data to provide the Total Magnetic Anomaly or IGRF-corrected Total Magnetic Intensity data set (Billay et al., 2014; Craill et al., 2019). The detail in the acquired data can be enhanced by applying various filters. These filters, which highlight magnetic anomalies, have different functions and assist with the interpretation (Billay et al., 2014; Craill et al., 2019) and include:

(i) *Reduced-to-Pole:* This operator is applied to the magnetic data in order to minimise the effects of inclination and position the observed magnetic anomaly above the source body (Ansari and Alamdar, 2009; De Castro et al., 2014; Wemegah et al., 2015). This method is based on the assumption that the observed magnetic anomalies are due to induced magnetisation and that very minimal remanent magnetisation occurs in an opposite direction to that of the current Earth's magnetic field (Gunn et al., 1995). This transform has been applied to remove the effects of magnetic inclination and for improving accuracy in the location of magnetic sources relative to geologic features.

(ii) *Analytical Signal:* This filter combines both the vertical and horizontal derivatives and can be used to decipher edges and depths of causative bodies (Wijns, 2005; Cooper, 2014; Nxantsiya,

2017). The amplitude of the analytical signal may also be directly related to the amplitude of magnetisation (MacLeod et al., 1993). The assumption, regarding two-dimensional magnetic features, is that the related anomalies are independent of dip and direction of the magnetisation (MacLeod et al., 1993; Hinze et al., 2012). This filter has therefore been applied to the IGRF-corrected magnetic data to generate a map with magnetic signatures that are independent of remanent magnetisation.

(iii) *First Vertical Derivative:* This filter helps enhance magnetic anomalies arising from near surface (high frequency) magnetic bodies (Hinze et al., 2012; Wemegah et al., 2015). It enhances the edges of magnetic anomalies and shallow features providing a better separation of closely spaced sources (Crail et al., 2019). Therefore, the First Vertical Derivative map tends to give a sharper image than that of the Total Magnetic Anomaly map (Wemegah et al., 2015; Crail et al., 2019).

The linear magnetic anomalies were characterised as wide (low frequency, regional anomalies) and narrow (high frequency, local anomalies) in similar to that defined by Wemegah et al. (2015) and Oladunjoye et al. (2016). These linear anomalies were displayed in ArcGIS and mapped on screen using the human eye without applying any length rule.

The total geomagnetic anomalies from the Earth Magnetic Anomaly Grid map were used to understand the magnetic anomaly features of the offshore region (Maus et al., 2009). The resolution of the total intensity geomagnetic anomaly map is 2-arc-minutes (Maus et al., 2009).

3. Results

The results section comprises four data sets from four different methods, namely field observations, geochemistry, drill core logging and aeromagnetic survey data. First to be described are the results from field mapping, which showed five different geological packages in the area, namely (a) the basalts and rhyolites of the Lebombo Group, (b) the intrusive rhyolites of the Ntabankosi Suite, (c) the basaltic and rhyolitic volcanics of the Bumbeni Complex, (d) the sedimentary rocks of the Msunduze Formation, and (e) the overlying sedimentary packages of the Zululand Group. The characteristics and extent of the geological units are described below and, where the geological units were deformed, structural data are described.

3.1. Field Observations (Lithostratigraphy and Structural)

3.1.1. Lithostratigraphy

Field observations from the lithostratigraphic units of the Sabie River and Jozini Formations (Lebombo Group), Bumbeni Complex, Ntabankosi Suite, Msunduzi Formation and Mzinene Formation (Zululand Group) comprising the study area are described in detail below.

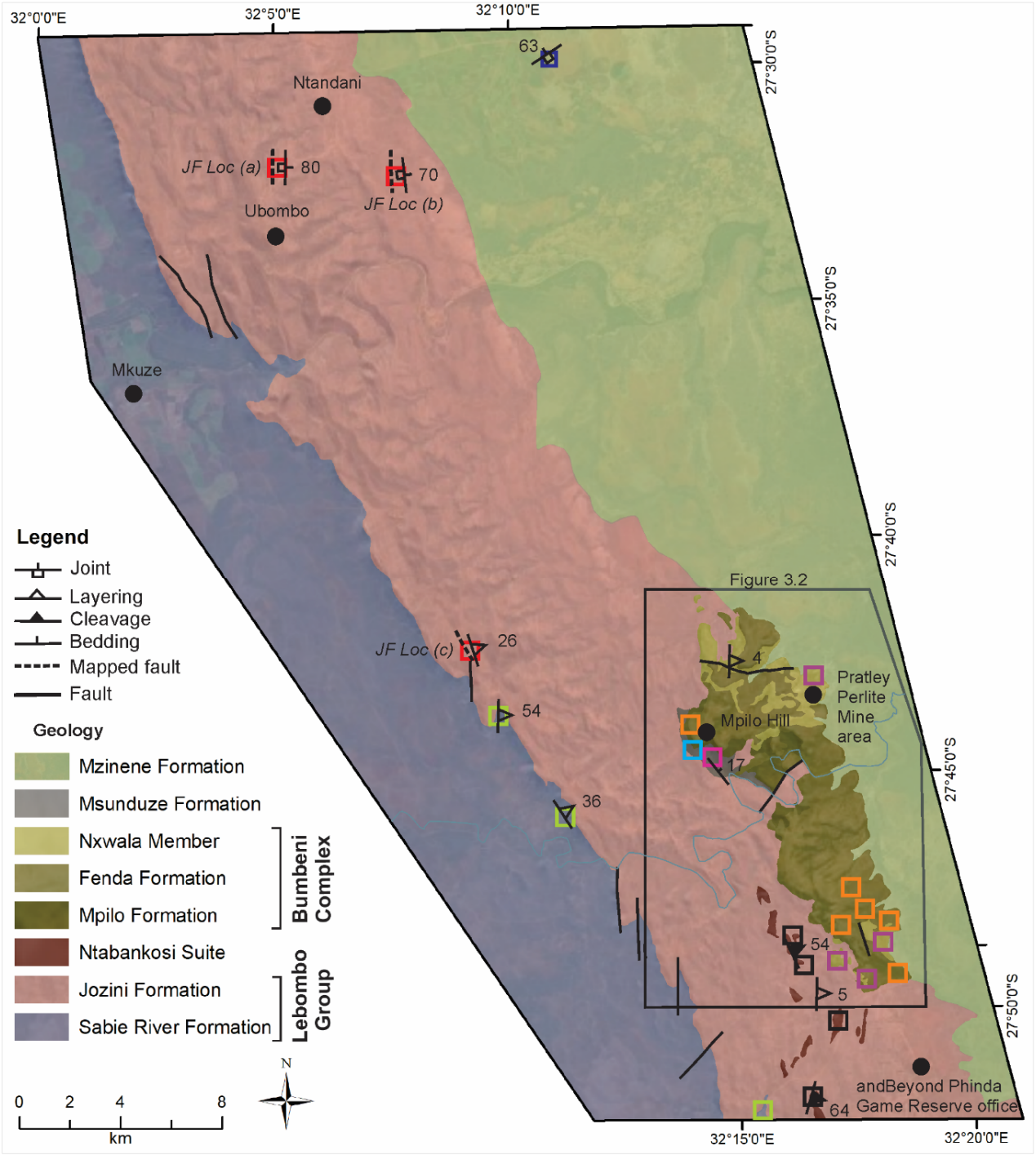

Figure 3.1: The field relationship of the different lithologies in the study area and the field area outline in which the geological and structural observations and data were collected during field work (map modified after the 1: 1 000 000-scale geological map of South Africa, Council for Geoscience, 2019). Localities (Loc) are highlighted in coloured squares; the Sabie River Formation (chartreuse), the Jozini Formation (red squares and with JF Loc a–c for localities associated with major faults) and the Ntabankosi Suite (black). The lithological units of the Bumbeni Complex are highlighted; Mpilo Formation (cyan square), Fenda Formation (orange squares) and Nxwala Member (purple squares). The localities in the Msunduze and Mzinene Formations are shown with magenta and dark blue squares, respectively. The collected field data include: joint, layering, cleavage, bedding and the mapped fault data. The faults from the 1: 1 000 000-scale geological map of South Africa (Council for Geoscience, 2019) are shown with solid black lines. The black polygon indicates the position of Figure 3.2.

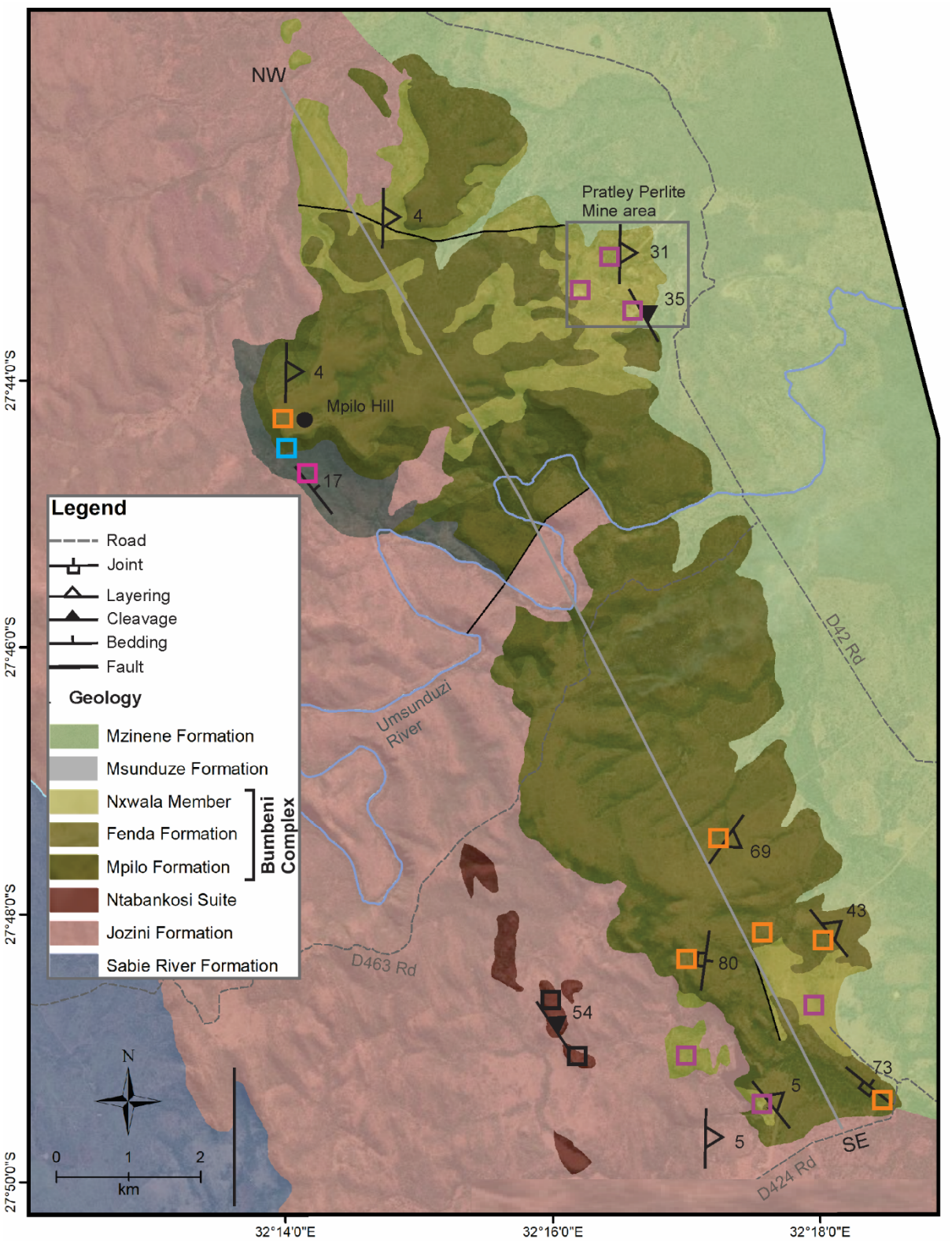

Figure 3.2: An enlarged view of the geological map of the Bumbeni Complex indicating areas in which the geological and structural observations and data were collected during field work. Localities in various lithological units are highlighted in coloured squares (see Figure 3.1 for colour codes). The Pratley Perlite Mine area, in which geological and structural observations and data were collected from the Nxwala Member, is highlighted. The grey NW-SE oriented line was used to derive the cross-section shown in Figure 3.5.

3.1.1.1. Lebombo Group

(i) Sabie River Formation

The Sabie River Formation, which forms the lowermost unit in the field area, consists of dark-coloured, fine-grained basalt flows that are usually amygdaloidal, separated by relatively sharp contacts and can be up to 1 m-thick (Fig. 3.3). The amygdales are pipe-shaped (up to 4-cm-long) (Fig. 3.3a) and rounded (up to 2 cm in diameter) (Fig. 3.3b). The pipe-shaped amygdales are predominantly at the base of individual lava flows. The basalts of the Sabie River Formation crop out in the southwest portion of the study area and usually dip between 34°–54° towards the northeast and east.

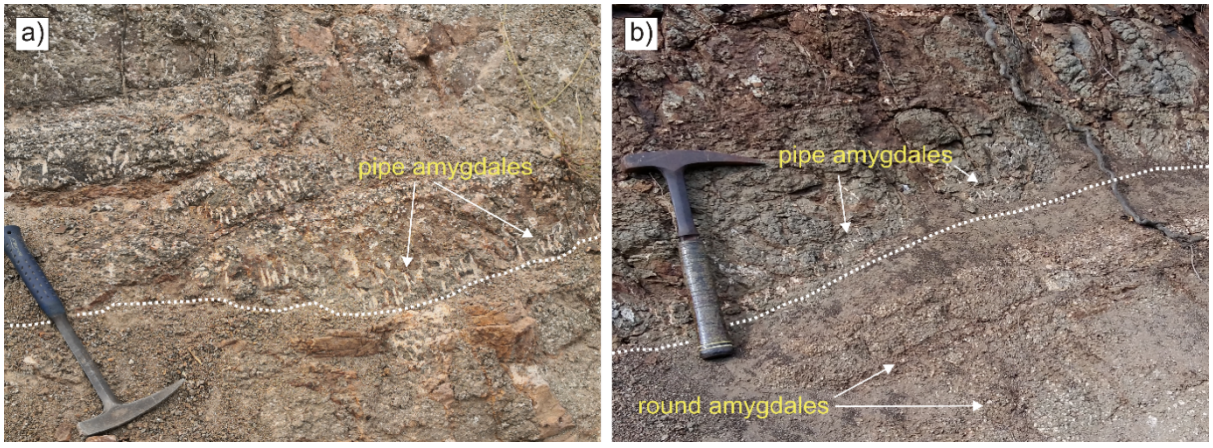

Figure 3.3: Photographs of the Sabie River Formation basalt taken in different localities showing (a) pipe amygdales at the base of an individual flow and (b) round amygdales along the upper contact of the lower lava flow and pipe amygdales in the upper basaltic unit.

(ii) Jozini Formation

The Jozini Formation comprises greyish red to multiple red-coloured, fine-grained locally banded rhyolite flows (Fig. 3.4). The thicknesses of individual flows vary from 5- to 10-m-thick and are characterised by a massive central zone overlain by a pumice-rich, auto-brecciated crust (Fig. 3.3b). The Jozini Formation occurs stratigraphically above the Sabie River Formation basalts and crops out in prominent north-south orientated ridges, which form the Lebombo mountains.

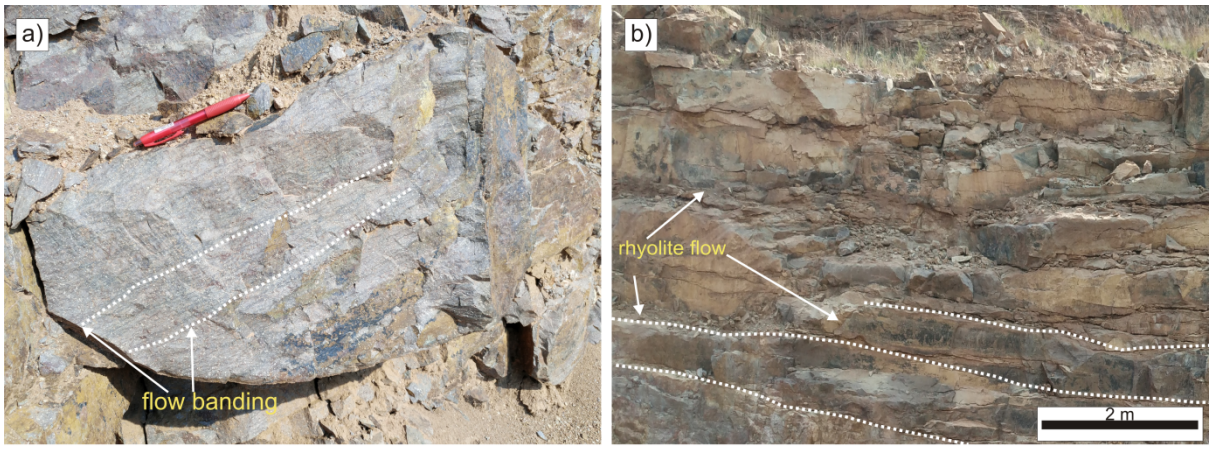

Figure 3.4: (a) Flow banding developed in the porphyritic rhyolite. (b) Lava flows typical of the Jozini Formation rhyolite. The flow banding and individual rhyolite flows are shown with dashed white lines.

3.1.1.2. Ntabankosi Rhyolite Suite

The Ntabankosi Rhyolite Suite comprises rhyolite domes and dykes that are typically pink to reddish brown, fine-grained and porphyritic and intrude the Jozini Formation (Fig. 3.5a). These rhyolites show localised folding, contorted flow banding (Figs. 3.5b and c) and a well-developed fracture cleavage (Fig. 3.5d). The thicknesses of individual flow bands vary from 1- to 30-cm-thick. The Ntabankosi Suite is exposed south of the Msunduzi River where the domes generally form prominent hillocks whilst dykes crop out as roughly north-south oriented, irregular ridges (Figs. 3.1 and 3.2).

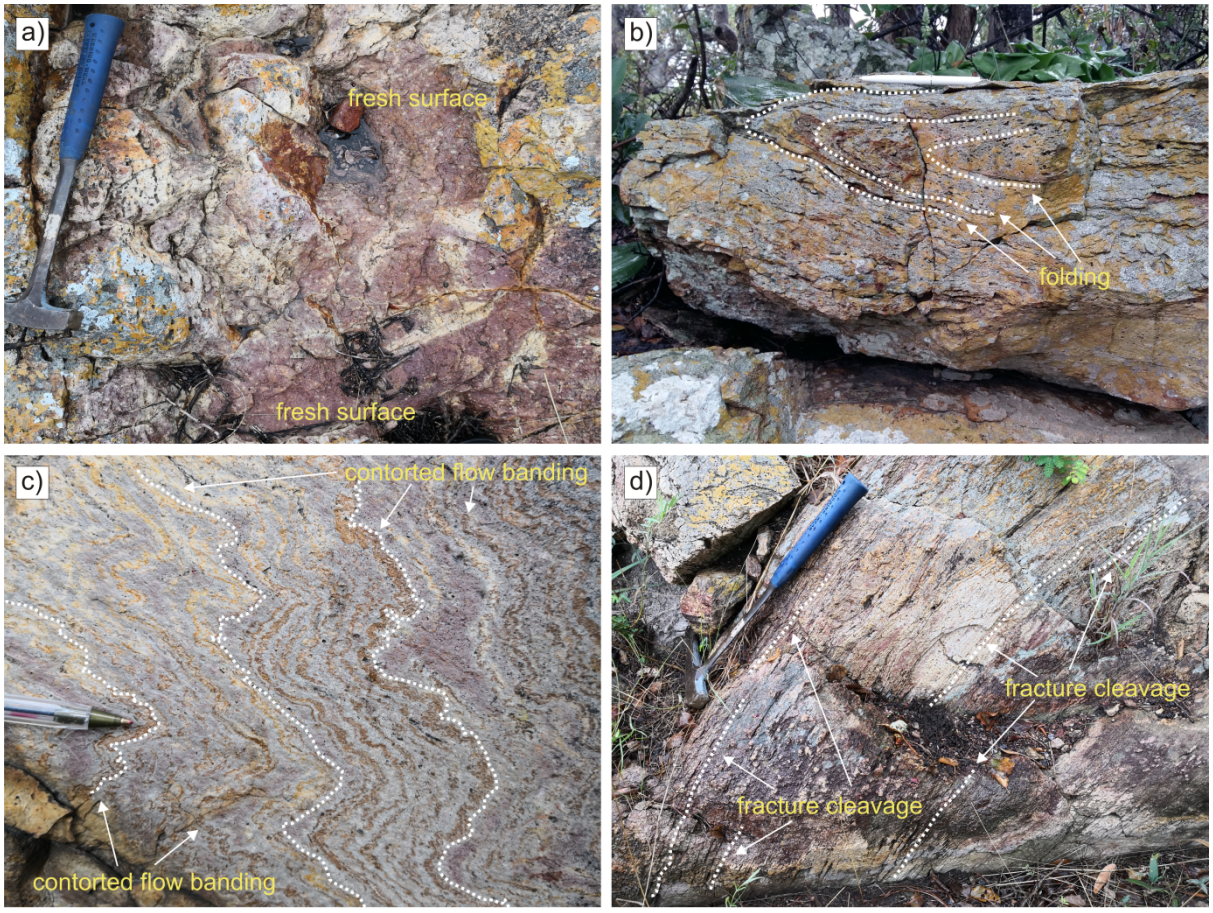

Figure 3.5: Photographs of the Ntabankosi Rhyolite Suite. (a) Fresh exposure of the fine-grained porphyritic rhyolite, (b) localised folding, (c) contorted flow banding and (d) a distinct fracture cleavage.

3.1.1.3. Bumbeni Complex

The Bumbeni Complex forms the western limit of the Bumbeni Ridge and crops out towards the southern end of the Lebombo mountains where it is incised by the Msunduzi River. The complex extends ~8 km north and ~ 9 km south of this river, in the Mkuze and &Beyond Phinda Game Reserves.

(i) Mpilo Formation

The Mpilo Formation comprises fine-grained, light brownish grey amygdaloidal and vesicular basalt (Fig. 3.6a). The amygdales contain quartz and calcite and are sub-rounded to elongate in shape and up to 4 cm in diameter (Fig. 3.6b). The Mpilo Formation unconformably overlies the Jozini Formation and it is best exposed at Mpilo Hill and in irregular outcrops north and south of the Msunduzi River.

Figure 3.6: Photographs of basalts of the Mpilo Formation with hammer for scale. (a) Excavation exposure of the amygdaloidal and vesicular nature of the basalts, with (b) the amygdales and vesicles shown in detail.

(ii) Fenda Formation

The Fenda Formation is the most extensive formation of the Bumbeni Complex cropping out in two regions, namely the northern and southern regions; the northern region occurs north of the Msunduzi River and the southern region extends from the south of the Msunduzi River to the southern end of the complex (Fig. 3.2). It unconformably overlies the Mpilo Formation basalt or the Jozini Formation where the former is not developed.

The Fenda Formation in the north forms the high ground of the Mpilo Hill and comprises light grey-coloured rhyolite and locally banded pyroclastic deposits (Fig. 3.7a and b). Irregular outcrops of these pyroclastic rocks occur below the rhyolite and consist of lapillistone and tuff (Fig. 3.7c). The lapillistone and tuff comprise angular to sub-rounded and elongated lapilli-sized pumice, crystal fragments and ash embedded in a fine-grained siliceous matrix (Fig. 3.7d).

In the southern region, the rhyolite flows are grey to greyish pink-coloured, banded and non-banded (Fig. 3.8a) and intercalated with pyroclastic deposits comprising crystal tuffs and pumice layers (Fig. 3.8b). The individual lithological units of the Fenda Formation are up to 10-m-thick and are commonly capped by auto-brecciated pumice-rich flow-tops. In places the rhyolite flows have been eroded with only remnants of flow toes and irregular chilled contacts preserved (Fig. 3.8c and d).

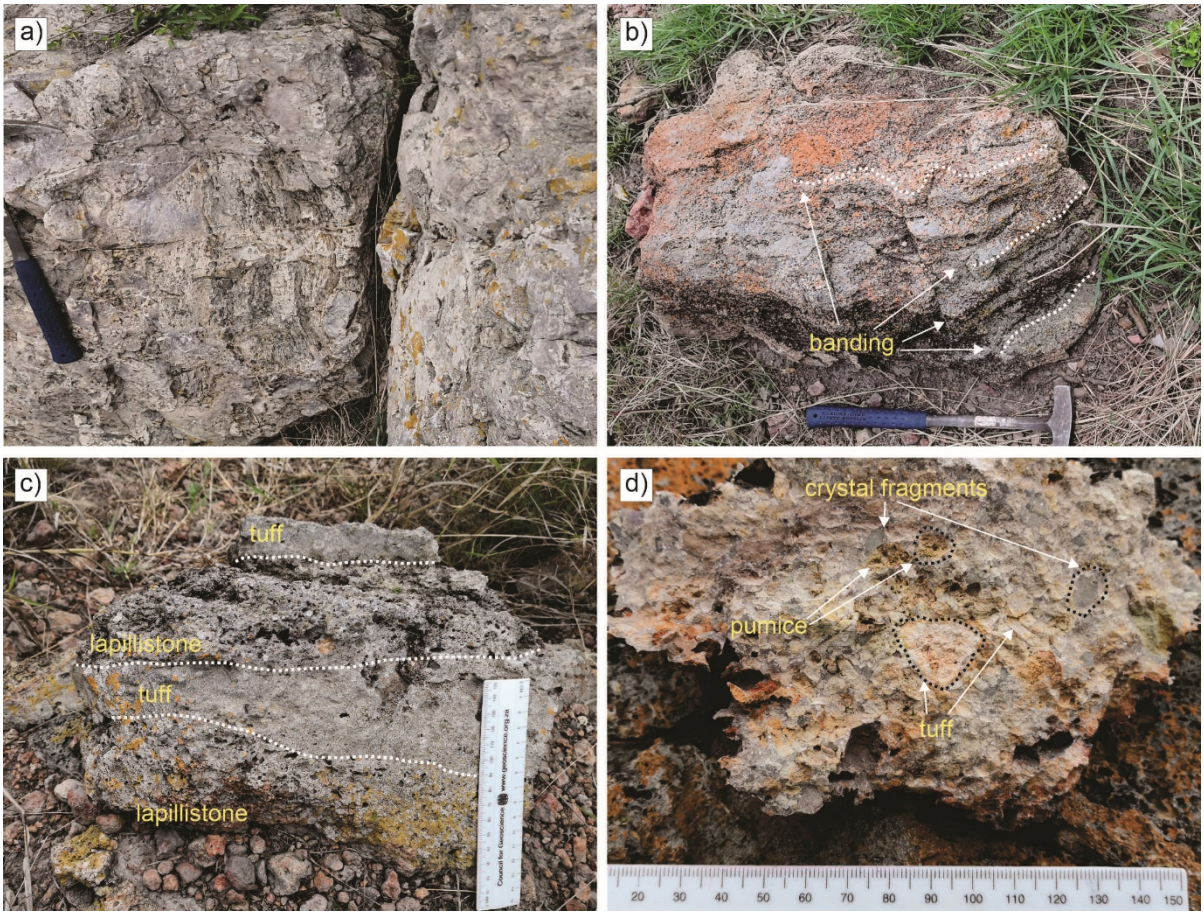

Figure 3.7: Photographs taken at Mpilo Hill, north of the Msunduzi River. (a) The grey-coloured rhyolite unit and (b) the banded pyroclastic deposits of the Fenda Formation (hammer for scale). (c) Intercalated lapillistone and tuff units. (d) A close-up view of the clast supported lapillistone where the different pyroclasts are shown with dashed black lines (scale in mm).

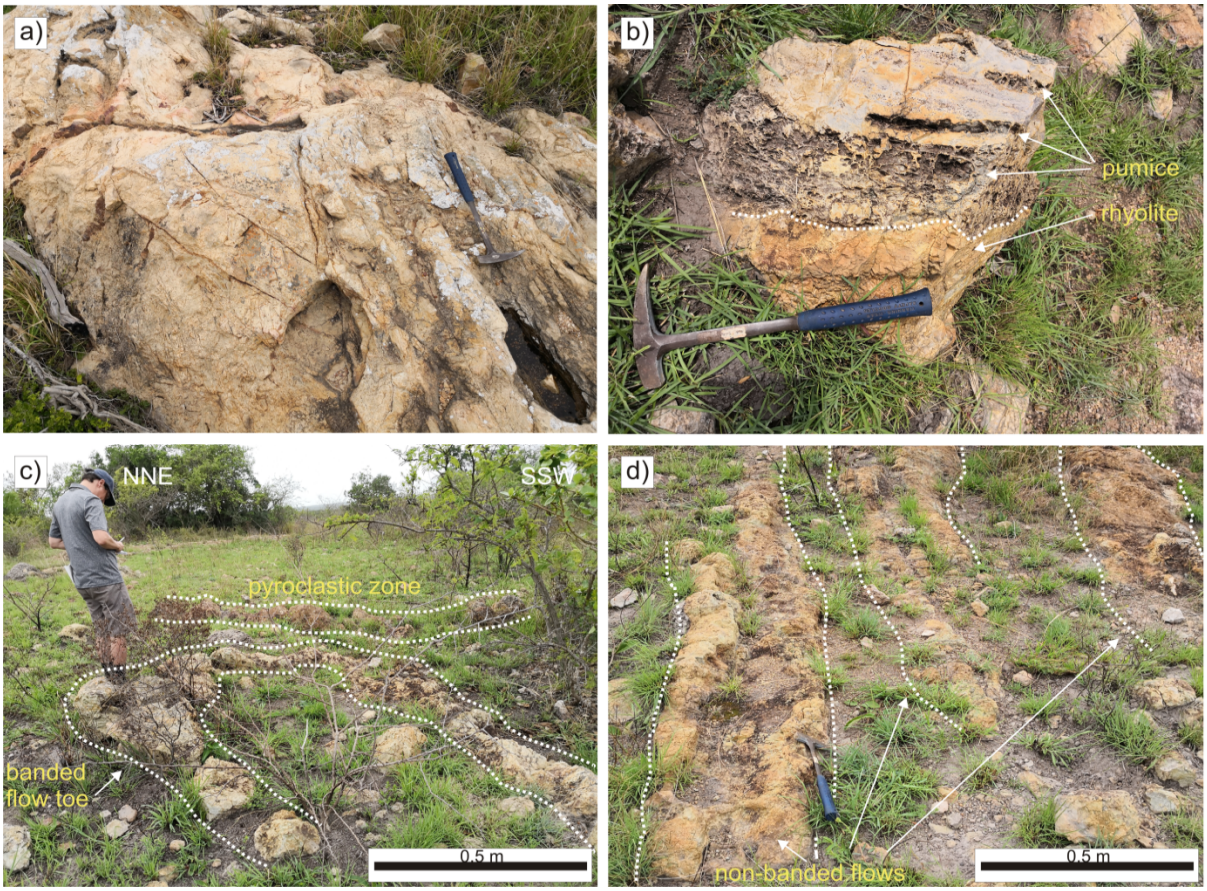

Figure 3.8: Example of rocks of the Fenda Formation in southern localities with hammer for scale. (a) The greyish pink-coloured rhyolite and the characteristic pumice layers (b) Continuous and non-continuous bands of pumice intercalated with rhyolite horizons. (c) An example of an east verging flow toe associated with a ~30-cm-wide pyroclastic zone. (d) Preserved irregular chilled contacts between rhyolite flows.

(iii) Nxwala Member

The Nxwala Member of the Fenda Formation crops out in two regions; namely the northern and southern exposures. The northern exposure is the type area for the Nxwala Member and occurs on the eastern flanks of the Mpilo Hill at the Pratley Perlite Mine in Mkuze Game Reserve (Figs. 3.1 and 3.2). The southern exposures occur in limited outcrops south of the Msunduzi River (Figs. 3.1 and 3.2).

The Nxwala Member comprises a complexly interlayered succession of proximal-to-source pyroclastic deposits, such as pyroclastic breccia, lapillistone and perlitic pitchstone and perlitised tuff, which are exposed in three Pratley Perlite Mine (PPM) localities (Locality 1-3) (Fig. 3.9). Each pit exposure shows a marked variation within the stratigraphy of the Nxwala Member with limited lateral continuity of individual rock units (Fig. 3.9).

In PPM-Locality 1, a complex intercalation of rhyolitic tuff, pyroclastic breccia, perlite and rhyolite occurs (Fig. 3.10). These rocks are generally flat-lying and in places, form horizontal contacts with individual perlite units (Fig. 3.10a). The pyroclastic breccia is a sequence flow that truncates the perlite in a topographic low and comprises rhyolite, tuff and perlite occurring as lapilli, bombs and blocks set in ash-tuff matrix (Figs. 3.10b–d). Individual bombs and blocks vary in size from 6 to 50 cm in diameter. The perlite horizon sporadically shows autobrecciated flow tops comprising angular to rounded fragments of perlite in a light grey matrix (Fig. 3.11).

The second locality, PPM-Locality 2, represents a topographically higher unit (its lithostratigraphical position being interminable with the other localities), and is a ~10-m-thick ash-fall tuff deposit (Fig. 3.12). The tuff is whitish-cream with randomly distributed glass fragments (from 0.1 to 0.5 cm in diameter) and it is overlain by subordinate perlite (Fig. 3.12). The contact between the perlite and tuff is marked by a ~30 cm-thick alteration zone (Fig. 3.12).

At PPM-Locality 3 a black-coloured, porphyritic perlitised obsidian/perlitic pitchstone is exposed (Fig. 3.13a). It is characterised by randomly distributed, sub-rounded and sub-angular (~0.6 m in diameter) lithophysae (high crystallisation domains) (Fig. 3.13a) and well-defined compositional banding with 0.2 to 2 cm-thick bands (Fig. 3.13b).

The southern exposure of the Nxwala Member comprises pyroclastic deposits similar to those in the northern exposure, however, no pyroclastic breccia, perlitised tuff and pitchstone are observed in outcrop. Here, the Nxwala Member is predominated by greyish pink and to cream-coloured poorly-sorted and pyroclast-supported lapillistone and tuff (Fig. 3.14). Some of the tuff horizons are well-bedded, with bedding draped over volcanic bombs, whereas other tuff units contain lithophysae that range in size from ~4 to 20 cm in diameter (Figs. 3.14b and c).

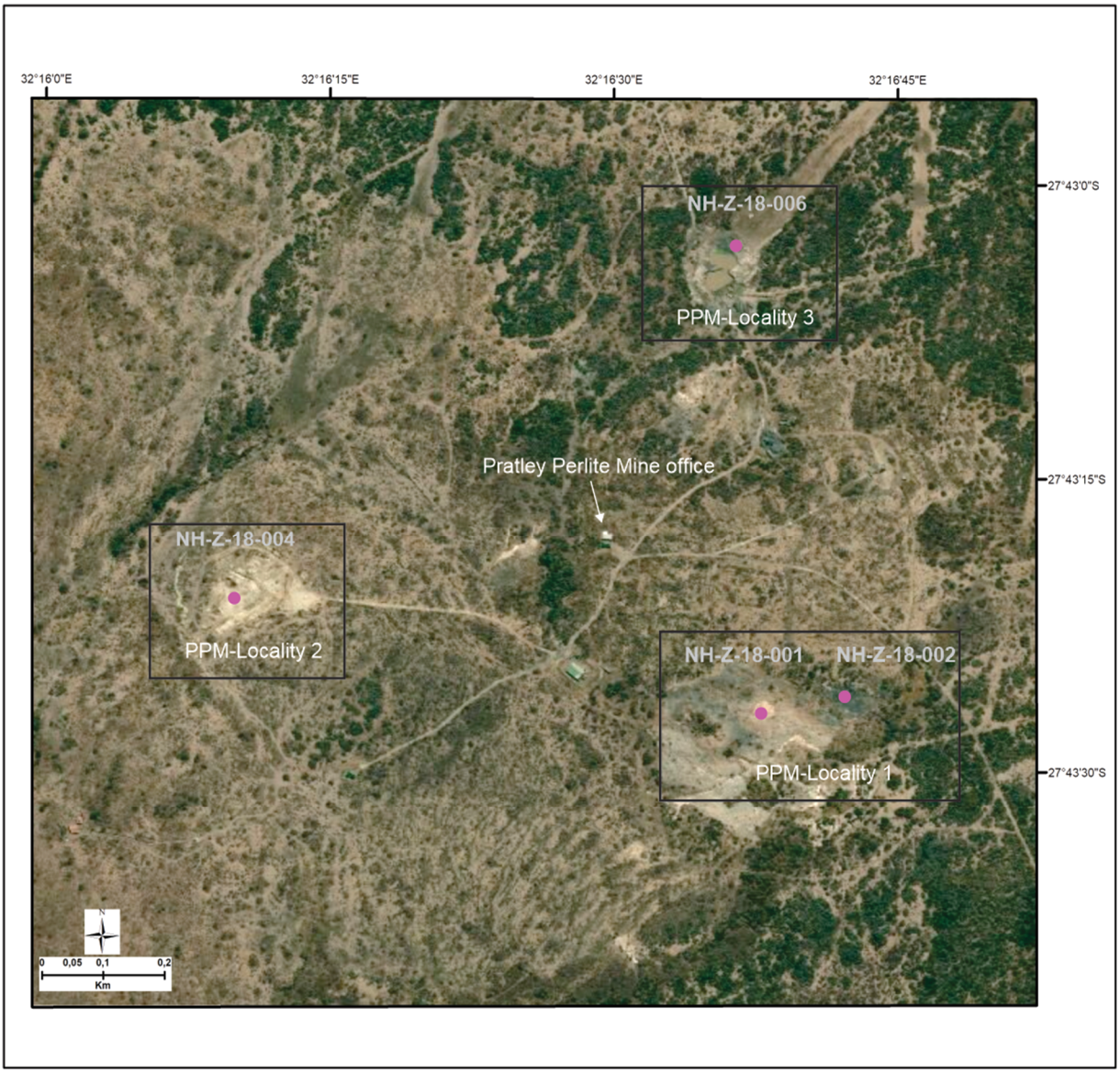

Figure 3.9: Map of different pit exposures within the type area of the Nxwala Member in the Pratley Perlite Mine. The different localities in the Pratley Perlite Mine (PPM) are named PPM-Locality 1 to 3. Sample locations in each PPM-Locality are shown with a purple circle and are labelled; NH-Z-18-001 (tuff), NH-Z-18-002 (perlite), NH-Z-18-004 (tuff), NH-Z-18-006 (perlitic pitchstone). More detailed descriptions on sampled rock types are available in Appendix 1–3.

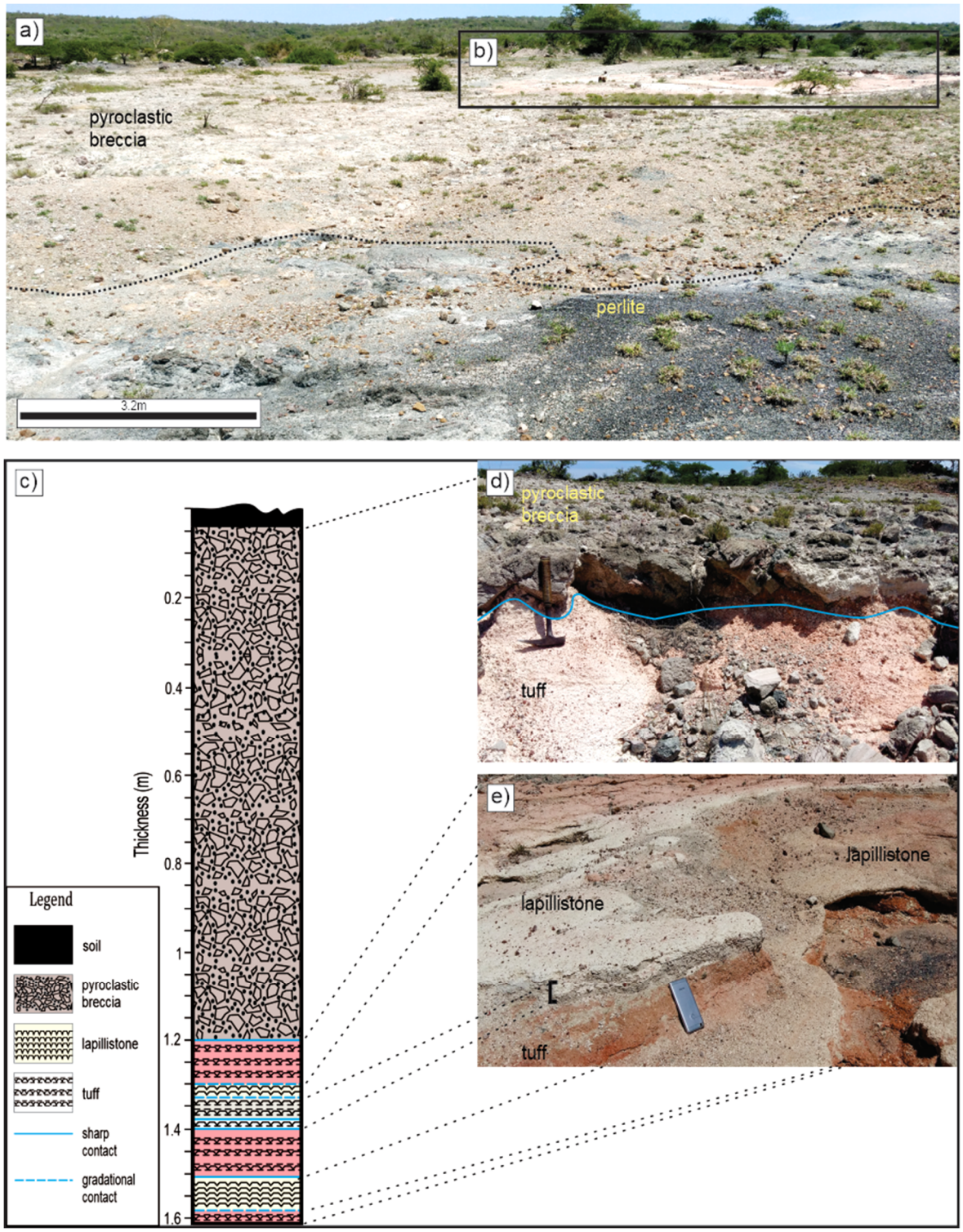

Figure 3.10: (a) Pyroclastic breccia and perlite exposed in PPM-Locality 1. The irregular boundary between perlite and the pyroclastic breccia is shown with a dashed black line. (b) Coarsening-upward succession of tuff and lapillistone. (c) Lithostratigraphic column illustrating the various rock types, contact relationships and thicknesses of the tuff and lapillistone succession in (b) (Refer to Appendix 4 for more detailed description on each unit and thicknesses). (d) A sharp contact between the pyroclastic breccia and the underlying tuff deposit. (e) The grey and multiple red-coloured tuff and whitish-cream lapillistone units (the pattern on the legend represents tuff and colours highlight the different tuff units).

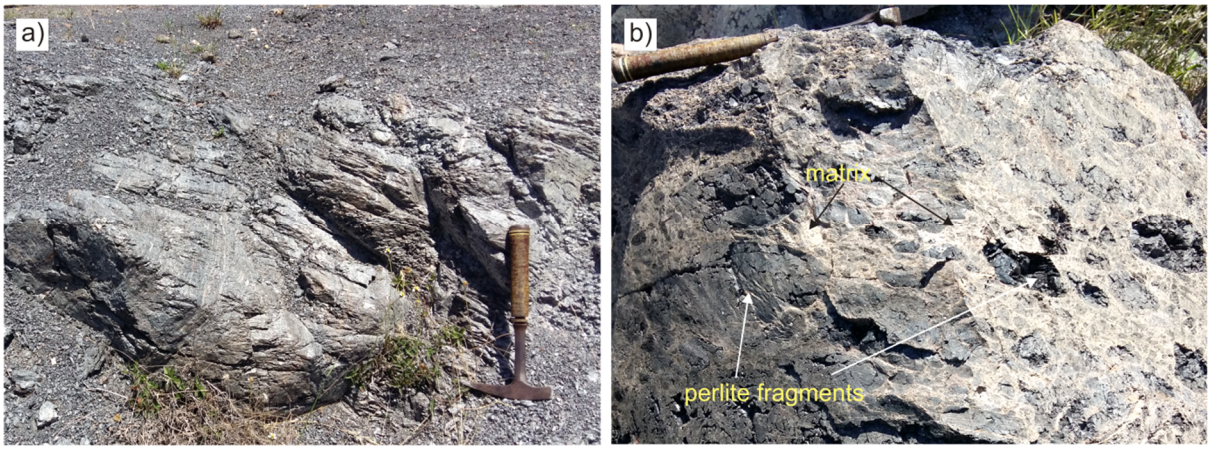

Figure 3.11: (a) The distinctive perlite exposed at PPM-Locality 1. (b) An autobrecciated flow top with perlite fragments set in a light grey matrix.

Figure 3.12: The tuff and perlite unit developed in PPM-Locality 2. (a) The perlite unit is generally dark grey to black and occurs as a lens-shaped unit above the tuff. The sharp contact between the underlying tuff and the perlite is marked by an irregular white-coloured alteration zone (up to 30-cm-thick) shown with a dashed black line. (b) Lithostratigraphic column for the tuff and perlite. The thickness variation and contact between the tuff and perlite is shown (Refer to Appendix 5 for detailed thicknesses).

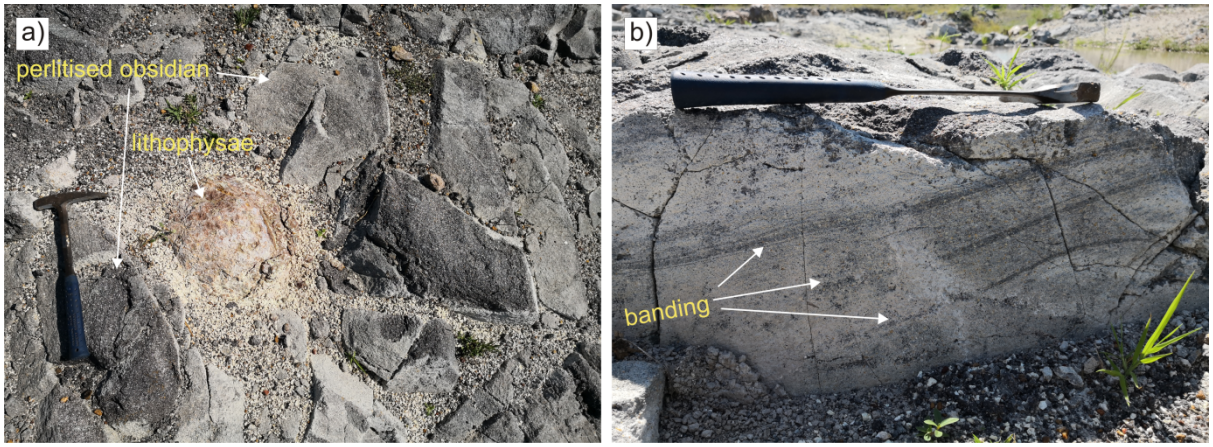

Figure 3.13: (a) Perlitic pitchstone with an in situ lithophysae. (b) Small-scale (0.2-2 cm-thick) banding typical of the perlitic pitchstone.

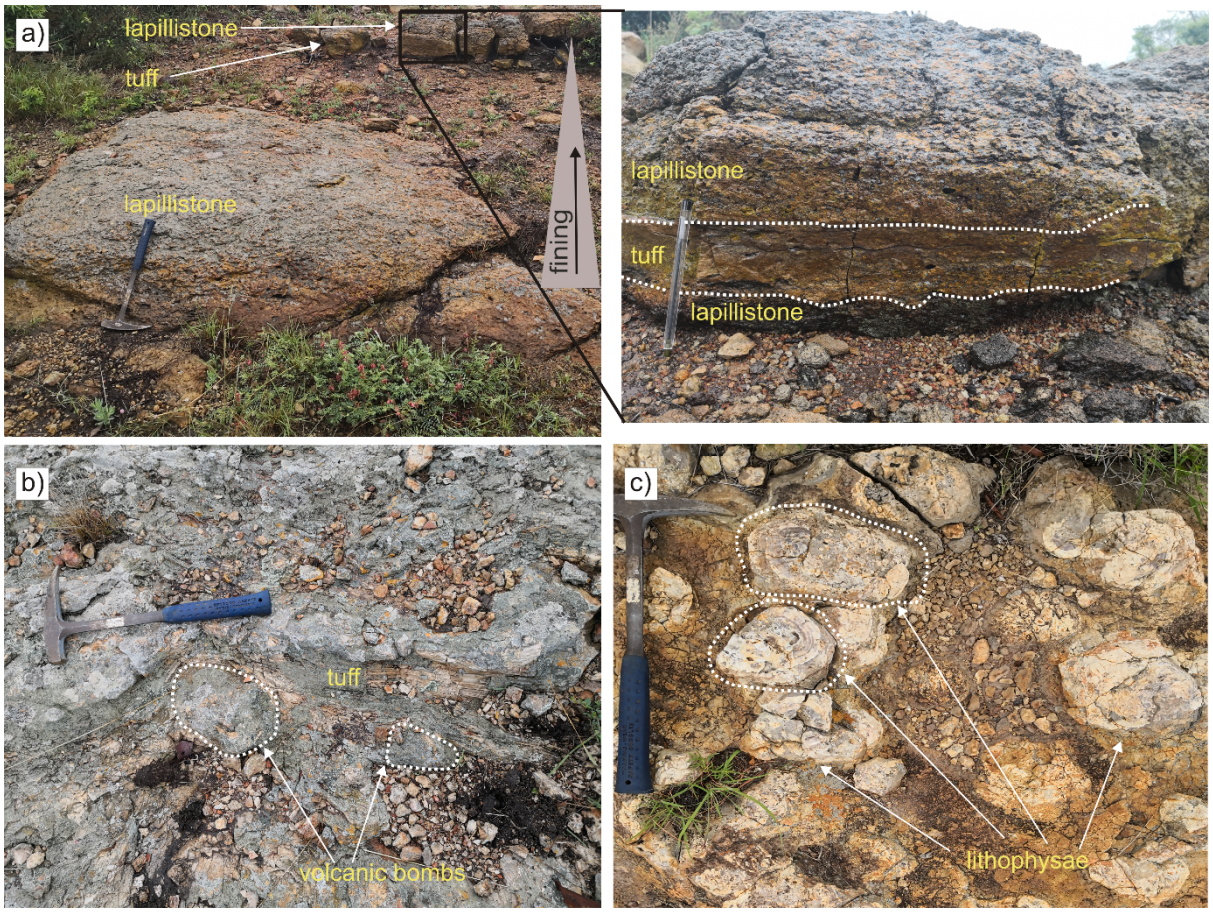

Figure 3.14: (a) The lapillistone (~70-cm-thick) unit interbedded with tuff. The insert shows a close-up view of the lapillistone and a 6-cm-thick ash unit. (b) Tuff with bomb-sized pyroclasts in laminated tuff. (c) The sub-rounded lithophysae in tuff characteristic of the Nxwala Member.

3.1.1.4. Msunduze Formation

The exposure of the Msunduze Formation is confined to a small area at the base of Mpilo Hill, north of the Msunduzi River and is characterised by a succession of interbedded conglomerate and sandstone units that dip at 17° towards the northeast (Fig. 3.15). The conglomerates are massive, matrix-supported and predominantly consist of well-rounded to sub-rounded, rhyolitic to basaltic pebbles and cobbles set in fine-to medium-grained, greenish and dark tuffaceous and siliceous matrix (Fig. 3.15). Towards the top of the succession, the conglomerates are commonly interlayered with fine-grained, greyish pink to moderate pink sandstone units, 10–50 cm-thick. Although the unit stratigraphically overlies the rhyolites of the Jozini Formation, no contacts are observable between the Msunduze Formation and the volcanics of the Bumbeni Complex making its stratigraphic position relative to the complex questionable.

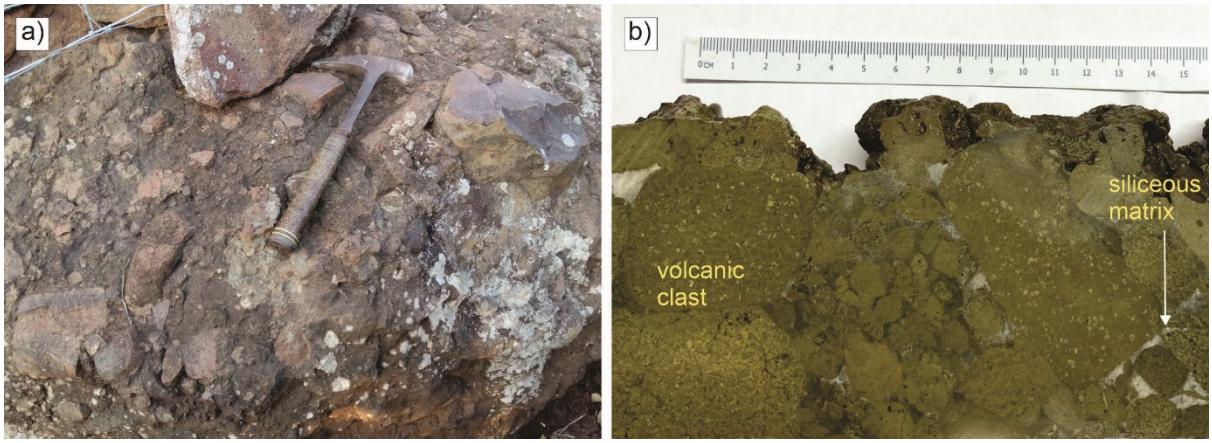

Figure 3.15: (a) Matrix-supported conglomerate with well-rounded to sub-rounded pebbles and cobbles set in fine-to medium-grained, reddish brown and greenish matrix. (b) A photograph of a polished hand specimen of the conglomerate showing a close-up view of the different clast shapes and sizes.

3.1.1.5. Zululand Group

(i) Mzinene Formation

The Mzinene Formation comprises deeply weathered, crudely-bedded fossiliferous siltstones interbedded with lenses of fine-grained sandstones (Fig. 3.16). The siltstone and sandstone units contain randomly distributed, sub-rounded angular carbonate concretions (Fig. 3.16). These rocks rest nonconformably on the Jozini Formation, the felsic volcanic rocks of the Bumbeni Complex and the Ntabankosi Suite. The sedimentary rocks of the Mzinene Formation crop out sporadically to the east of the Lebombo mountains on the western margins of the Maputaland Plain.

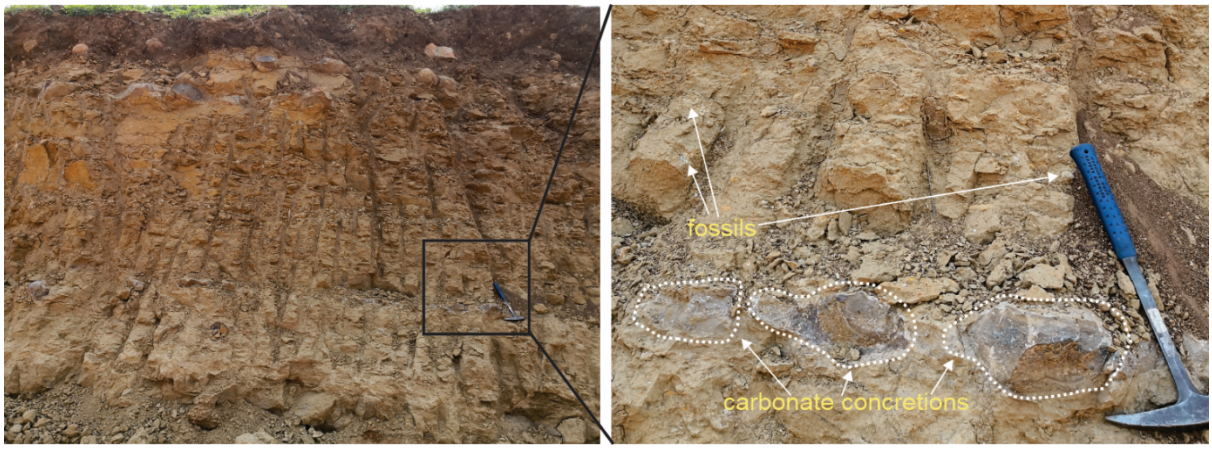

Figure 3.16: The siltstone of the Mzinene Formation with carbonates concretions. The insert shows a close-up view of the fossiliferous siltstone unit and the carbonate concretions.

3.1.2. Field Structural Data

For ease of interpretation, the fracture measurements from the Jozini Formation are separated into localities (e.g., the Jozini Formation localities-JF Loc) termed JF Loc a—c for areas that are associated with major fault zones (Fig. 3.17). The different images associated with each lithology shows the morphology of the fractures.

3.1.2.1. Lebombo Group

(i) Sabie River Formation

The Sabie River Formation basalts were affected by systematic and columnar jointing and faulting (Fig. 3.18). The systematic joint sets are steeply dipping to sub-vertical (57°–88°) planar joints, with three dominant orientations, namely NW-SE, N-S and E-W and a minor NE-SW orientation (Fig. 3.19a). The NNE-SSW oriented fault (with a lack of noticeable kinematic indicators) dips at 38° towards the west (Fig. 3.19b).

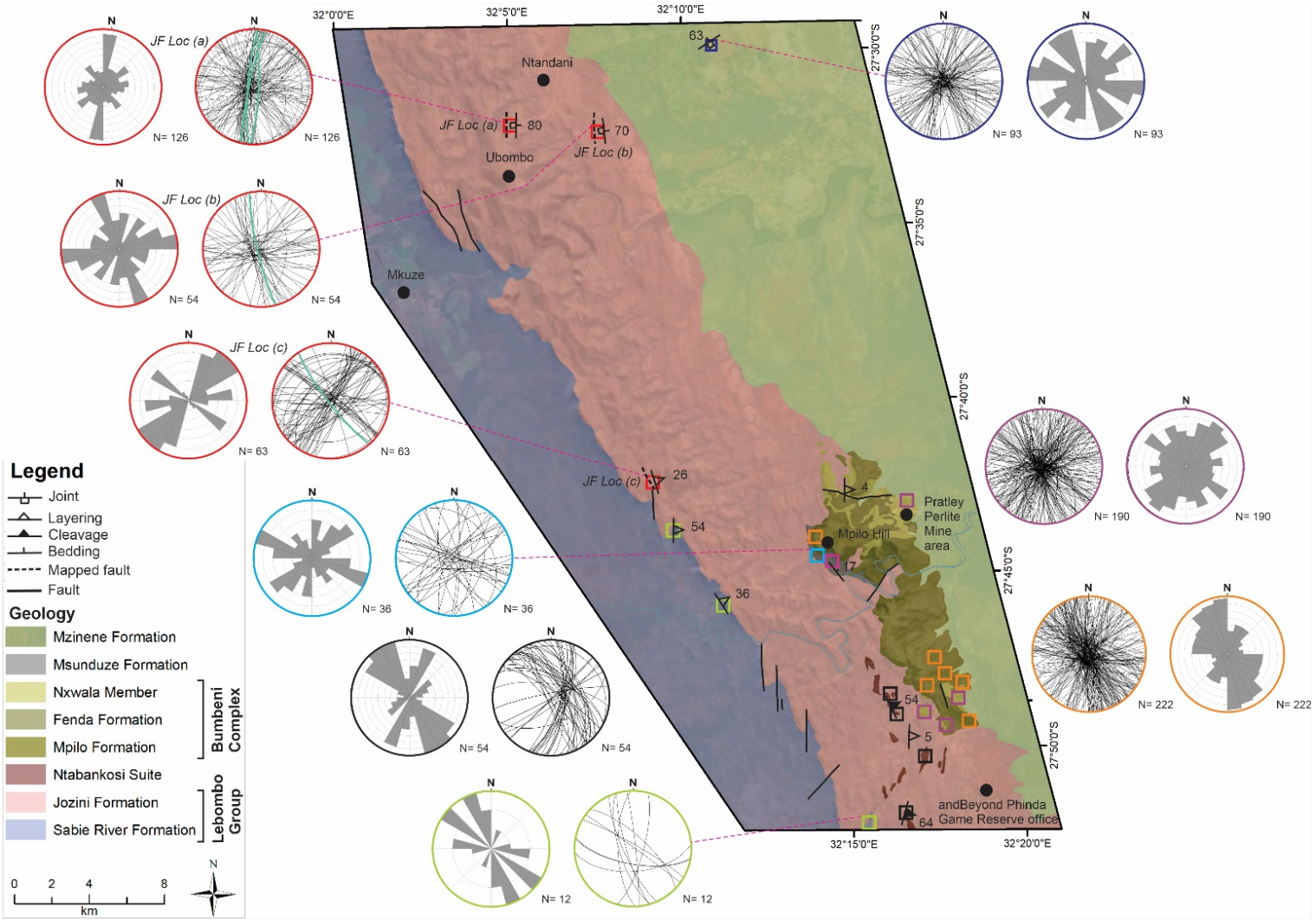

Figure 3.17: The areas where structural data were collected are highlighted with coloured squares; the Sabie River Formation (chartreuse), the Jozini Formation (red) and the major faults (green lines) orientations and associated joints are also shown-JF Loc a—c (the data is interpreted in the Structural section of this study) and the Ntabankosi Rhyolite Suite (black). The collected field data include: joint, layering, cleavage, bedding and the mapped fault data. The faults from the 1: 1 000 000-scale geological map of South Africa (Council for Geoscience, 2019) are shown with solid black lines. The lithological units of the Bumbeni Complex are also highlighted; the Mpilo Formation (cyan square), the Fenda Formation (orange squares) and the Nxwala Member (purple squares). The Mzinene Formation is shown with a dark blue square. Stereonet plots representing joint orientations associated with each lithological unit are shown. The rose diagrams are used for simple representation of joint orientation.

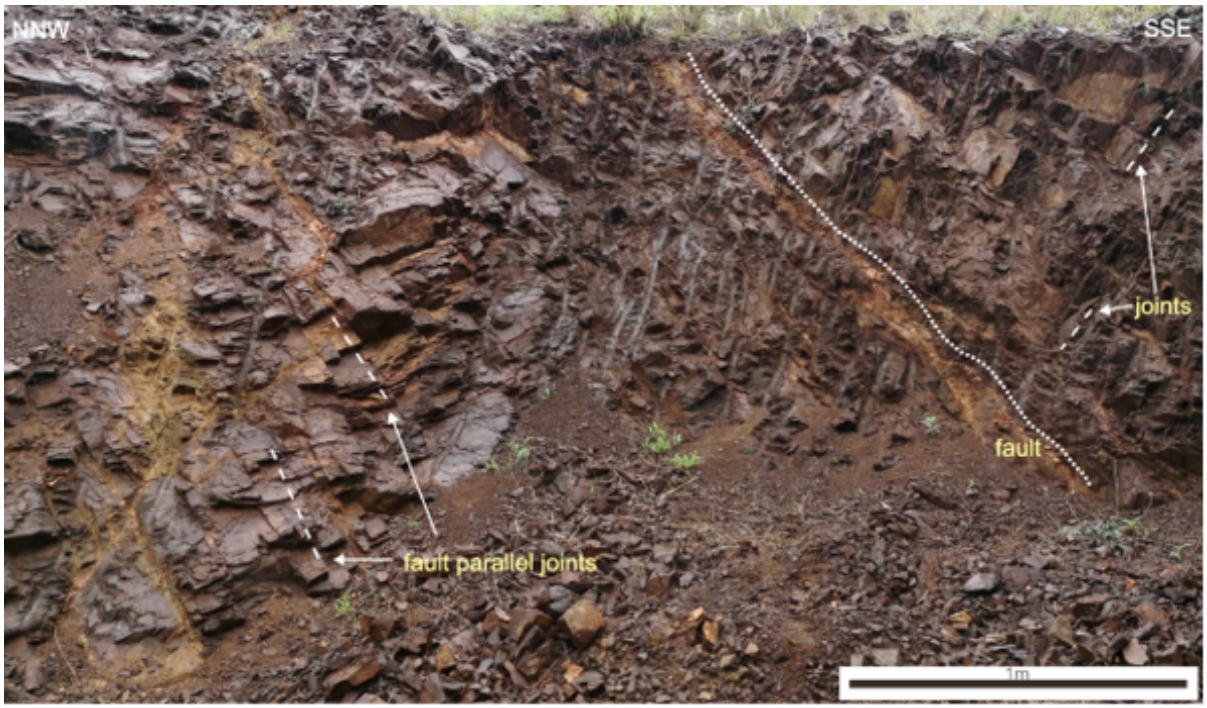

Figure 3.18: The joints in the Sabie River Formation and a NNE-SSW striking fault with a 38° dip towards the west (dip azimuth of 290°).

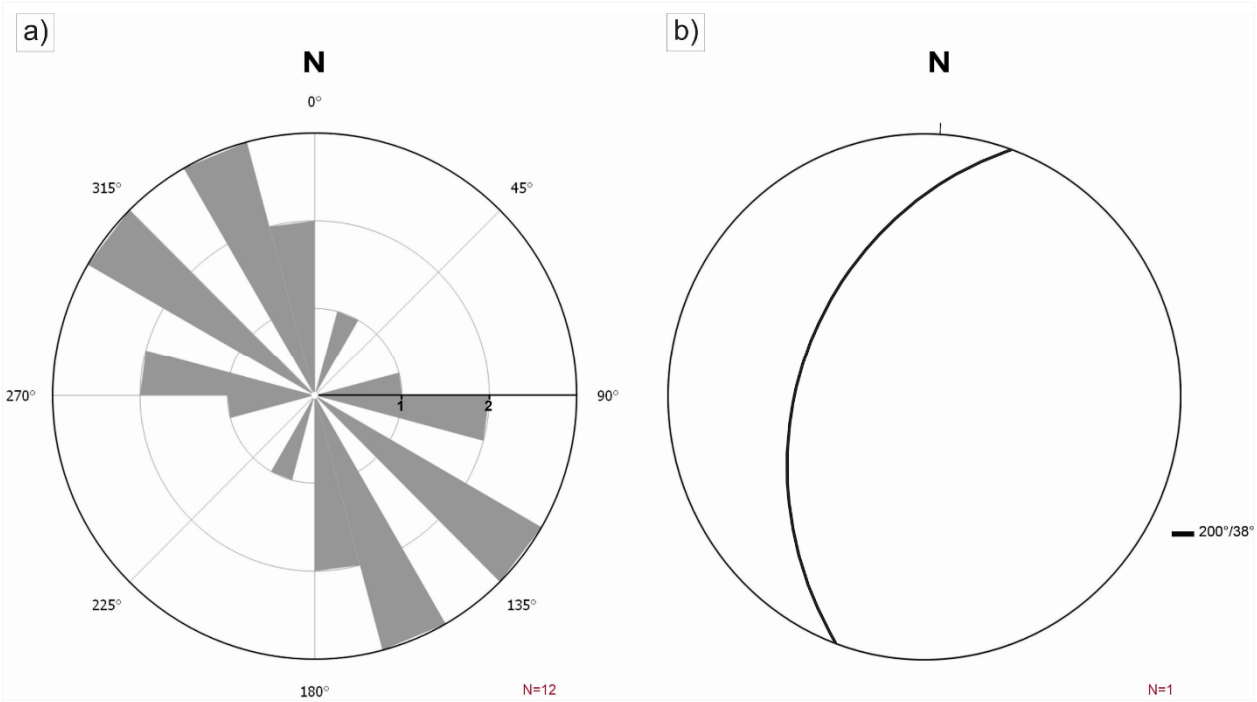

Figure 3.19: (a) The rose diagram, with 15° bin sizes, illustrates the different orientations of the joints in the Sabie River Formation basalt, showing the dominant and minor trends in the joint orientation data. (b) Lower hemisphere, equal angle stereonet of the fault (strike and dip; 200°/38°).

(ii) *Jozini Formation*

The Jozini Formation rhyolites have been affected by brittle faulting with ~2-m-wide, N-S oriented faults (Fig. 3.20). The dextral strike-slip fault surfaces have sub-vertical dips (80°–82°) towards the west (azimuths 275°–282°) and east (dip and dip azimuth 094°/74°) (Fig. 3.21a). The slickenside lineations on these surfaces plunge between 10°–26° with trends between 008°–039° (Fig. 3.21a). The fault core zones generally comprise ~10 cm to ~1-m-wide, clast-supported breccias with rhyolitic clasts ranging from sand to pebble in size (Figs. 3.20a and 3.21b). The associated damage zones are characterised by sub-vertical to vertical joint planes.

The massive zones of the rhyolite flows are commonly characterised by subparallel, planar and systematic joint sets (Fig. 3.22). The JF Loc (a) area reveals N-S oriented faults and a distinct N-S joint set orientation characterised by steeply inclined to vertical planes (50°–87°) that dip towards the east and west (Fig. 3.23). A second distinct E-W orientation is characterised by steeply inclined to vertical planes (64°–86°) (Fig. 3.23a). The two minor joint plane orientations present in this locality, include the NNE-SSW and NE-SW oriented joint planes with dip angle measurements that range between 30°–90° and the NW-SE striking joints which are mainly characterised by steeply inclined to vertical planes (61°–88°) (Fig. 3.23a).

The JF Loc (b) locality reveals a ~100 m-long N-S oriented fault and dominant NNE-SSW, NE-SW and NW-SE joint set orientations and a minor E-W orientation (Fig. 3.24). The NNE-SSW and NE-SW joints are mainly moderately inclined to vertical (43°–90°), although a few shallow dipping joints are present (dips of 03°–30°). The E-W striking joints are characterised by a combination of shallowly to steeply (12°–86°) dipping planes. In the JF Loc (c) locality, the southwest dipping normal fault is NW-SE striking and the joint surface measurements reveal distinct NW-SE and E-W orientations and minor NNE-SSW to NE-SW and N-S orientations (Fig. 3.25). The NW-SE and E-W striking joint planes are generally steep to vertical (63°–90°). The NNE-SSW and NE-SW (70°–87°) and also the N-S (43°–87°) joint planes are steep to sub-vertical.

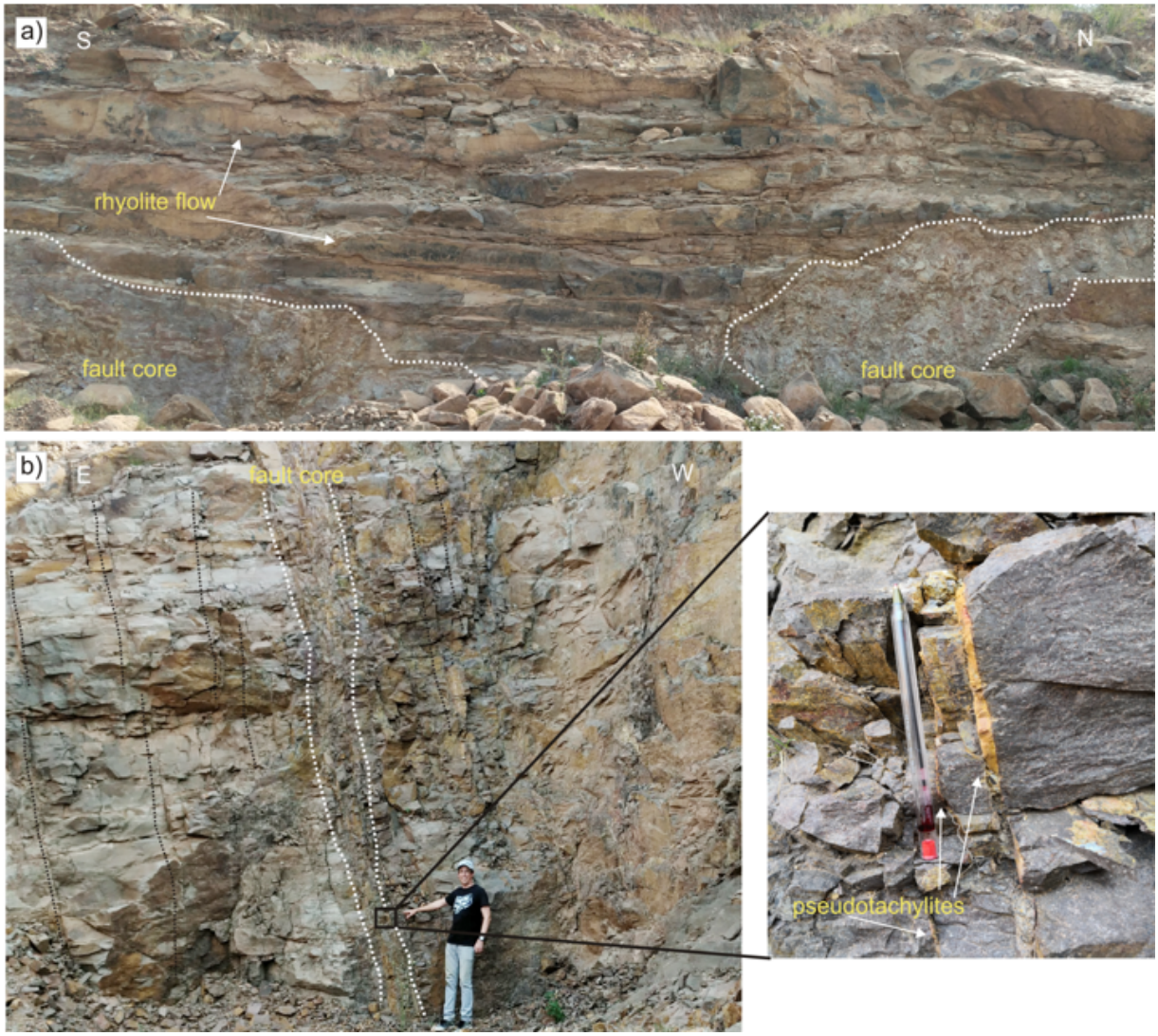

Figure 3.20: (a) Jozini Formation rhyolite flows with flow parallel joints developed above and below the individual flow units and the associated N-S oriented fault core shown with dashed white lines; the photograph was taken parallel to the fault orientation in the JF Loc (a) area. (b) A cross-sectional view of the vertical to sub-vertical fault parallel joints. The fault zone is shown with dashed white lines and the fault parallel joints are shown with dashed black lines. The insert shows the characteristic pseudotachylites that are developed in the fault core.

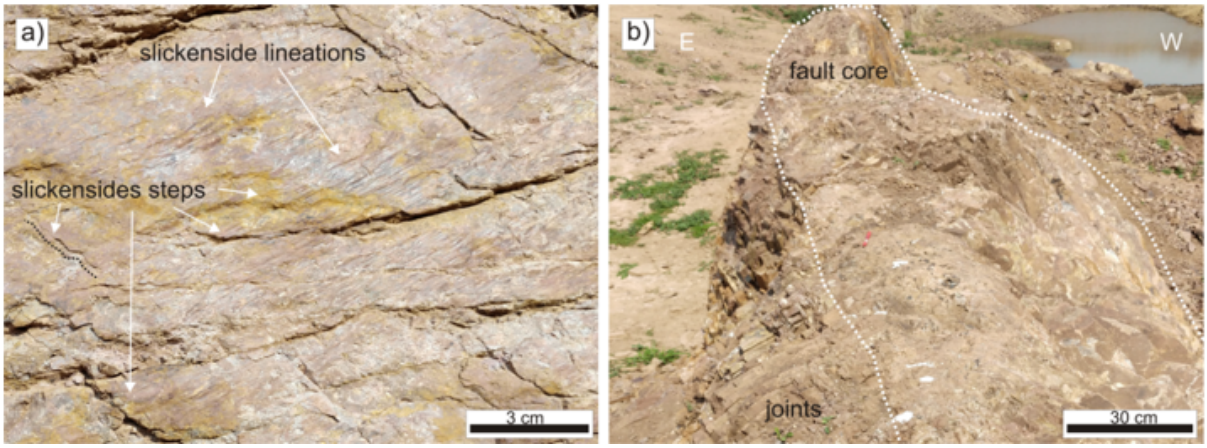

Figure 3.21: (a) A cross-sectional view of strike-slip movement in a joint surface revealed by slickenside steps. The dextral strike-slip fault is N-S striking with dip and dip azimuth of 80°/275° and lineation measurement of 26°/039° (plunge and plunge direction). (b) A top view of the fault with associated fault breccia and the fault-associated systematic joints. The fault is N-S striking and the photograph was taken facing to the south.

Figure 3.22: A sharp contact between the underlying rhyolitic tuff and overlying rhyolite flow with a dip of 26° towards 084°. The fault is NW-SE striking fault with dip and dip azimuth of 78°/229° and is a tilted normal fault (Fig. 3.25b). The major fault structures within the Jozini Formation reveal a N-S strike and dip azimuth between 271°—282°. The fault plane here is now inclined at 78° to the southwest as shown in this photograph.

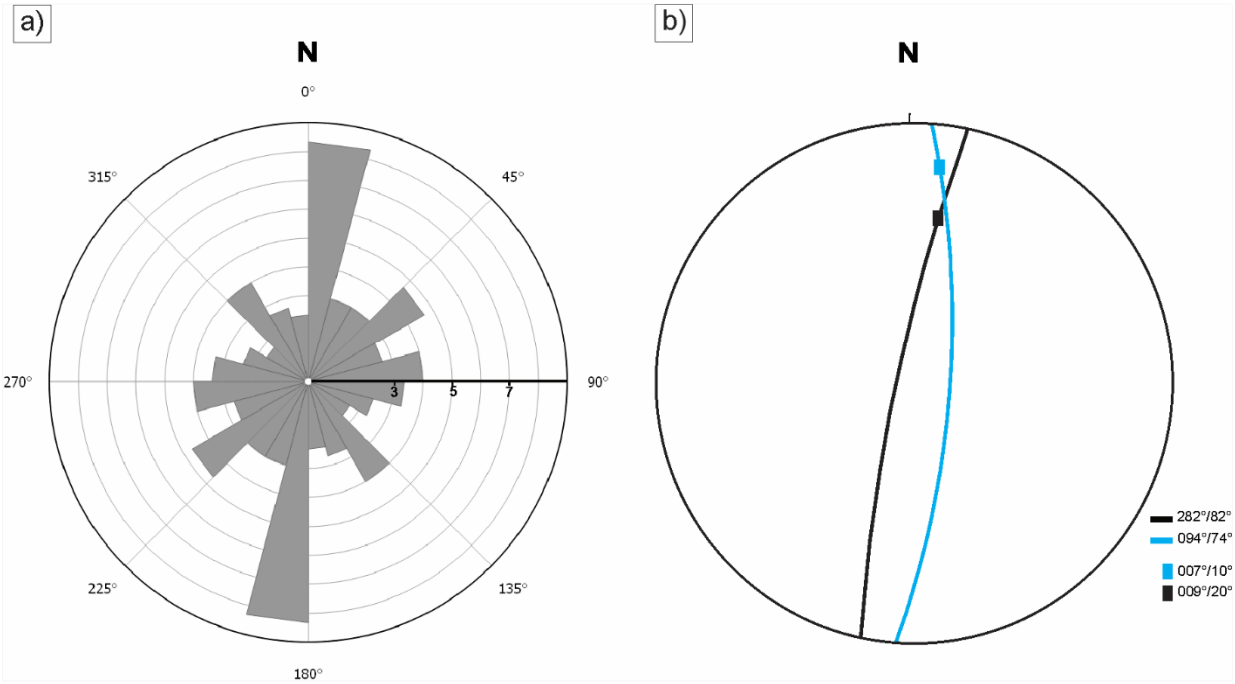

Figure 3.23: (a) The orientations of the joint planes measured in JF Loc (a) (Fig. 3.17) are represented on a rose diagram. For the rose diagram a bin size of 15° has been used. (b) Fault data plotted on lower hemisphere, equal angle stereonet (dip azimuths and dip angles are shown on the bottom right). Lineations are shown as coloured rectangles with the colour corresponding to the associated fault.

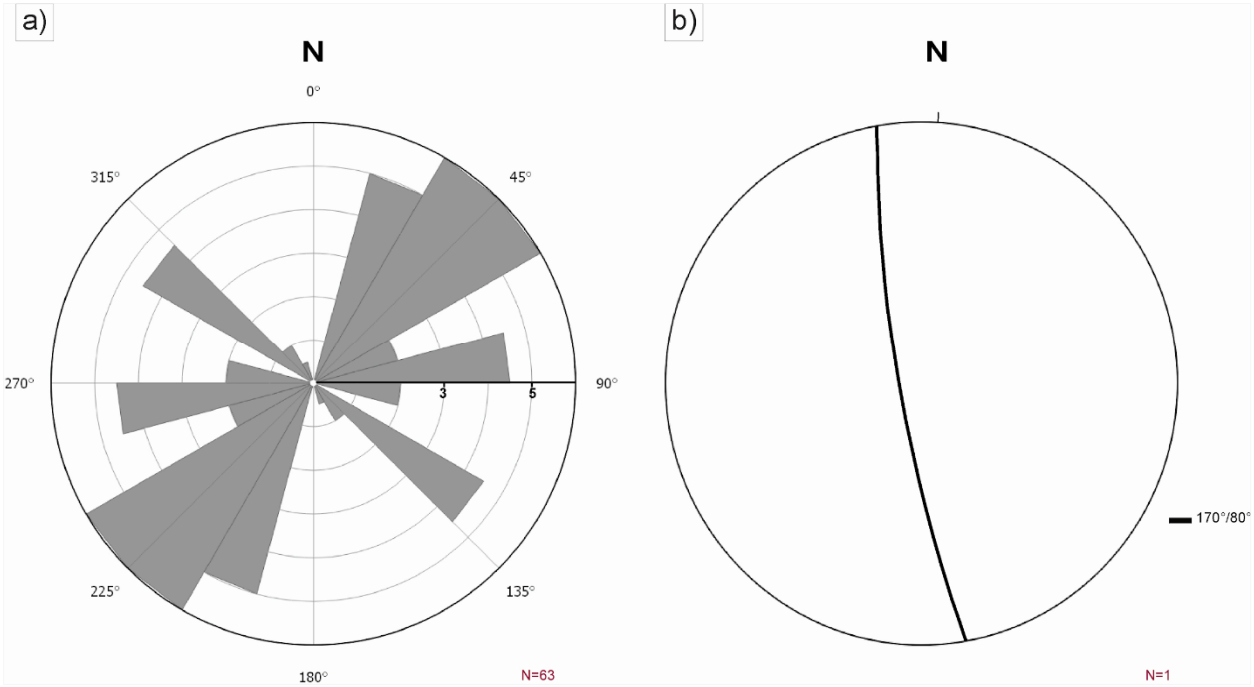

Figure 3.24: (a) The orientations of the joint planes measured in JF Loc (b) are presented on a rose diagram. For the rose diagram a bin size of 15° has been used. (b) Lower hemisphere, equal angle stereonet of the fault (strike and dip of the fault is shown on the bottom right).

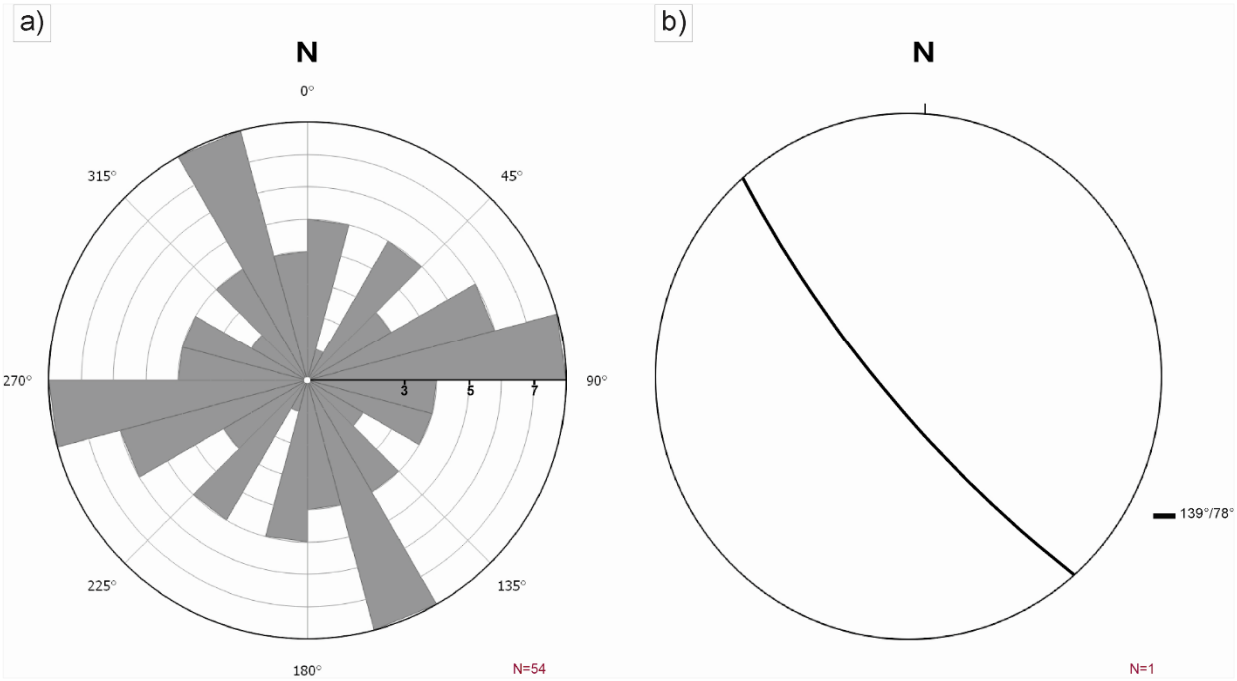

Figure 3.25: (a) The orientations of the joint planes measured in JF Loc (c) are represented by a rose diagram (a bin size of 15° has been used). (b) Fault plotted on lower hemisphere, equal angle stereonet (strike and dip of the fault is shown on the bottom right).

The collected field data from the Jozini Formation rhyolites in three localities (JF Loc a–c), grouped into a 10° interval from either side of the shear fracture directions of a Riedel shear system, are shown in Table 1. Table 1 shows a high number of R and Y-shears relative to the R', T and P-shears. From the two hundred and forty three systematic joints, the Riedel shear fractures represent 65% and the non-Riedel shear fractures 35%.

Table 1: Systematic joint data from the Jozini Formation rhyolites in three localities (JF Loc a–c). The table shows the 10° intervals for each shear fracture orientations and the number of fractures in each interval are shown in each column.

Outcrop area	Number of fractures (n)	R (015°) *Interval: (005°–025°) (185°–205°)*	R' (075°) *Interval: (065°–085°) (245°–265°)*	P (165°) *Interval: (155°–175°) (335°–355°)*	T (045°) *Interval: (035°–055°) (215°–235°)*	Y (000°) *Interval: (170°–190°) (350°–010°)*	Joints outside the major shear fracture orientations
JF Loc a	126	24	12	8	19	27	36
JF Loc b	63	6	7	1	19	0	30
JF Loc c	54	2	11	8	7	6	20
Total	243	32	30	17	45	33	86
Percentage (fracture orientations)		65%					35%

3.1.2.2. Ntabankosi Rhyolite Suite

Closely spaced, systematic joints and fracture cleavage are dominant structural features evident in the rhyolitic units of the Ntabankosi Suite. The joint surfaces are predominantly planar but curved joint planes are also visible (Fig. 3.26). The Ntabankosi Suite reveals three major fracture orientations (Fig. 3.27), namely; the dominant NW-SE oriented joint planes with dips between 59°–89°, the NE-SW orientation with steeply dipping (54°–84°) and sub-vertical (86°–89°) northeast and southwest dipping joint surfaces, and the N-S oriented eastward dipping planes, yielding dips between 56°–73°. There is a lack of E-W oriented joint planes.

Figure 3.26: (a) The fracture cleavage and planar to curved joints developed in rhyolites of the Ntabankosi Suite. The joints and fracture cleavage are parallel and are shown with dashed white lines.

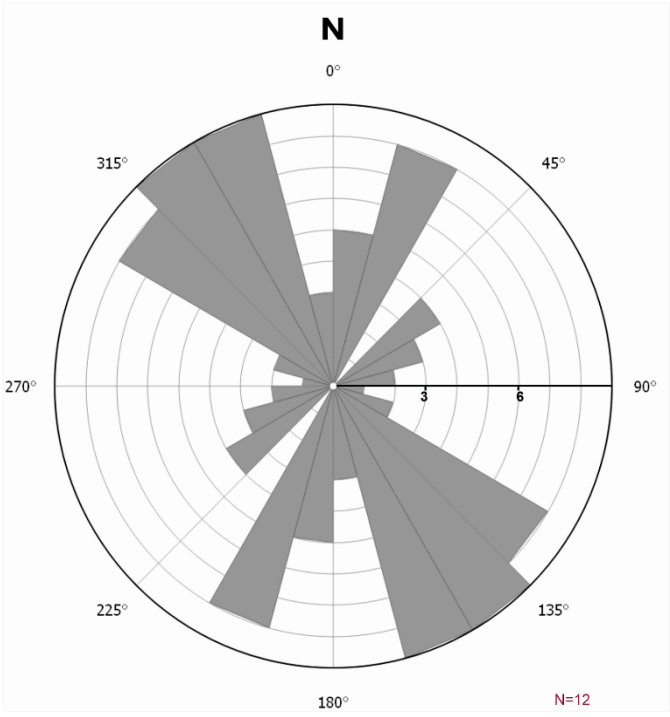

Figure 3.27: Rose diagram showing the different joint surface orientations. For the rose diagram a bin size of 15° has been used.

3.1.2.3. Bumbeni Complex

(i) Mpilo Formation

The Mpilo Formation basalt has planar joints (Fig. 3.28), with dominant NW-SE and NE-SW orientations and minor N-S and E-W orientations (Fig. 3.29). The NW-SE oriented joints are shallowly to steeply inclined (36°–89°) towards the southwest and northeast, whilst the NE-SW oriented joints dip between 59° and 90° towards the northwest and southwest. The N-S striking joint surfaces dip steeply (65°–85°) towards the east and the E-W oriented joints dip steeply (72°–89°) towards the south.

Figure 3.28: Steeply dipping joints in the Mpilo Formation basalt. Hammer handle for scale (20 cm long).

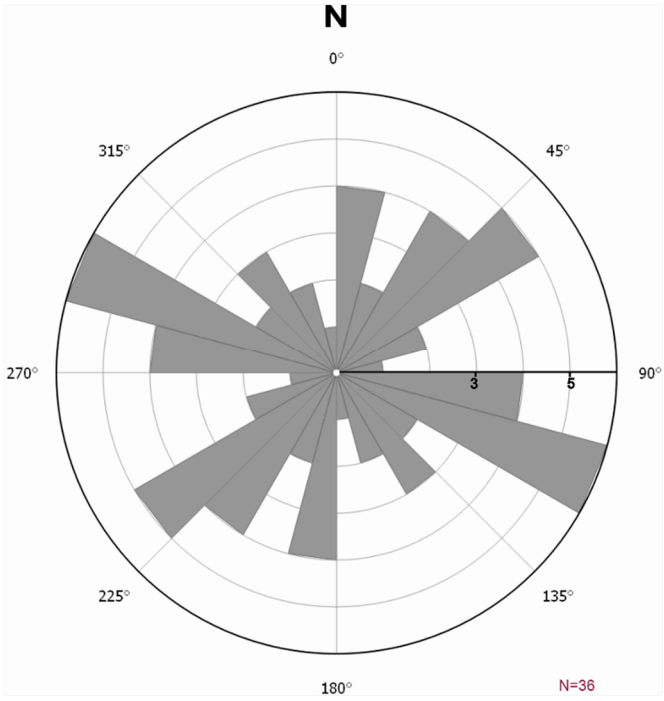

Figure 3.29: Rose diagram with 15° bin sizes showing fracture orientation distribution in the Mpilo Formation.

(ii) Fenda Formation

The systematic joints in the rhyolitic rocks of the Fenda Formation are planar and steeply dipping (Figs. 3.30). The dominant joint surface measurements reveal a distinct NW-SE orientation with dips ranging between 48° and 90° (Fig. 3.31). These joints are dipping towards the southwest and northeast. A

second NE-SW oriented joint set dips (52°–90°) with varying (east, west, southeast and northwest) azimuths. A third E-W oriented joint set dips (62°–89°) towards the north and south. A minor N-S joint orientation is also visible and is characterised by steep (52°–90°) east and west dipping joint planes (Fig. 3.31).

Figure 3.30: The photograph shows the morphology of joint planes developed in rocks of the Fenda Formation. The joint planes in some outcrops are slightly curved. The hammer handle points towards the top of the rhyolite unit.

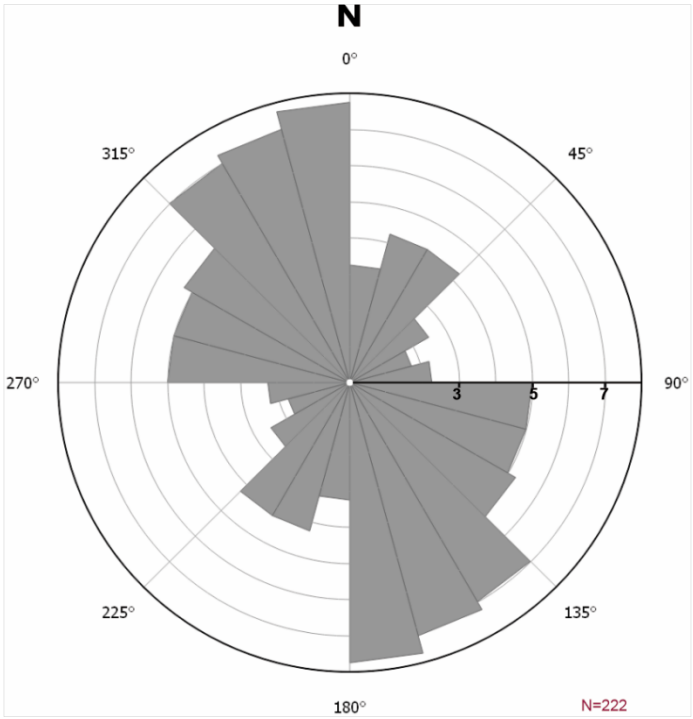

Figure 3.31: A rose diagram with 15° bin sizes showing the joint orientations in the Fenda Formation.

(iii) Nxwala Member

Lithological units of the Nxwala Member have been affected by jointing and localised faulting and also small-scale folding in tuffaceous units (Fig. 3.32 and 3.33). The lithological units of this member reveal dominantly planar, steeply inclined and sub-vertical to vertical systematic joint sets. The dominant joint sets are oriented NW-SE and NE-SW, with the NW-SE oriented joints dipping between 56° and 90° towards the southwest and northeast. The NE-SW oriented joints have dips ranging between 49° and 90°. There are two minor joint orientations; a N-S joint set dipping between 52°–90° towards the east and west, and an E-W set dipping between 56°–90° towards the north and south.

The brittle faulting developed in the tuff is characterised by brecciated fault zones and well-developed damage zones. A fault developed in the ash tuff outcrop in the PPM-Locality 2 area is NE-SW oriented, steeply dipping (dip and strike of 85°/044°) with a ~30-cm-wide fault core (Fig. 3.32a). A second fault, characterised by a ~40 cm-wide fault core, is NW-SE oriented with dip and strike of 54°/328° (Fig. 3.32b).

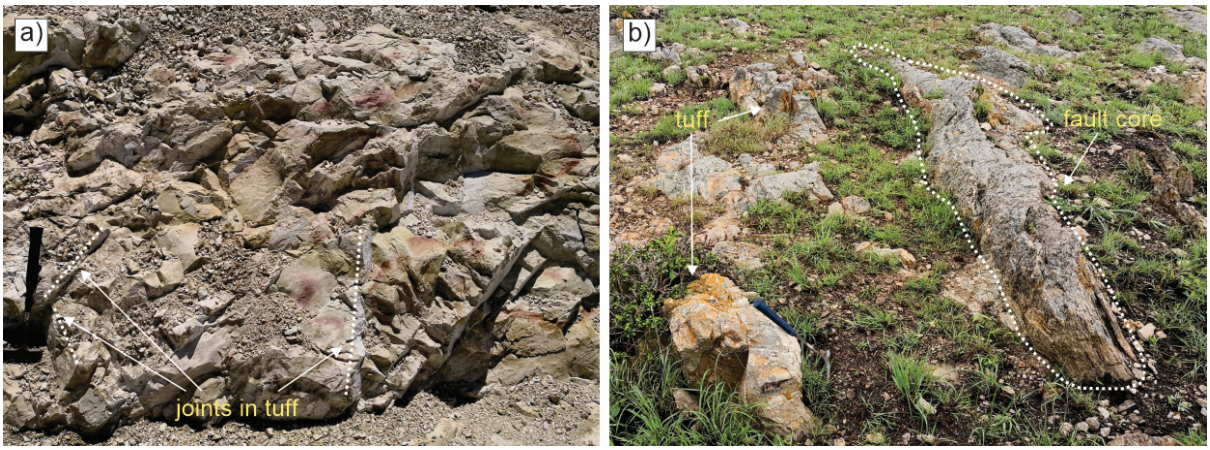

Figure 3.32: (a) Characteristic jointing developed in the tuff of the Nxwala Member which is exposed in PPM-Locality 2 shown in Figure 3.9. (hammer for scale). (b) A NW-SE striking fault associated with the tuff deposits exposed in the southern outcrops of the Nxwala Member (hammer for scale).

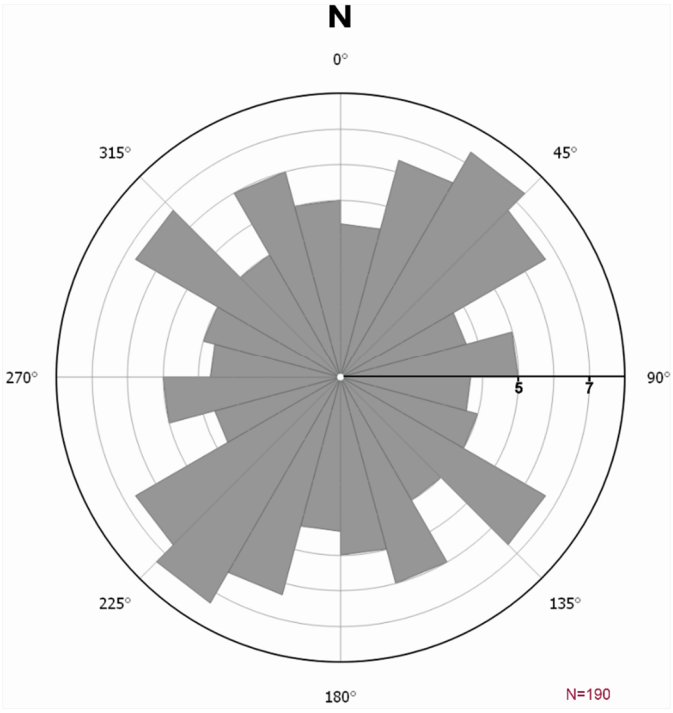

Figure 3.33: Rose diagram, with 15° bin sizes, showing the different joint surface orientations in the Nxwala Member.

3.1.2.4. Zululand Group

(i) Mzinene Formation

The Mzinene Formation reveals steeply dipping, vertical and sub-vertical planar systematic joint sets (Figs. 3.34). The dominant joint surface measurements reveal a distinct NW-SE orientation with dips ranging between 73° and 90° (Fig. 3.35). These joints are dipping towards the southwest and northwest. A second NE-SW oriented joint set has dips ranging between 74° and 90°. The third distinct E-W oriented joint set is characterised by dips ranging between 64° and 87° with joint planes dipping towards the north and south. The fourth distinct N-S oriented joint set, which is perpendicular to the E-W joint orientation, is characterised by sub-vertical (70°–90°) joint planes dipping towards the east and west (Fig. 3.35).

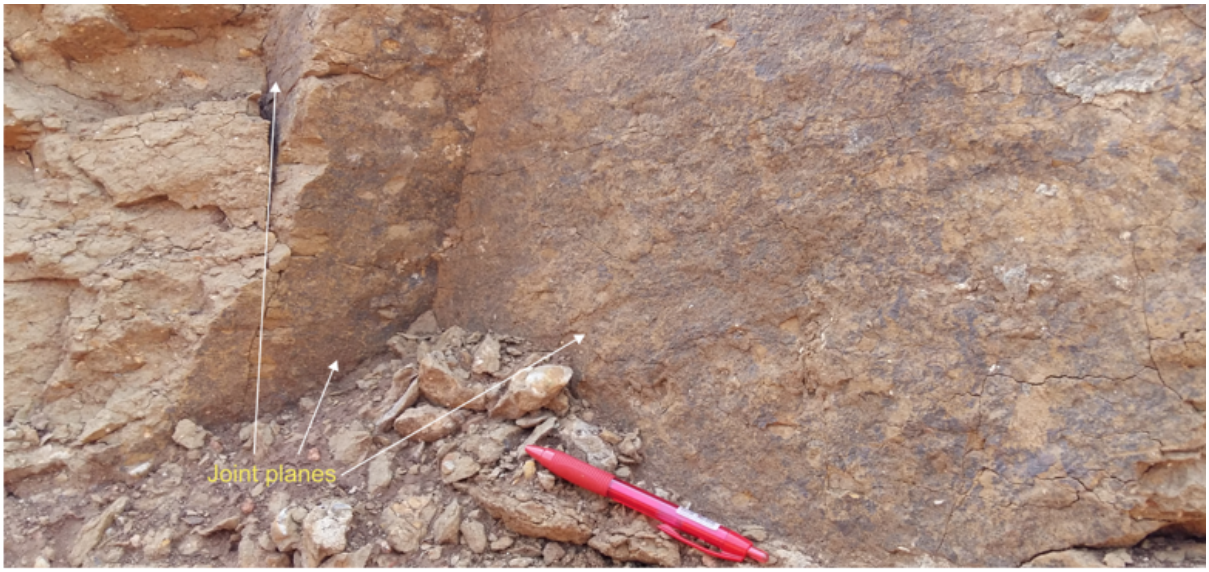

Figure 3.34: A close-up view of the planar joint surfaces in the siltstone of the Mzinene Formation.

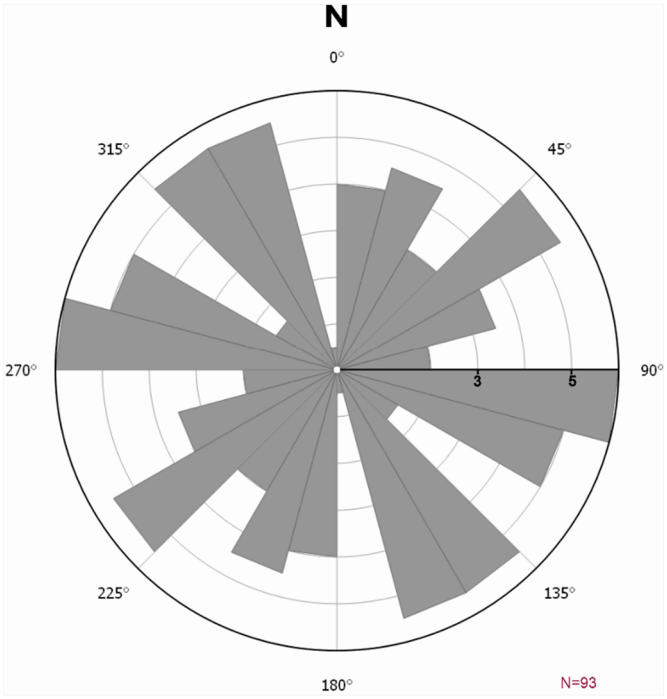

Figure 3.35: Rose diagram, with bin size of 15°, for the joint surface measurements in the Mzinene Formation.

3.2. Whole-rock geochemistry

The geochemistry results from rocks of the Nxwala Member are shown in the Total alkalis versus silica (TAS) classification diagram (Fig. 3.36). The pyroclastic rocks of the Nxwala Member in this study are acidic with SiO_2 contents ranging between 71.5–72.5 wt% (Fig. 3.36). These rocks are potassic (3.48–4.62 wt% K_2O) with high Al_2O_3 contents (12.02–13.94 wt%). The Na_2O contents of these rocks ranges between 1.53 to 3.67 wt% whereas the Fe_2O_3 (t) (0.95–1.69 wt%) and CaO (0.64–1.41 wt%) contents are low. These rocks are further characterised by low TiO_2 (0.13–0.22 wt%), MgO (0.05–0.72), MnO (0.015–0.033 wt%), P_2O_5 (0.013–0.035 wt%) and Cr_2O_3 (0.006 –0.013 wt%). In addition, the pyroclastic rocks of the Nxwala Member are classified as rhyolites on the total alkalis versus silica classification diagram with Na_2O+K_2O values ranging between (5–7.9 wt%) (Fig. 3.36).

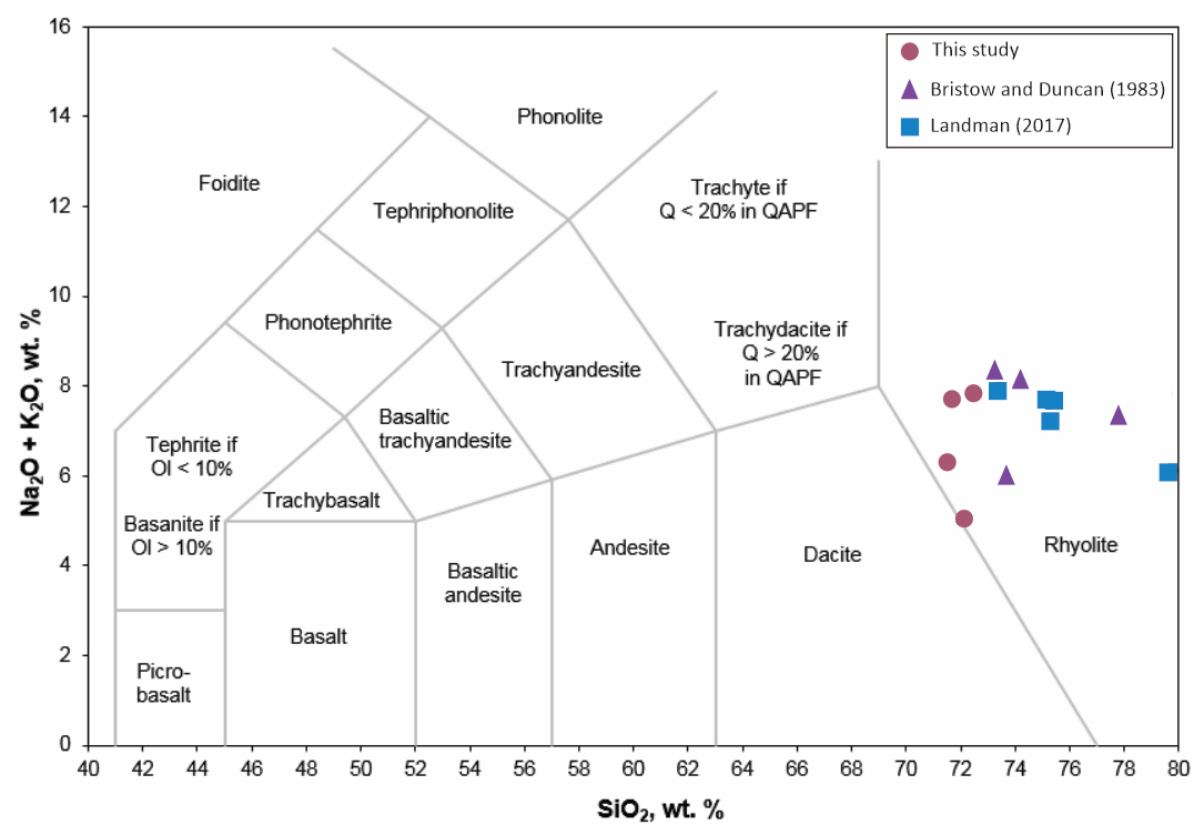

Figure 3.36: TAS classification diagram for the rocks of the Nxwala Member in the northern region of the Bumbeni Complex (sample localities are shown in Figure 3.9) and pyroclastic rocks of the NZA borehole (after Le Bas et al., 1986). This classification diagram shows the similarities in analytical results from the Nxwala Member volcanics, in the northern region of the Bumbeni Complex; (i) in this study, (ii) in Bristow and Duncan (1983) and (iii) from pyroclastic rocks of the NZA borehole (after Landman, 2017). Only the data from the pyroclastic rock samples of Bristow and Duncan (1983) were plotted on the TAS classification diagram and any two sets of results acquired from the same sample (e.g., L507) were averaged. For the NZA borehole, only the data comparable to the analytical results in this study were plotted for ease of comparison. More detailed descriptions and complete results on sampled rock types are available in Appendices 1–3.

3.3. Drill core

The ZB borehole intersection within the Zululand Basin indicates that the basement consists primarily of rhyolitic volcanics. The pyroclastic deposits of the Bumbeni Complex are intersected in the borehole NZA (proximal to the mapped Bumbeni Complex), whilst mafic volcanics are intersected in the more distal ZD borehole (Fig. 1.6).

3.3.1. NZA drill core

The Bumbeni Complex lithologies were intersected by the NZA borehole at approximately 571– 521.21 m depth (surface elevation of ~521 m above mean seal level) and are ~50-m-thick (Fig. 3.37). These pyroclastic rocks reveal a broad coarsening-upward succession of fine-grained tuff to poorly-sorted lapilli tuff and lapillistone (Fig. 3.38).

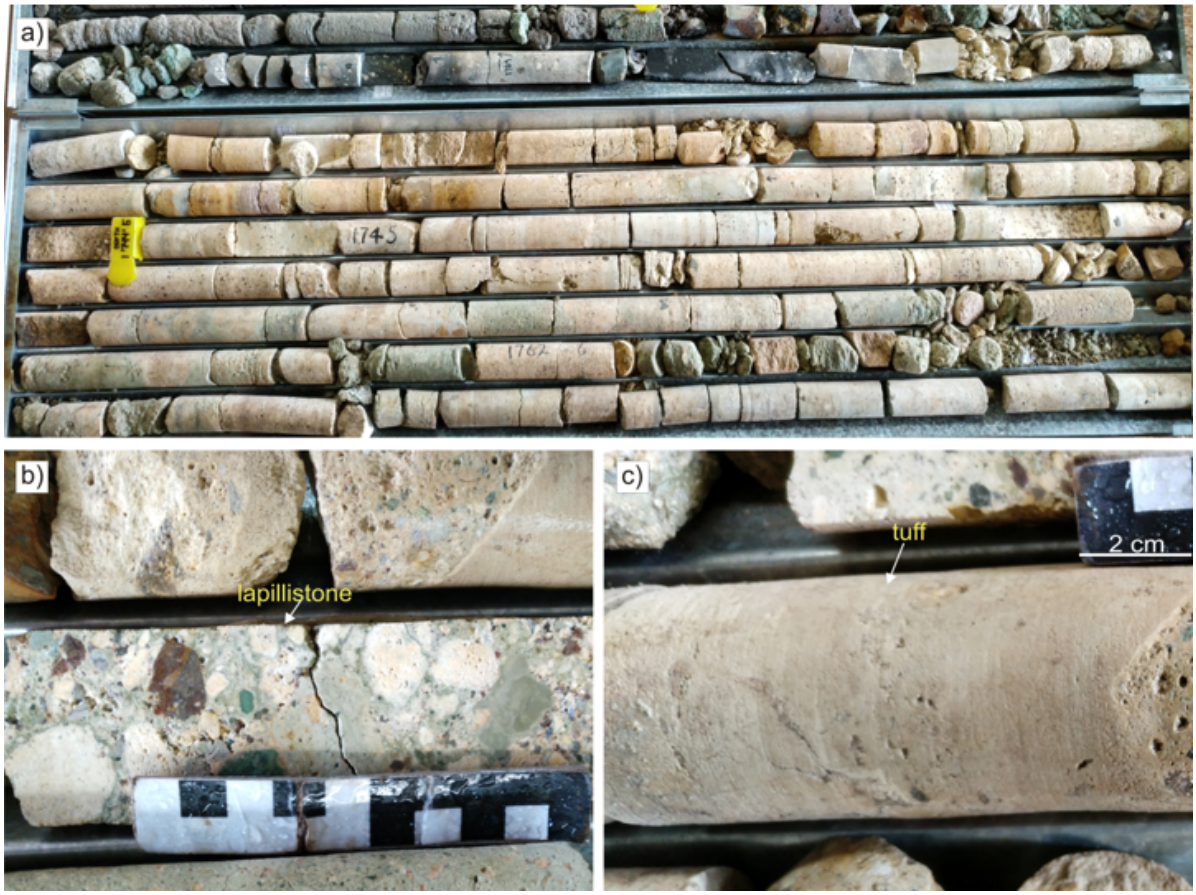

Figure 3.37: Photograph of the core tray of the NZA drill core showing (a) pyroclastic deposits of the Bumbeni Complex. The drill core shallows towards the top of the photograph. (b) Poorly-sorted lapillistone and fine-grained tuff (c) characteristic of the pyroclastic deposits seen in the NZA drill core.

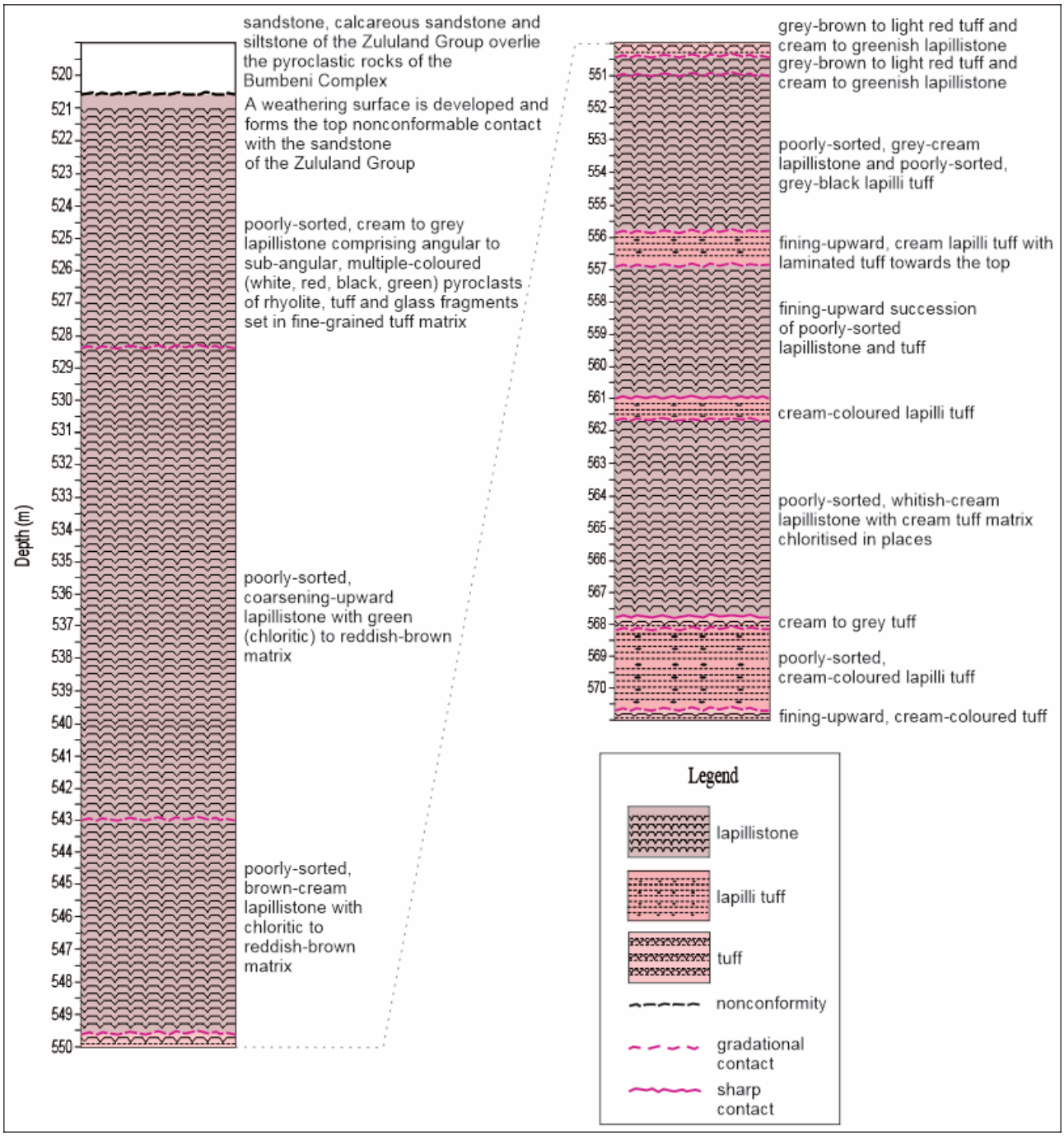

Figure 3.38: The stratigraphic log of the NZA borehole, which intersects the pyroclastic rocks of the Bumbeni Complex. The lithostratigraphic column displays the thickness variation and contact relationships between the tuff, lapilli tuff and lapillistone. The nonconformable contact between pyroclastic rocks of the Bumbeni Complex and the Zululand Group is also shown. A more detailed description of the pyroclastic rocks of the NZA drill core is available in Appendix 6. The pyroclastic rocks of the Bumbeni Complex are overlain by ~1740 m of core, from 50 to 1790 m depth, comprising sedimentary rocks of the Zululand Group. For the purposes of this study the overlying lithostratigraphic units were not logged.

3.3.2. ZB drill core

The ZB borehole intersects grey-coloured, porphyritic rhyolite flow units between 1545.75–1427.57 m depth (surface elevation of ~1524.75 m above mean seal level) (Fig. 3.39). The tops of individual lava flows are marked by a tuff horizon or autobrecciated flow tops (Figs. 3.39b and c). In places, these flows are fractured and brecciated with fractures usually comprising thin veins of calcite and red jasper (Fig. 3.39c). The various rhyolite flow units are also represented on a simplified lithostratigraphic column (Fig. 3.40).

Figure 3.39: (a) Core tray of the ZB rhyolite flows with the depth of the core shallowing towards the top of the photograph. (b) Individual tuff units that mark the top of each rhyolite flow. (c) Shows a rhyolite flow and autobrecciated flow tops. The rhyolite rock fragments are generally cemented by a siliceous (red jasper) matrix.

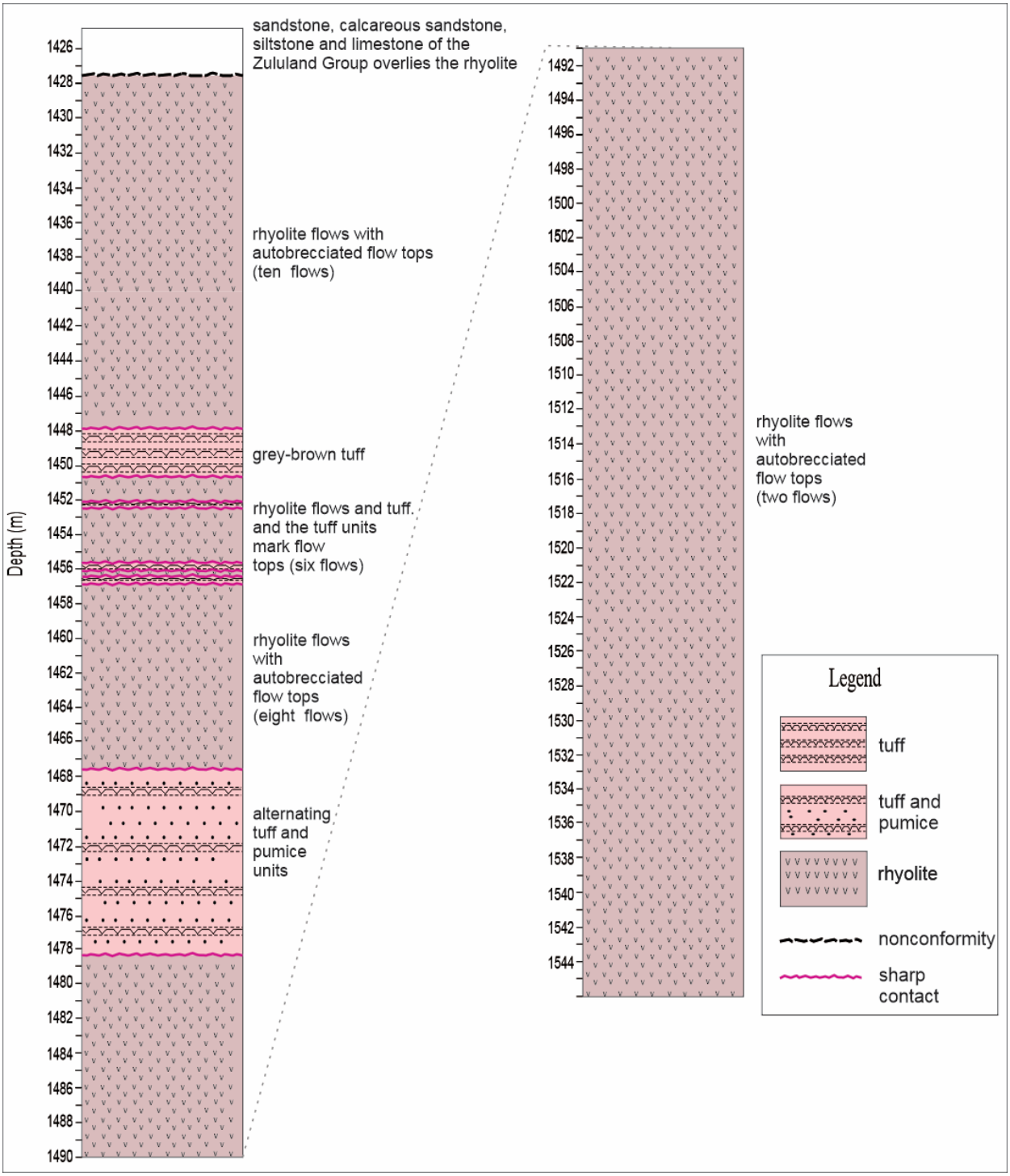

Figure 3.40: Simplified stratigraphy of the logged ZB borehole. The Lithostratigraphic column displays the various rhyolite flows, thickness variation and contact relationships between the rhyolite and tuff units. The nonconformable contact between pyroclastic rocks of the Bumbeni Complex and the Zululand Group is also shown (Refer to Appendix 7 for more detailed descriptions and depths of the rhyolite flows and tuff). The rhyolites are overlain by 4678 m of core, from 0 to 4674 m depth, consisting of sedimentary rocks of the Zululand Group (which were not logged).

3.3.3. ZD drill core

The mafic volcanic rock and brown tuff of the 1071-m-long ZD borehole, with a surface elevation of ~1050 m above mean seal level, is shown in Figure 3.41. The mafic rock is dark grey, coarse-grained comprising angular to and sub-angular, dark, pale green and reddish-brown minerals set in a fine crystalline matrix (Figs. 3.41a and b). The top of the lava flow is marked by a fine-grained, brown tuff horizon (Figs. 3.41c and 3.42).

Figure 3.41: Photograph of the core tray ZD showing (a) the mafic lava and a close-up view of the lava (b). Note the dark and reddish-brown minerals set in fine crystalline matrix. (c) The insert shows a close-up view of the overlying tuff.

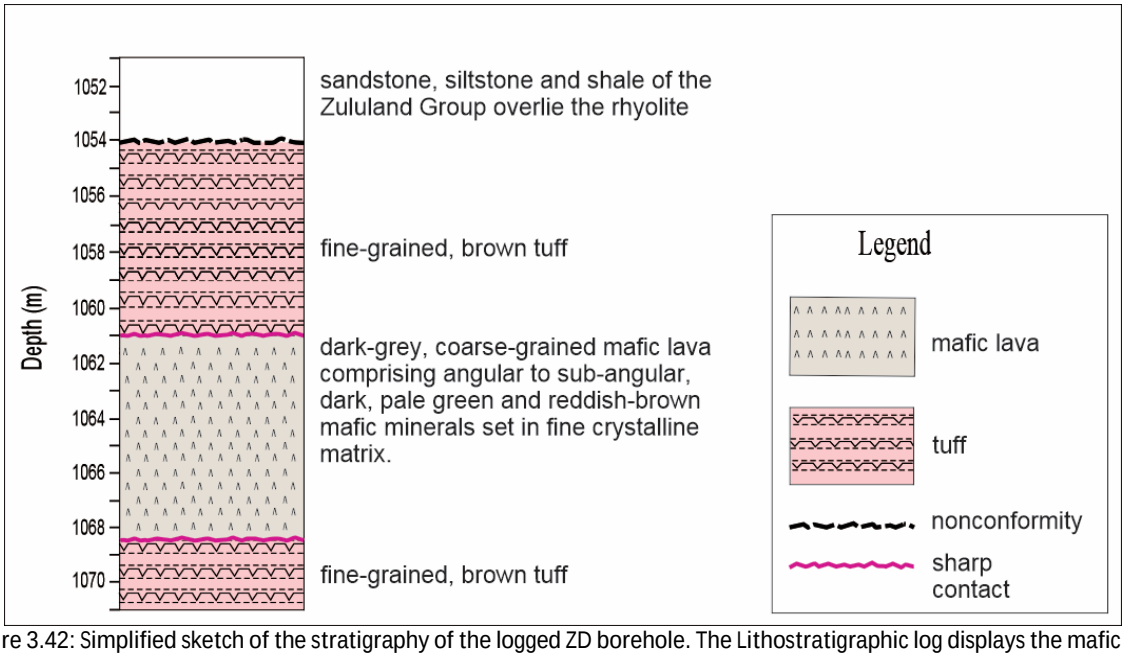

Figure 3.42: Simplified sketch of the stratigraphy of the logged ZD borehole. The Lithostratigraphic log displays the mafic lava flow, thickness variation and contact relationships between the lava and tuff units. The nonconformable contact between tuff and the Zululand Group is also shown. The mafic lava is overlain by 1054 m of core, from 0 to 1054 m depth, consisting of sedimentary rocks of the Zululand Group (which were not logged) (Refer to Appendix 8 for descriptions and depths of the mafic lava and tuff).

3.4. Aeromagnetic Data Analysis

The processed aeromagnetic data reveals distinct magnetic signatures in the study area as shown in Figures 3.43 and 3.44. There is a general decrease in the magnetic intensity from west to east. This trend is observed in the Total Magnetic Anomaly, which decreases from 32000 to 0 nT and in the Reduced-to-Pole map, which decreases from +250 to -150 nT (Figs. 3.43 and 3.44a). Furthermore, the combination of the coherent distinct linear magnetic signatures, revealed by the overall magnetic texture mainly defined by the Total Magnetic Anomaly data which is a product of the IGRF-corrected Total Magnetic Intensity data, Reduced-to-Pole, First Vertical Derivative and Analytical Signal data, allow for the identification of magnetic domains (Figs. 3.43–3.45).

There are four domains (Domains 1–4) identified in the study area, which are separated by distinct regional magnetic discontinuities (Fig. 3.45). Domain 1 occurs in the western area, Domain 2 spans the central and northern areas, Domain 3 occurs in the eastern area and Domain 4 corresponds with the southern area. Each domain is characterised by distinct (linear and curvilinear) magnetic anomalies/lineaments. These lineaments are characterised as wide (low frequency, regional anomalies) and narrow (high frequency, local anomalies) in space (Fig. 3.45).

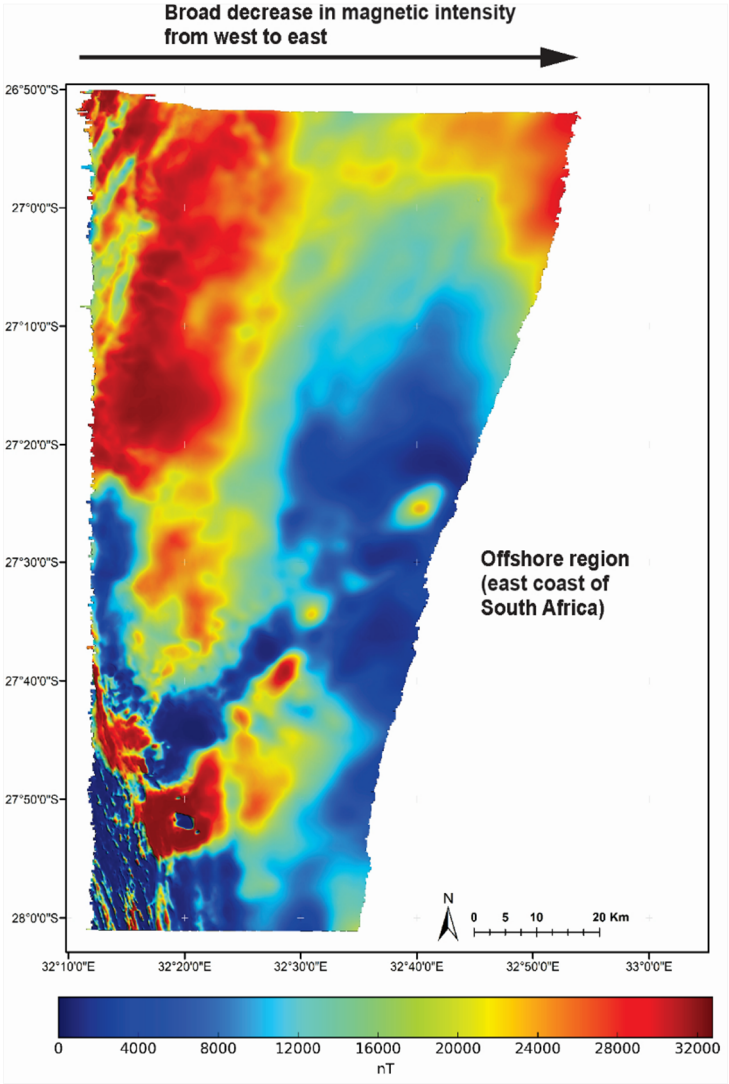

Figure 3.43: Total Magnetic Anomaly (IGRF-corrected data set) of the study area. Histogram equalized map showing a variation in colours where the red and blue colours represent magnetic high to low regions, respectively. For example, the western region is dominated by magnetic high areas and the eastern region is characterised by magnetic low areas.

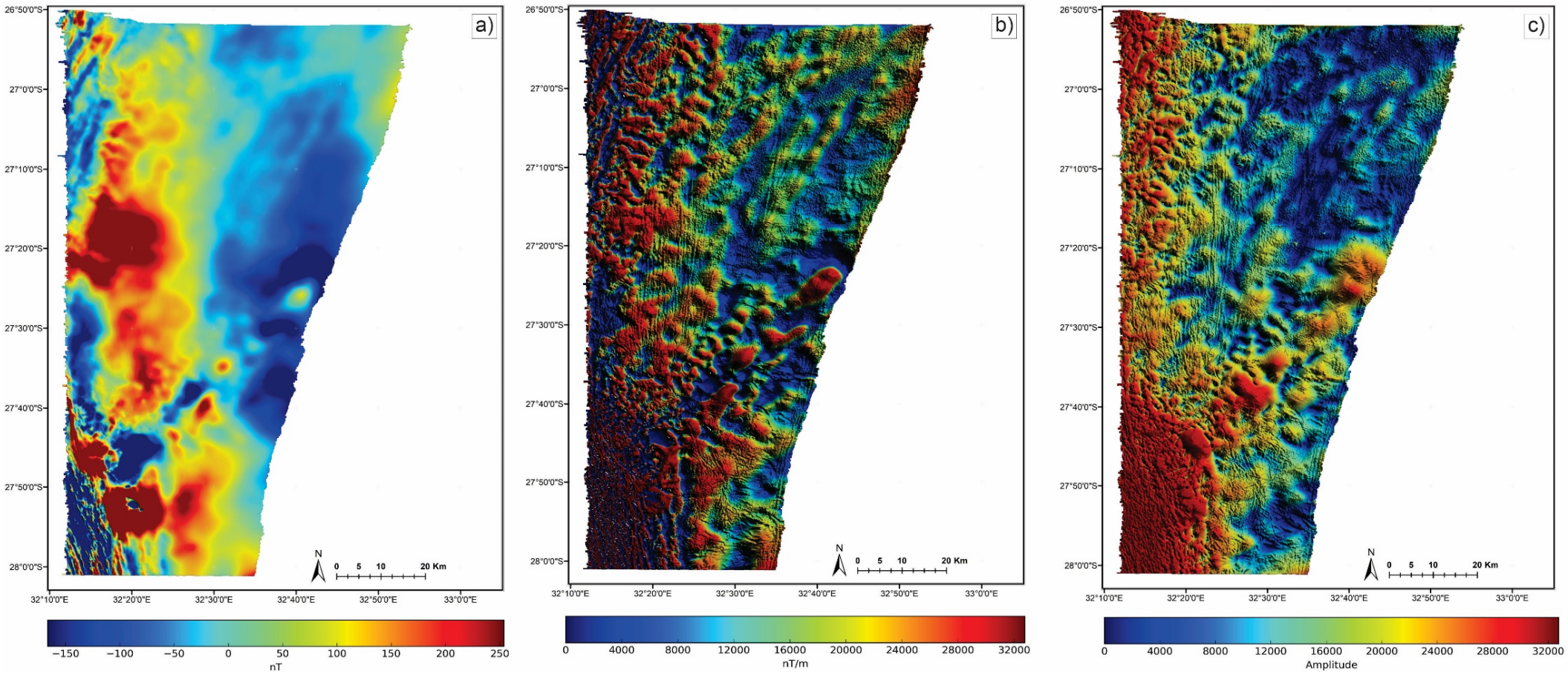

Figure 3.44: Processed airborne magnetic data. The data is histogram equalized and shows a variation in colours with red and blue representing regions of magnetic high and low values on these maps, respectively. (a) Reduced-to-Pole operator improves the accuracy in the location of magnetic sources relative to geological features. (b) First-Vertical Derivative map shows the low frequency magnetic anomalies and these anomalies are enhanced providing a better separation between those that are closely spaced. (c) Analytical Signal data has an amplitude which is independent of the direction of the magnetisation source. The amplitude and frequency of the data relates to that of the magnetised source.

3.4.1. Identification of Magnetic Domains including the Bumbeni Complex and Lineament

3.4.1.1. Domain 1

Domain 1 covers the western extent of the study area and extends from the south to the north comprising magnetic values ranging from a minimum of -150 nT to a maximum of +250 nT in the Reduced-to-Pole data set (Figs. 3.44c and 3.45a). The northern section of Domain 1 is characterised by NNE-SSW trending, wide parallel lineaments, whereas the southern section consists of closely spaced, NNW-SSW and N-S oriented high frequency lineaments (Fig. 3.45). This domain includes the Bumbeni Complex, which is associated with high and low magnetic signatures (Fig. 3.45). The northern portion of the complex is characterised by a broad magnetic low signature, whereas the central and southern sections comprise magnetic high and low signatures, respectively (Fig. 3.45). The area east of the Bumbeni Complex is characterised by a distinctive, roughly circular, high frequency, negative magnetic anomaly with an amplitude of approximately -150 nT (Fig. 3.45), identified by a grey polygon in Figure 3.45a.

3.4.1.2. Domain 2

To the east of Domain 1 is Domain 2, which is bound by Domain 3 to the east. In the southern portion of the study area, the boundary of Domain 2 is defined by a NE-trending magnetic low zone that is the northern boundary of Domain 4 (Fig. 3.45). Domain 2 is characterised by a high to intermediate magnetic intensity and minor diffuse magnetic low areas and consists of minor NE trending wide lineaments occurring northwest of Domain 3 and the southwestern portion of the Bumbeni Lineament, which is characterised by NE-striking, disjointed remanently magnetised cylindrical anomalies (Figs. 3.43 and 3.45). Domain 2 is further characterised by NW-SE, N-S and E-W oriented, closely spaced narrow lineaments that are clearly visible in the First Vertical Derivative map (Fig. 3.45b). In places, these narrow lineaments cross-cut the wide lineaments and each other.

3.4.1.3. Domain 3

Domain 3 is restricted to the northeastern portion of the study area and is predominantly defined by a broad magnetic low region in the Total Magnetic Anomaly data and also in the Reduced-to-Pole data (Figs. 3.43 and 3.45a). In the Reduced-to-Pole data this region is characterised by low values ranging from -150 nT to 0 nT (Fig. 3.45a). Domain 3 consists of a NE-SW trending high frequency lineament occurring in the northwest. This domain also consists of the northeastern portion of the Bumbeni Lineament, which is characterised by disjointed cylindrical anomalies with normal magnetisation (Fig. 3.45). Domain 3 is further characterised by NW-SE, N-S and E-W oriented, closely spaced high

frequency lineaments which cross-cut each other and the NE trending low frequency lineament. These anomalies do not reveal any consistent pattern in their cross-cutting nature across this domain.

3.4.1.4. Domain 4

Domain 4 occurs in the southern portion of the study area and is flanked to the east by Domain 1 and to the northeast by Domain 3. It is separated from Domain 2 in the north by the Bumbeni Lineament. Domain 4 is a region of high to medium magnetisation (0 to +25 nT) characterised by high frequency magnetic signatures. This domain comprises closely spaced, low frequency NW-SE, N-S and E-W striking lineaments that show minor cross-cutting relationships with no consistent pattern (Fig. 3.45).

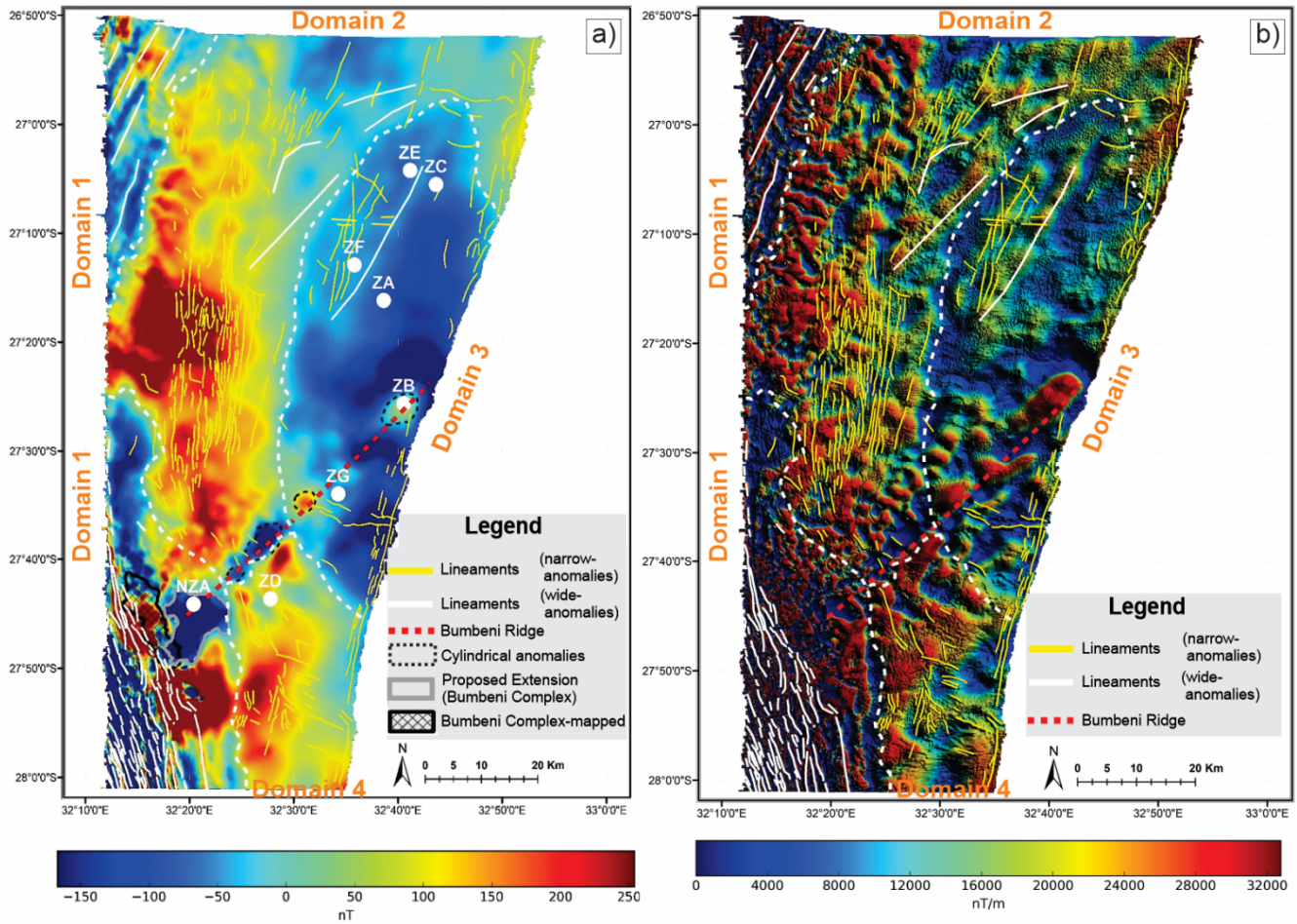

Figure 3.45: Histogram equalized processed airborne magnetic data with red-high and blue-low magnetic signatures. (a) The Reduced-to-Pole map of the study area showing Domains 1–4. Lineaments are shown as white and yellow lines. The domain boundaries are shown with dashed white lines. The NE striking Bumbeni Ridge/Lineament is shown with a dashed red line and intersects Domains 1–3 and represents the boundary between Domains 2 and 4. The locations and names of the boreholes are shown with labelled white circles. The black polygon to the west of the NZA borehole shows the extent of the mapped Bumbeni Complex as shown in Figure 1.6. The grey polygon shows a proposed extension of the Bumbeni Complex beyond its earlier mapped extent. (b) The different domains and the narrow and wide lineaments and the Bumbeni Ridge/Lineament are shown in the First-Vertical Derivative map of the study area.

4. Discussion

4.1. Geological evolution of the basement

The basement rocks in the study area comprise the volcanic rocks of the Lebombo Group, which range in composition from nephelinites, picrites and basalts to rhyodacites and rhyolites (Marsh and Eales 1984; Duncan et al., 1997; Riley et al., 2004). These rocks are subdivided, from old to young, into the Mashikiri, Letaba, Sabie River, Jozini, Mbuluzi and Movene Formations (Duncan and Marsh, 2006; Klausen, 2009). The basal Mashikiri Formation nephelinites are SiO_2 undersaturated and are enriched in incompatible trace elements (Watkeys, 2002; Riley et al., 2004), which suggests they were derived from melting of a metasomatically-enriched subcontinental lithospheric mantle (Hastie et al., 2013). These nephelinites are overlain by the Letaba Formation picrite basalts of the northern Lebombo region (Duncan and Marsh, 2006; Hastie et al., 2013) and likely formed from metasomatically-enriched subcontinental lithospheric mantle (Bristow et al., 1984); or mixing between asthenospheric mantle and subcontinental lithospheric mantle (Ellam and Cox, 1991; Sweeney et al., 1991) or from a heterogeneous source (Jourdan et al., 2007b; Jourdan et al., 2009).

The overlying basalts of the Sabie River Formation cover most of southern Africa (Duncan and Marsh, 2006), including the southern portion of the Lebombo mountains and the current study region, and vary from low and high-Ti-Zr compositions (Duncan et al., 1984; Watkeys, 2002). The low-Ti-Zr basalts, found in the southern Lebombo, Lesotho, central Botswana and central Namibia, are attributed to an asthenospheric source that equilibrated with refractory mantle before eruption (Sweeney et al., 1991), whereas a lithospheric mantle source is ascribed for the high-Ti-Zr basalts that occur in the northern Lebombo region and in Zimbabwe (Fig. 1.2) (Duncan et al., 1984; Watkeys, 2002). The Sabie River Formation is unconformably overlain by rhyodacites and rhyolites of the Jozini Formation and the Mbuluzi Formations, with the latter occuring in Eswatini (Duncan and Marsh, 2006; Hastie et al., 2013). The Jozini Formation displays little chemical variation along its length (Bristow and Saggerson, 1983a) with the rhyolitic rocks only showing apparent differences in their trace element signatures (Bristow and Saggerson, 1983b).

4.2. Deformation of the Lebombo Group

The Sabie River Formation basalts are characterised by NNE-SSW oriented faults (Fig. 3.18). The orientation of these faults is consistent with E-W oriented tectonic extension. The faulting in these

basalts is here ascribed to the E-W oriented paleo-extensional tectonic event of the initial stages of Gondwana break-up in the early Jurassic (~180–175 Ma) (Watkeys and Sokoutis, 1998; Watkeys, 2002).

Field evidence in this study suggests that the majority of faults, which are normal and strike-slip faults, occur in the competent rhyolites of the Jozini Formation. The presence of pseudotachylites in the fault zone suggests that rapid frictional melting occurred at some time during slip faulting at shallow depths (Fig. 3.20), similar to that described by Killick (1988) and Reimold (1995). The major NW-SE oriented, normal fault occurring in the Jozini Formation that is inclined at 78° to the southwest (Fig. 3.22), is inferred as having formed during a prevailing regional extensional event. This event is attributed to stage one of Gondwana break-up related to E-W directed regional extension (Watkeys and Sokoutis, 1998; Watkeys, 2002). The NW-SE-orientation of this normal fault may have resulted from rotation during subsequent tectonic tilting of the Lebombo Group volcanics (Watkeys and Sokoutis, 1998; Klausen, 2009; Hastie et al., 2011b).

The planar systematic joint sets occurring in the Jozini Formation rhyolites reveal distinct NW-SE, E-W, N-S and NNE-SSW to NE-SW joint orientations. A portion of the N-S oriented systematic joint sets most likely formed during E-W directed regional extension related to stage one (~180–175 Ma) of Gondwana break-up (Watkeys and Sokoutis, 1998; Watkeys, 2002), which likely occurred simultaneously with the 173±0.7 Ma Rooi Rand Dyke Swarm intrusion into the Lebombo Group similar to that described by Armstrong et al. (1984) and Meth (1996). Field evidence combined with the dextral strike-slip movement occurring in the Jozini Formation rhyolites and the orientations of associated systematic joint sets, suggests that these systematic joint sets are representative of a dextral strike-slip system and can be interpreted on a dextral Riedel shear system (Fig. 4.1). It is not crucial for all the shears to exist but the presence of R-shears is mandatory for faults that form in the Riedel shear system (Davis et al., 2000). The 65% representation of the Riedel shear fracture orientations, suggests that these systematic joint orientations are well constrained and can are interpretable on a Riedel shear system (Table 1) (Fig. 2.1).

The N-S oriented dextral strike-slip faults and joint sets are here inferred as P-shears, the NNE-SSW oriented joint sets as R-shears and the T-fractures are represented by the NE-SW oriented joint sets. The E-W oriented fractures are interpreted in this study as R'-shears (Fig. 4.1). The presence of the N-S oriented, dextral strike-slip faults suggests that a rotation in the paleo-stress regime from a vertical σ_1 to a horizontal NE-SW oriented σ_1 may have occurred during deformation to favour the formation of these faults. This deformation event may be associated with the offshore dextral strike-slip movement of the Gastre Fault-Agulhas Falklands Fracture Zone system (Ben-Avraham et al., 1997;

Watkeys, 2002), which is here attributed to the second deformation event (175–155 Ma) of Gondwana break-up (Fig. 1.3c).

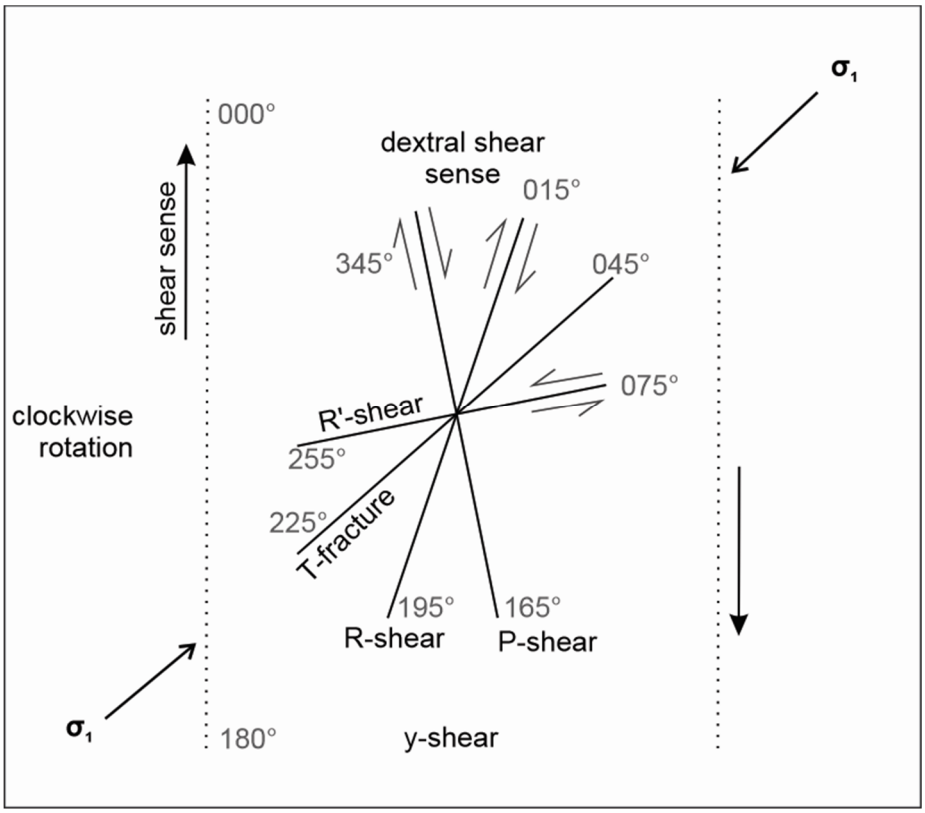

Figure 4.1: Idealised Riedel shear system diagram used in this study to interpret fracture orientations in terms of dextral strike-slip system. Modified after Bartlett et al. (1981), Woodcock and Fischer (1986) and Davis et al. (2000).

Analysis of the aeromagnetic data reveals distinct trends in the geological relationships and tectonic architecture of the basin. There is a broad decrease of magnetic intensity from west to east across the study area (Figs. 3.43 and 3.45). Sedimentary rocks generally show poor magnetic signatures (Gunn et al., 1995; Curto et al., 2014), therefore, the eastward decrease in magnetisation is inferred as the product of poor magnetisation in the eastward-thickening of the sedimentary rocks of the Zululand and Maputaland Groups in the Zululand Basin. The aeromagnetic data defines four distinct magnetic domains (Domains 1–4) (Fig. 3.45). The northern section of Domain 1 is characterised by NNE trending low frequency lineaments related to deep structures (Fig. 3.45). These structures show no clear correlation with the Lebombo Group geology, however, their close proximity to the Lebombo mountains, their orientation and the magnetic high signatures (that are characteristic of mafic igneous rocks or fractures), these structures can be attributed to three potential sources. These magnetic structures could thus be sourced from (1) the NNE-SSW oriented faults developed in the Sabie River Formation which are most likely related to the initial stages of Gondwana break-up in the early Jurassic (~180–175 Ma) (Figs. 1.3a and b) (Watkeys and Sokoutis, 1998; Watkeys, 2002), (2) the 173±0.7 Ma

N-S trending mafic dykes of the Rooi Rand Dyke Swarm, which are intrusive to the Lebombo Group (Fig. 4.2), and (3) basement fractures not previously identified during field mapping in this region. The N-S oriented lineaments, in the southern region of Domain 1, correlate well with the Lebombo Group and it is here postulated that these lineaments are related to N-S oriented dextral strike-slip reactivation of the N-S oriented normal faults characteristic of the Jozini Formation rhyolites (Fig. 3.45).

Domain 2 is the central domain of the study area and comprises minor NE trending low frequency lineaments in the northeast that are related to deep sources, the SW portion of the Bumbeni Lineament and the NW-SE, N-S and E-W oriented, closely spaced high frequency lineaments related to shallow structures (Fig. 3.45). The low frequency lineaments cross-cut each other, the NE trending wide lineaments in the northeast and the Bumbeni Lineament, which suggests that the shallow structures occurred at different times and post-date the occurrence of the deep structures and the Bumbeni Lineament.

Domain 3 is limited to the eastern portion of the study area and is largely defined by a zone of broad magnetic low, in the Total Magnetic Anomaly and Reduced-to-Pole maps, indicating a region of low crustal magnetisation similar to that described by Curto et al. (2014) and Hanyu et al. (2017). Domain 3 is characterised by a NE trending deep seated, linear magnetic structure in the north, and the NW-SE, N-S and E-W oriented, closely spaced high frequency lineaments that are attributed here to shallow structures; most likely fractures (Fig. 3.45). These shallow structures, based on similar magnetic intensity, texture and orientations, could be similar to those in Domain 2. Furthermore, the shallow structures cross-cut each other and the deep-seated, linear structure, suggesting that these younger shallow structures developed at different times and post-date the occurrence of the deep-seated structure. The deep-seated, linear structure is in close proximity to the ZE borehole which intersects a volcanic rock at the base (Fig. 1.6) (Viljoen et al., 2011; Chabangu et al., 2014). Therefore, this structure may be related to a basement fracture system not previously identified in this region.

Domain 4 is limited to the southern portion of the study area and is characterised by NW-SE, N-S and E-W oriented, closely spaced, high frequency lineaments related to shallow structures (Fig. 3.45). These structures are most likely fractures similar to those of Domains 2 and 3, based on their magnetic intensity, texture and orientations.

Based on the orientation of the basement structures in Domains 2 and 3 and the shallow structures and the observed cross-cutting relationships evident in the Domains 2, 3 and 4 (Fig. 3.45), it is inferred here that these structures were formed by different paleo-stress regimes that would have occurred

with progressive tectonic deformation. The paleo-stress directions would have been responsible for the basement structures with the subsequent rotation in the paleo-stress orientations through time forming the younger fractures. This long-lived event is attributed here to the second and third deformation events and can be constrained between stages 2 and 3 (175–135 Ma) of Gondwana break-up, which is associated with the offshore dextral strike-slip movement related to the Gastre Fault-Agulhas Falklands Fracture Zone system (Figs. 1.3c and d) (Ben-Avraham et al., 1997; Watkeys, 2002).

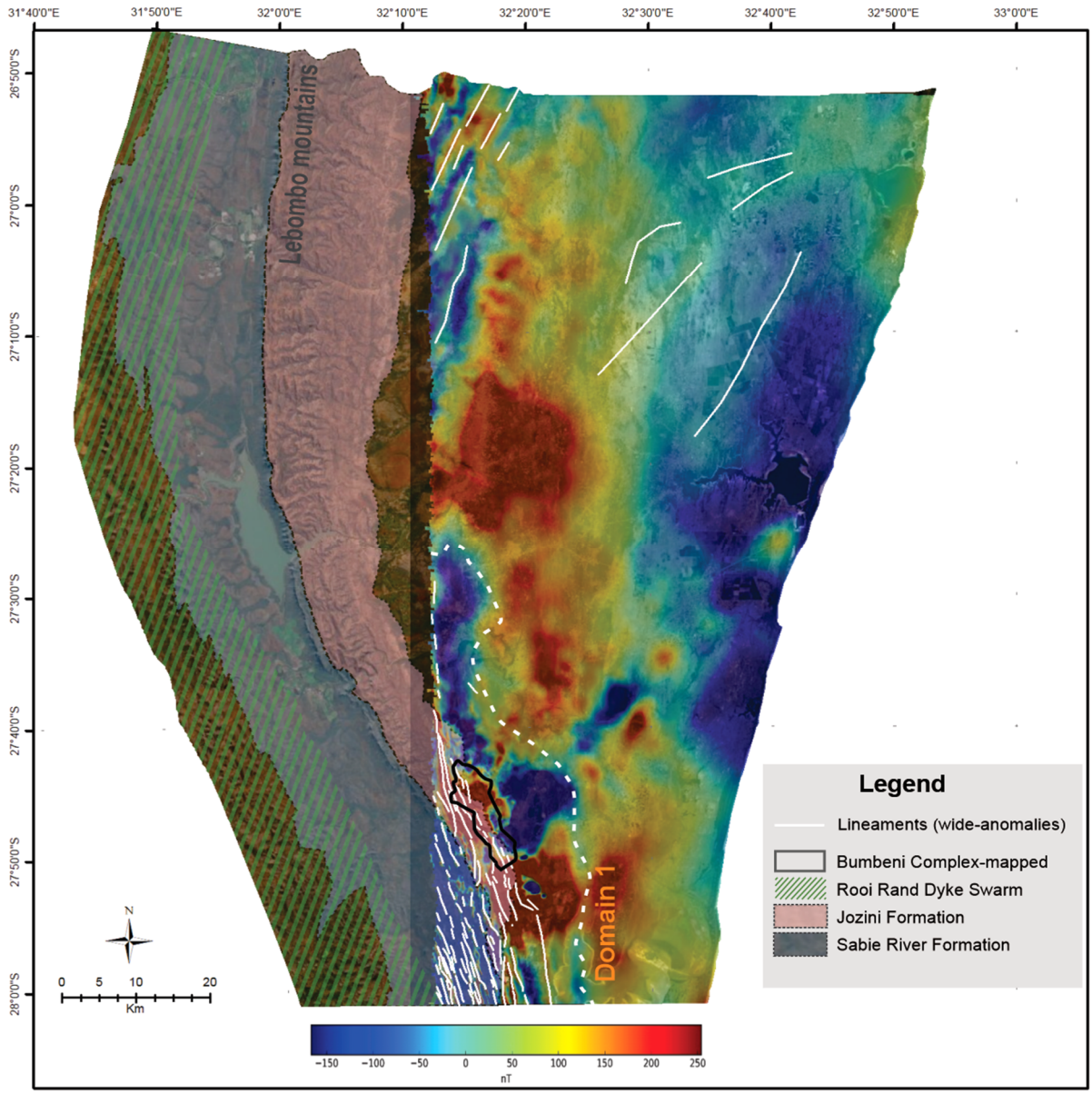

Figure 4.2: Simplified geology of the study region superimposed on the Esri satellite World Imagery (modified after the 1: 1 000 000-scale geological map of South Africa, Council for Geoscience, 2019). The Reduced-to-Pole map shows the low frequency, wide lineaments. The figure highlights the positional correlation between the wide lineaments and the Sabie River and Jozini Formations (Lebombo Group), particularly in the southern region of Domain 1. The green hatching represents the area where Rooi Rand Dykes occur, which intrude the Lebombo Group (modified after Meth, 1996 from Saggerson and Bristow, 1983). The black polygon shows the surface extent of the Bumbeni Complex.

4.3. General morphology of the Bumbeni Complex

The Bumbeni Complex occurs as two adjacent roughly circular igneous bodies, and comprises two volcanic successions, the lower mafic volcanic Mpilo Formation, and the upper felsic volcanic Fenda Formation (Fig. 4.3). The Fenda Formation consists of the pyroclastic deposits of the Nxwala Member, which appear to be developed towards the base of this formation.

Field observations indicate that the ~40-m-thick, amygdaloidal and vesicular basalts of the Mpilo Formation crop out in the northern region of the Bumbeni Complex and disconformably overlie the rhyolites of the Jozini Formation (Fig. 4.3). The Mpilo Formation is here correlated with a sub-circular high magnetic anomaly, based on the position of the mapped complex, which is typical for mafic intrusive bodies (e.g., Gunn et al., 1995) (Fig. 3.45a). Basaltic magmas typically ascend through fractures as dykes to feed basaltic lava eruptions at the surface (Gudmundsson, 1984; Muirhead et al., 2014). Therefore, based upon the positional correlation combined with the presence and extent of the high magnetic anomaly typical for mafic intrusive bodies, it is inferred that the Mpilo Formation is intrusive into the underlying Sabie and Jozini Formations and that it extends beyond the current outcrop extent.

The Mpilo Formation is unconformably overlain by the Fenda Formation, which is the most extensive formation of the Bumbeni Complex, comprising ~80% of the complex (Figs. 3.1–3.2). The Fenda Formation also overlies the Jozini Formation, particularly where the Mpilo Formation is not developed. The Mpilo Hill area comprises light grey-coloured rhyolite flows and locally banded, poorly-sorted rhyolitic pyroclastic deposits of the Fenda Formation (Fig. 3.7), where the rhyolite flows generally overlie the pyroclastic deposits. Whereas the interbedded poorly-sorted lapillistone, tuff, welded tuff, pyroclastic breccia, perlitised tuff and perlitic pitchstone of the Nxwala Member are exposed east of the Mpilo Hill, in the Pratley Perlite Mine area (Figs. 3.9–3.13). The perlite of the Nxwala Member has only been observed in the Pratley Perlite Mine area and forms as an alteration product of tuff, rhyolitic lava and obsidian flows similar to that discussed by Sa'ad et al. (2010) and Hinojosa-Prieto et al. (2016). Small-volume pyroclastic flows travel short distances and generally form thick structureless deposits (Sparks, 1976), which suggests that the presence of the pyroclastic breccia in close proximity to the source area is associated with the catastrophic collapse of an eruptive column (Sparks, 1976; Fischer, 1979). The variability in the textural appearance of these rocks combined with their lithological relationships suggests thet there were repetitive (chaotic) cycles of volcanic eruption and deposition. These repetitive cycles are attributed to various phases of dome building and collapse that typically accompany plinian-style eruptions (Bristow and Duncan, 1983).

South of the Msunduzi River, the rhyolite flows are intercalated with pyroclastic deposits comprising layers of tuff, poorly-sorted lapillistone and pumice (Figs. 3.8a and b). The individual lithological units of the Fenda Formation are up to 10-m-thick and are commonly capped by pumice-rich auto-brecciated flow-tops with individual flows identified by flow toe remnants and irregular chilled contacts (Fig. 3.8c and d). Field observations have revealed fine-grained, well-bedded tuff units that are interbedded with volcanic bombs (Fig. 3.14b). The presence of these tuff units below and above these volcanic bombs indicate that tuff accumulation occurred and at some time before and after their deposition. Furthermore, this relationship suggests episodes of violent eruption interspersed with periods of quiescence as defined by the fine-grained tuffaceous layers (Fig. 3.8b) (Walker, 1981).

The lithological units identified in the NZA drill core indicate that the basement succession comprises pyroclastic deposits. When analysing the results of this study, namely (a) the location of the NZA borehole relative to the Bumbeni Complex, (b) the textural similarities between the mapped Nxwala Member and the NZA drill core, and (c) the similarities in the major element geochemistry from pyroclastic rock samples collected in Pratley Perlite Mine area with the lithological units in the NZA borehole (Fig. 3.36) (Landman, 2017), it is inferred that the pyroclastic rocks intersected by the NZA borehole are of Fenda Formation affinity, in particular the Nxwala Member. This corroborates with the interpretations of Landman (2017) for the NZA borehole. Based on the similarities between the outcrop and borehole textures and lithological relationships, it is interpreted here that the rocks of the Fenda Formation in the southern region are a product of multiple, chaotic cycles of volcanic eruption accompanied by multiple rhyolite flows and deposition of pyroclasts, as seen in the northern region (Bristow and Duncan, 1983).

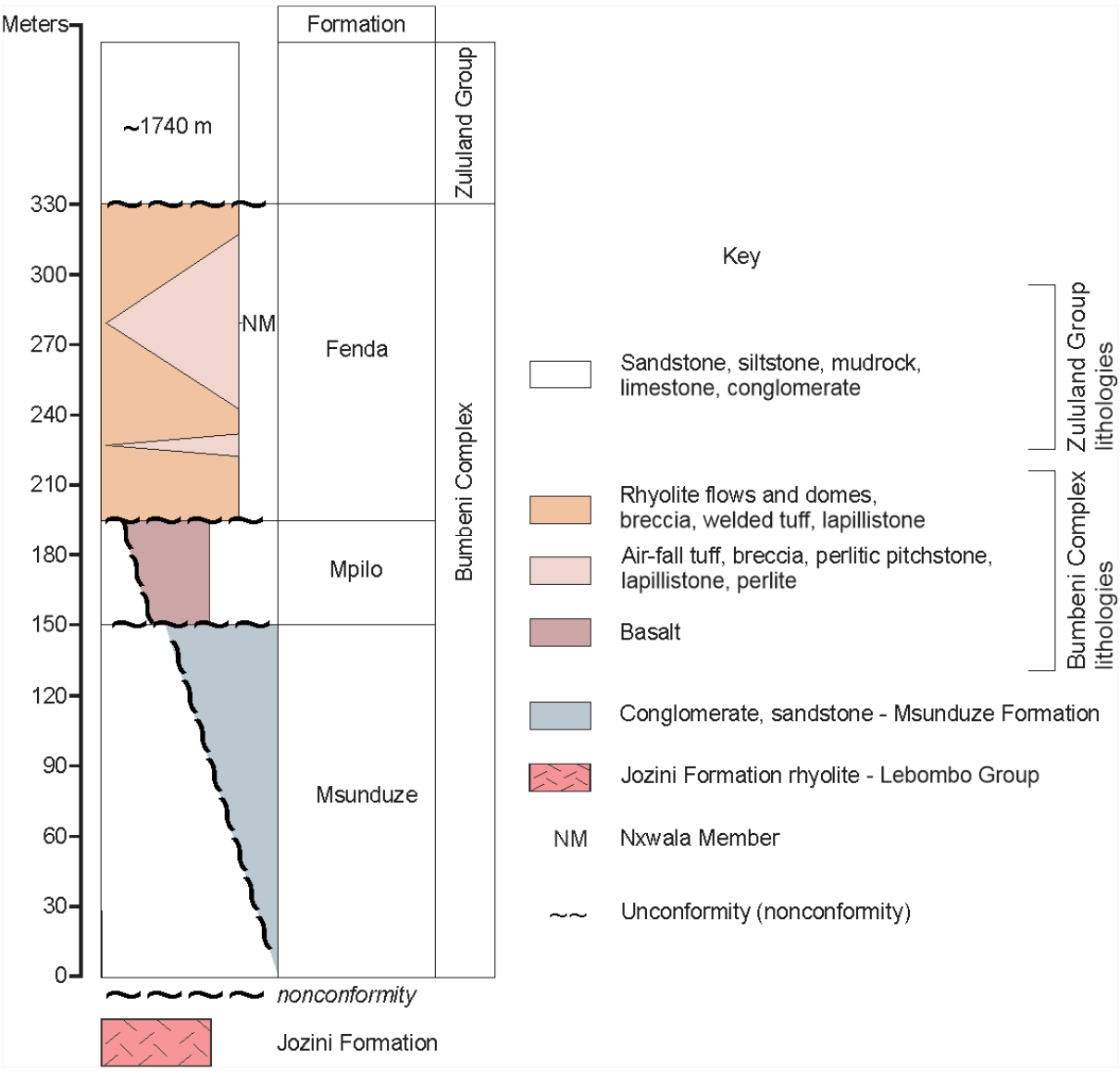

Figure 4.3: Generalised lithostratigraphic column and subdivision of the Bumbeni Complex and associated lithological units. The overlying Zululand Group that reaches a thickness of about 1740 m in the NZA borehole is also shown. Thicknesses are based on field mapping, drill core from the NZA borehole and those proposed by Cleverly and Bristow (1979) and Joubert and Johnson (1998).

From the information obtained in this study, it is inferred that the Bumbeni Complex formed as a result of a plinian eruption given that this eruption would have been characteristically violent, ejecting significant amounts of pumice accompanied by periods of dome building and collapse (Walker, 1981; Ashwell et al., 2018). This interpretation corroborates with the interpretations made by Bristow and Duncan (1983), where a small-scale eruption (~2 km^2) was inferred that equated to a relatively small magma chamber in the northern region, based on the presence of the Nxwala Member volcanics and their localised distribution. The associated magma chamber would have contained just sufficient

volatiles to cause small plinian eruptions, although not enough volatiles to cause and sustain a major eruption column (Bristow and Duncan, 1983).

In the aeromagnetic data, the distinctive, roughly circular, high frequency, magnetic low signature observed in Domain 1, which is associated with the pyroclastic rocks intersected by the NZA of possible Fenda Formation affinity, coincides with the magnetic low of the southern region of the Bumbeni Complex (Figs. 3.45a and 4.4). This indicates that these anomalies are likely the pyroclastic rocks of the Fenda Formation. It is suggested here that the roughly circular, magnetic low signature in Domain 1, most likely represents a subsurface extension of the complex. Thus, the Bumbeni Complex is larger than the surface extent as previously proposed based on gravity data (Barkhuizen, 1989).

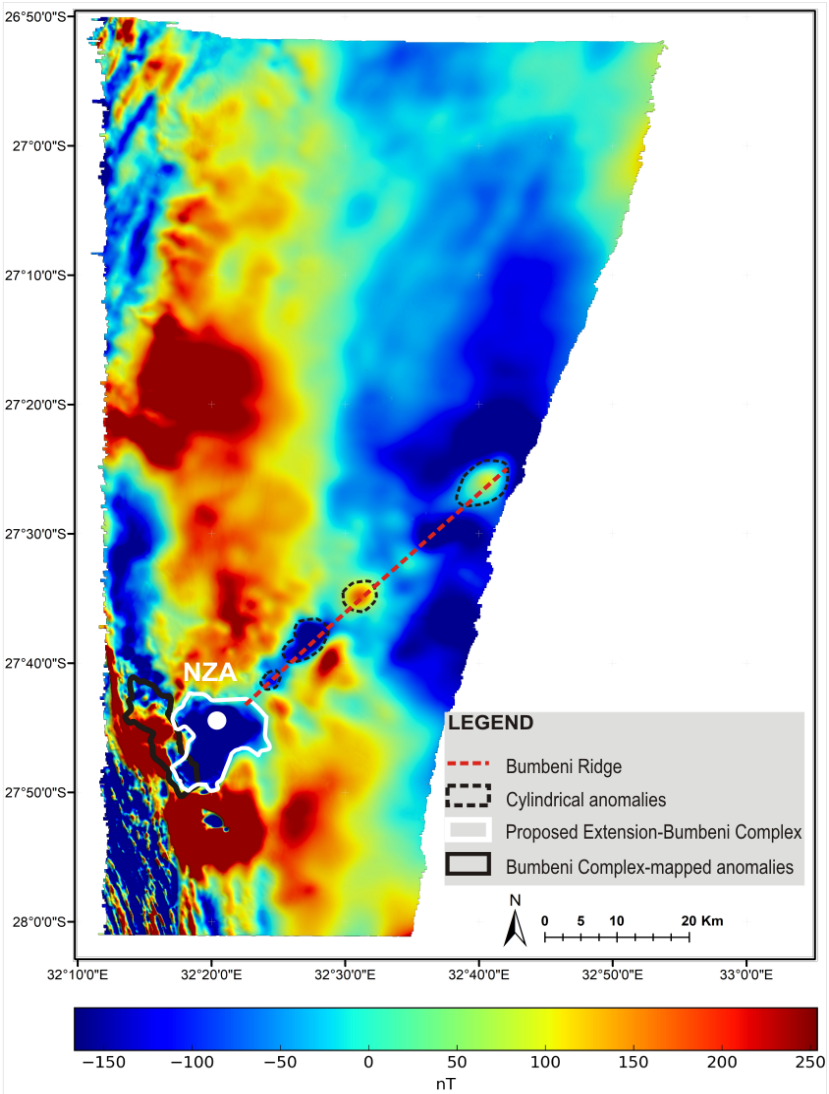

Figure 4.4: The surface extent of the Bumbeni Complex and its proposed extension (with black and white polygons, respectively) overlain on the Reduced-to-Pole map. The trend of the Bumbeni Lineament/Ridge and the position of the NZA borehole (white circle) are also shown.

4.3.1. Emplacement model for the Bumbeni Complex lithostratigraphy

The evolution of the Bumbeni Complex lithostratigraphy is here discussed in terms of an emplacement model using new and existing data (i.e., geological, geochemical and geophysical data), which involves the eruption and deposition of the Bumbeni Complex volcanics from two vents, namely the northern and southern vent regions (Figs. 3.36 and 4.5–4.7). The inferred northern eruption vent is positioned at the present location of the Mpilo Hill (Fig. 4.5). The area covered by the southern vent includes the central, southern and eastern parts of the complex with the eastern limit confined in some ~2.5 km distance southwest of the NZA borehole (Fig. 3.45). It is proposed that the eruption vents were active at some time during the Early Cretaceous after the deformation of the Jozini Formation rhyolites, based on the current age of the Bumbeni Complex of 133±5 Ma (Allsopp et al., 1984).

The northern region is characterised by ~225-m-thick sequence (Cleverly and Bristow, 1979), comprising rhyolite, a thick (>10 m) welded tuff deposit, obsidian flows, poorly-sorted pyroclastic deposits including a pyroclastic breccia, which is here interpreted as a near vent deposit derived from the collapse of an eruptive column. During emplacement and deposition of the viscous volcanic material (i.e., rhyolitic lavas), thick lithological units would develop proximal to the eruption vent, with minimal material extending to distal settings (Walker et al., 1973; Walker, 1981; Scutter et al., 1998). The areas of maximum thickness of the thick viscous lava, lava domes and thick tephra are abundant near volcanic centres and, therefore, indicate the most likely site of a vent (Self et al., 1986; MacLeod and Sherrod, 1988). Hence, it is inferred that the Fenda Formation formed proximal to a northern volcanic vent as the close spatial association of pyroclastic rocks with relatively thick welded tuff and obsidian flows (characterised by perlitic pitchstone in outcrop) is consistent with characteristics of proximal facies in other volcanic deposits (e.g., Korringa, 1973; Sparks et al., 1999). Although the distance of deposition from the source varies, some ash-fall tuff deposits (e.g., in areas farther than ~2 km north of this proposed vent location) most likely represent distal deposits. It is therefore concluded, based on field relationships, lithological characteristics and thicknesses, that the geology of the Bumbeni Complex in this region is in close proximity to a volcanic vent.

The existence of a southern vent is interpreted due to the presence of rhyolite flows, with short flow lengths (~1.2 m-long flows), containing chilled margins and preserved flow toes, which are inferred as forming proximal to vent emplacement (Walker et al., 1973; Harris and Rowland, 2009; Magnall et al., 2017). This southern region of the complex also reveals a proximal-to-source succession of tuff and angular-clast-dominated, poorly-sorted lapillistone similar to that found in the northern region. The field relationships and textural similarities combined with the proximal-to-source deposition

interpreted here for the Nxwala Member (in outcrop and in the NZA drill core) suggests that these rocks represent near-vent emplacement (Korringa, 1973; Walker, 1981; Sparks et al., 1999).

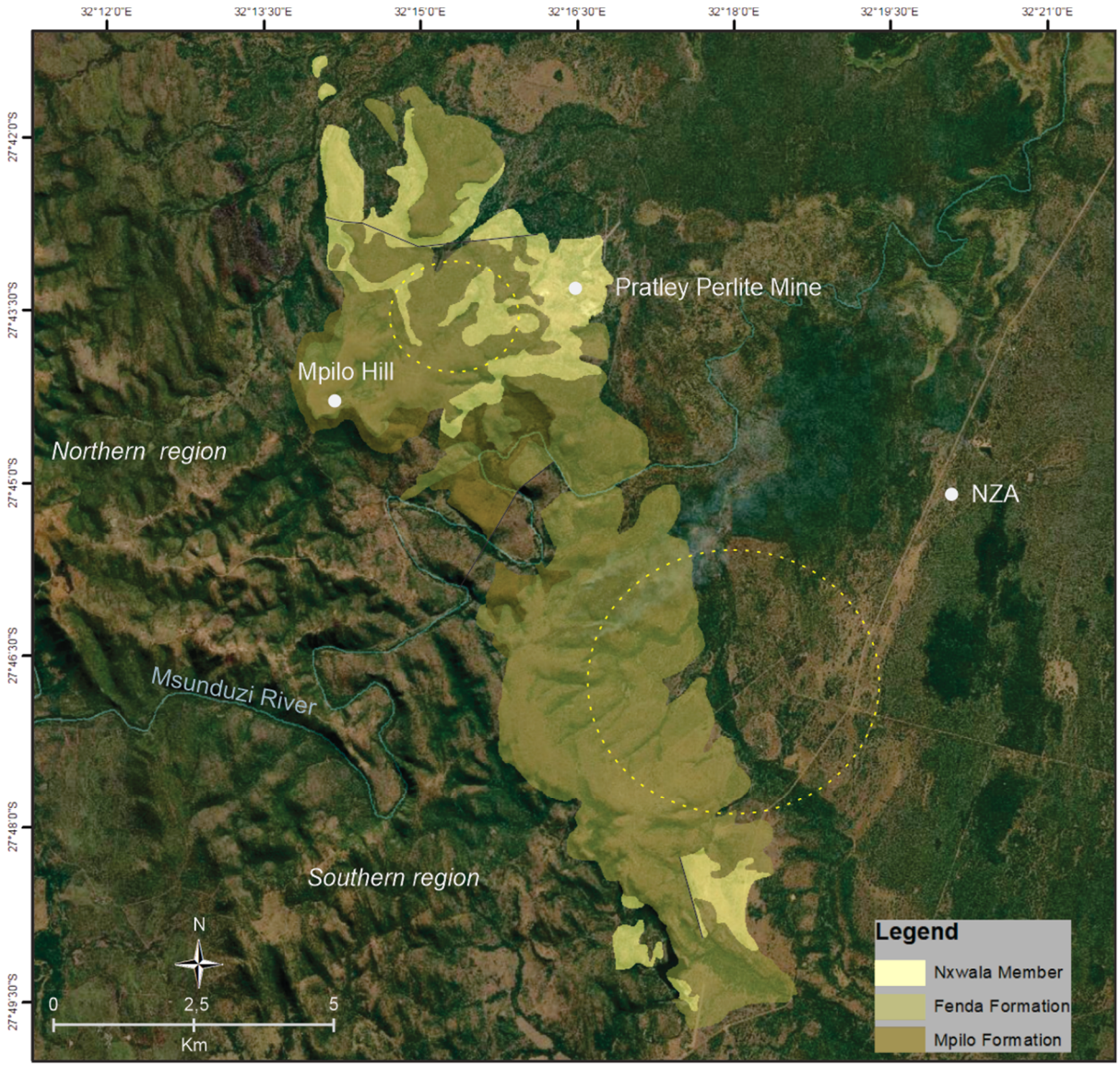

Figure 4.5: An Esri satellite World Imagery showing the mapped Bumbeni Complex (draped with the geological map as shown in Figures 1.6, 3.1 and 3.2). This figure also highlights the location of the proposed vent regions (highlighted with yellow circles) south and north of the Msunduzi River and the location of the NZA borehole. One eruption site is located in the northern region in the vicinity of the Mpilo Hill and the other in the southern region (more details on the eruption sites and associated lithological units are available in Figures 4.6 and 4.7).

Although compositional similarities between the rocks of the Nxwala Member in the northern region and those of the NZA borehole (southern region), have been observed in this study based on the available analytical data (in particular major element data) (Fig. 3.36) (Landman, 2017), it is difficult to infer that the magma source for the regions was the same. Trace element data for the rocks in the separate regions would be useful and could potentially provide evidence that these rocks originated

from a single magma chamber, as these analyses are useful in determining the origin and evolution of igneous rocks, however that is beyond the scope of this study. Based on this uncertainty towards a single magma chamber for the southern and northern regions of the complex and geochemical similarities in rocks of both regions, it is assumed here that the felsic rocks of the Bumbeni Complex may have formed from two geochemically similar felsic magma chambers, a northern and southern magma chamber, similar to that described by Walker (1981). It follows, based on the lithological relationships, the suggested vent regions and the assumption that felsic rocks of the Bumbeni Complex originated from two geochemically similar but separate felsic magma chambers, that the Cretaceous Bumbeni Complex represents a volcanic system with loci of eruptions in the north and south of the complex (Figs. 4.5–4.7).

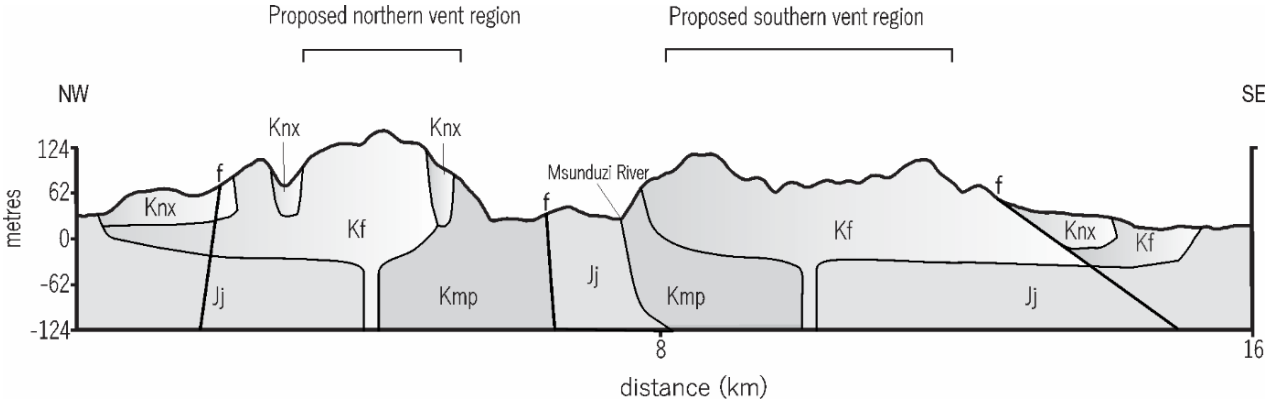

Figure 4.6: A NW-SE oriented idealised cross section across the Bumbeni Complex which intrudes the Lebombo Group. The cross section is representative of the surface geological relationships and postulated subsurface intrusion of the complex into the Lebombo Group. These lithological relationships are described in Section 3.1.1.3 with a schematic representation shown in Figure 4.7. The position of the cross section line is shown in Figure 3.2. The lithological units are coded according to the South African Committee for Stratigraphy (SACS); Jozini Formation (Jj), Mpilo Formation (Kmp), Fenda Formation (Kf) and Nxwala Member (Knx). The vertical scale is presented as elevation in metres (m) and as depth above and below mean sea level, respectively. The distance is presented in kilometres along the cross section line.

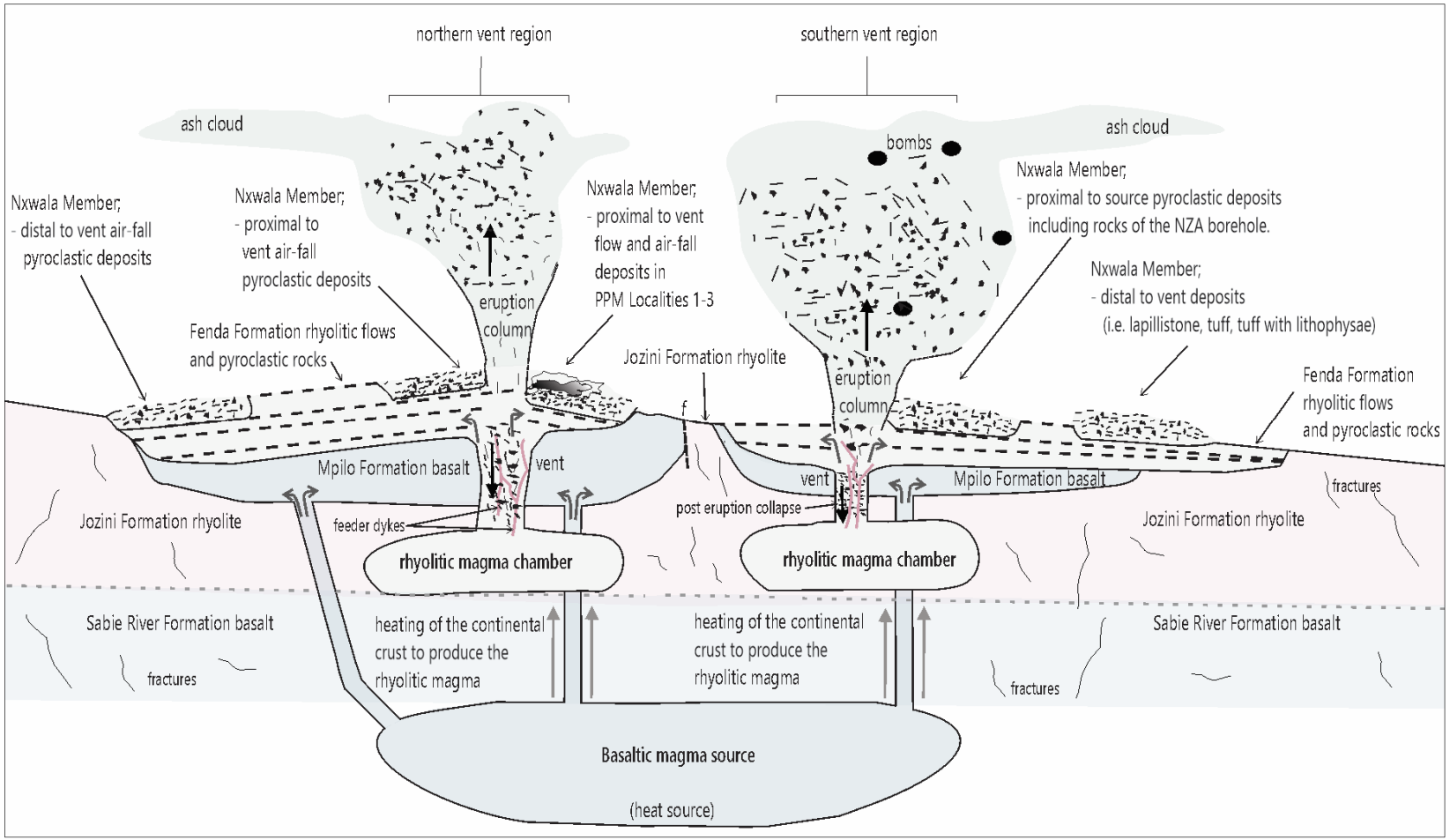

Figure 4.7: Schematic presentation showing the emplacement model proposed for the Bumbeni Complex lithostratigraphy (not to scale) and the intrusive relationship between the complex and the Sabie River and Jozini Formations. This diagram, from bottom to the top, shows the ascending basaltic magma which produced the Mpilo Formation lavas. This ascending hot basaltic magma generated a wide zone of melting of the continental crust and the acidic melts were produced in magma chambers. These acidic melts fed the volcanic activity most likely through feeder dykes (pink lines) which exploited pre-existing fractures. The Fenda Formation lithological units were formed from the repetitive (chaotic) cycles of volcanic eruption and deposition through the northern and southern vents. Intermittent post eruption collapse may have occurred in both the vents and on their flanks (black arrows in vents).

The mapped Bumbeni Complex is associated with the NNW-SSW deep-seated linear structures observed in the aeromagnetic data which are here correlated with the faults observed in the Jozini Formation. It is postulated that the Bumbeni Complex magma migrated to the surface through pre-existing fractures similar to that described by Goss et al. (2009), which are abundant in the area (Figs. 3.45, 4.2 and 4.6). This process is commonly seen along continental margins where magma chamber growth and evolution favour pre-existing structures (Hughes and Mahood, 2011).

The Bumbeni Complex, characterised by non-parallel, undulatory and non-systematic joint sets, which reveal NW-SE, NE-SW, N-S and minor E-W orientations, shows no evidence of major faults and only two small-scale (30 to 40-cm-wide), NE-SW and NW-SE oriented faults were observed in tuff units. Furthermore, no magnetic linear structures could be correlated here to any faulting in the Bumbeni Complex. It is proposed here, based on the non-systematic nature of the joint sets and the lack of any known post-Bumbeni Complex deformational event, that the joint sets developed in the complex were most likely caused by cooling or exhumation subsequent to erosion (e.g., Rogers et al., 1996; Arlegui and Simón, 2001; Weinberger et al., 2010). It is further proposed that the small-scale faults here are locally developed and cannot be associated with any known major tectonic event, perhaps they may have been produced by localised movement along joint surfaces, triggered by the chaotic cycles of volcanic eruption and column collapse. It is evident here, based on field evidence, structural and magnetic data analyses, that the structural framework of the Bumbeni Complex is distinctly different to that of the Sabie River and Jozini Formations (Lebombo Group).

4.4. Processes that led to the development of the Bumbeni System

4.4.1. The Bumbeni Ridge

The Bumbeni Lineament, which divides Domains 2 and 4 in the aeromagnetic data, and extends northeast from the proposed extension region of the Bumbeni Complex, comprises northeast-striking, disjointed cylindrical anomalies that are typical for plutonic bodies with remanent and normal magnetisation (Figs. 3.45 and 4.4). These cylindrical anomalies are in close proximity to the ZD, ZG and ZB boreholes, which intersect both mafic and felsic rocks at the base (Figs. 3.41 and 3.45). Based on the close proximity of the cylindrical anomalies and the presence of the volcanic basement rocks of the ZD, ZG and ZB boreholes, it is envisaged here that these anomalies are a result of plutonic bodies. These northeast trending plutonic bodies define the Bumbeni Ridge (Barkhuizen, 1989; Shone, 2006). It is further postulated here that the magma responsible for these plutonic bodies migrated upward through pre-existing fractures similar to that described by Goss et al. (2009) and Hanyu et al. (2017). Furthermore, based on the presence of positive and negative polarity periods in the Cretaceous

revealed by the geomagnetic timescale, it is inferred that these plutonic bodies are indicative of emplacement during positive and negative polarity periods which prevailed during the Cretaceous (Gradstein, 2012; Ogg et al., 2016; Hanyu et al., 2017).

4.4.2. Evolution of the Bumbeni Complex and Ridge

It is critical to produce a comprehensive evolution model of the Bumbeni Complex and Bumbeni Ridge to account for the orientation of the ridge and the presence of the complex at the south-western edge of the ridge. Thus, the processes that are attributed to the development of the volcanism responsible for the Bumbeni Complex and the Bumbeni Ridge are outlined here.

The field evidence reveals that the Bumbeni Complex comprises basaltic and rhyolitic rocks of the Mpilo and Fenda Formations, respectively, indicating bimodal volcanism. During ascension, the hot basaltic magma which produced the Mpilo Formation lavas, would have generated a wide zone of melting of the continental crust producing the acidic magma chambers responsible for the Fenda Formation (Fig. 4.7). The migration of the magma, from depth to surface, would have been facilitated by pre-existing fractures. These interpretations corroborate with bimodal basalt-rhyolite evolution related to areas of crustal extension in continental settings (Bhushan, 2000). Furthermore, they also corroborate with the interpretations made by Verma (2001) for (intracontinental) bimodal volcanism of the Meseta Río San Juan (Mexico), where basaltic magmas are ascribed to partial melting of the lithospheric mantle and the formation and eruption of rhyolitic magmas attributed to upwelling of the mantle and extensional tectonics. Therefore, it is suggested here that the bimodal volcanism related to the formation of the Bumbeni Complex, is typical for areas undergoing crustal extension. This is most likely related to local extension associated with the upwelling of the sublithospheric mantle. Although no chronological data are known for the volcanic rocks correlated here with the Bumbeni Ridge, the close spatial association of the magnetic reversals along the magnetised plutonic bodies defining the ridge (in Domains 2) with that of the proposed extension region of the Bumbeni Complex, suggest that these features are genetically related (Fig. 4.4). The magmas that produced these plutonic bodies would have ascended to shallower depths, most likely through weakened and stretched/thinned portions of the lithosphere (Anderson, 1994). Therefore, there must have been local extension along the ridge to allow for their intrusion (Bhushan, 2000; Tibaldi et al., 2017).

The upwelling of the sublithospheric mantle, which is considered here responsible for the formation of the Bumbeni Complex and the presence of the plutonic bodies defining the Bumbeni Ridge, requires a heat anomaly. There are two possible mechanisms of formation proposed here; (1) the presence of

a volcanic hot-spot activity and (2) upwelling of asthenopheric melt linked to crustal thinning during Gondwana break-up or potentially a combination of the two.

Firstly, it is possible that the origin of both the Bumbeni Complex and the Bumbeni Ridge could be related to mantle plume formation or volcanic hot-spot activity. Such a plume-related heat source could potentially be the Bouvet hot-spot as the hot-spot track has been aligned with the Lebombo mountain range (Fig. 4.8a) (Morgan, 1981, 1983) and its location in the Natal Valley (Figs. 4.8b and c), between South Africa and Antarctica, at ~140 Ma (Fig. 4.9) (Golonka and Bocharova, 2000). This occurred at a similar time to the creation of the Parana-Etendeka Provinces that were closely related to the Tristan da Cunha hot-spot during the opening of the Atlantic Ocean (Figs. 4.8c and 4.9) (Martin, 1987; Golonka and Bocharova, 2000; Mohriak et al., 2002). A hot-spot heat anomaly does not only affect the region directly above it, but it also influences areas further away from the hot-spot centre (Martin, 1987). This conclusion was reached by Martin (1987) after a Bouvet hot-spot related chemical anomaly was identified, which extended ~500 km east of the Bouvet Island. Based on along-isochron bathymetric and gravity anomalies of five hot-spots, Ito and Lin (1995) also showed that hot-spots produced mantle temperature anomalies that influenced ridge structures to a maximum distance of ~500 km, corroborating the conclusion reached by Martin (1987). Therefore, based on the ~140 and 120 Ma positions of the Bouvet hot-spot (Figs. 4.8a, c and 4.9), it is suggested here that the Bouvet hot-spot may have provided the heat anomaly that produced magmatism and plutonism in the Northern Natal Valley and in the regions currently occupied by the Bumbeni Complex and Ridge (Figs. 4.8 and 5). It is envisaged here that the hot-spot related heat anomaly was not effective enough to cause a significant melting anomaly to produce significant volumes of magma, based on the localised occurrence of the Bumbeni Complex.

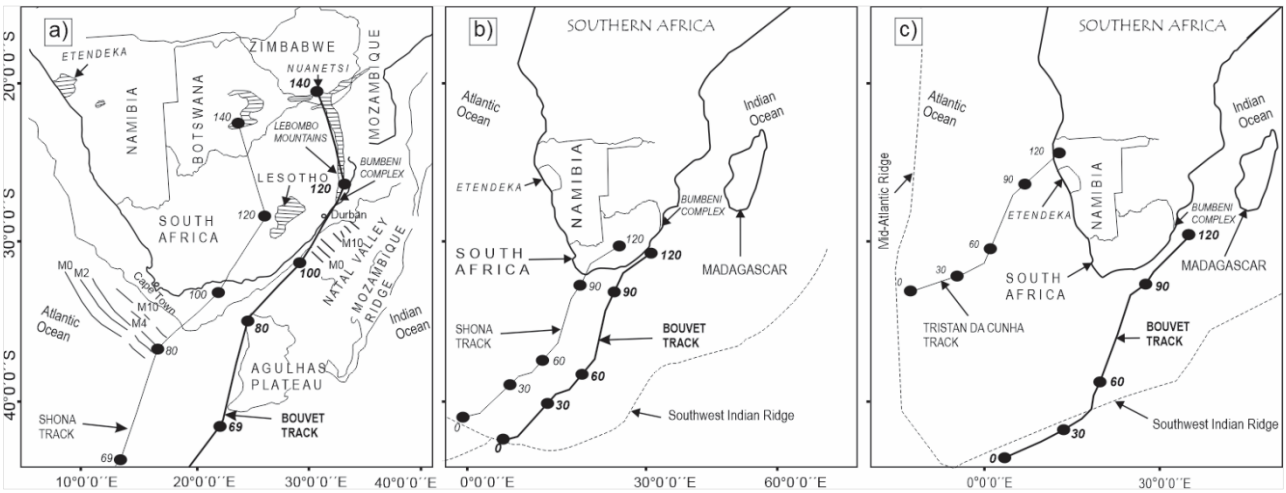

Figure 4.8: The modelled hot-spot tracks with similar ages of the Bouvet, Shona and Tristan da Cunha tracks, which are represented by solid lines with black dots. The dots are associated with ages, in millions of years, of radiometrically dated locations. (a) The location of the Bouvet hot-spot track relative to the Lebombo mountains (between 140–120 Ma), the Bumbeni Complex and the Northern Natal Valley (modified after Martin, 1987). (b) The Bouvet hot-spot track is located in the Natal Valley at 120 Ma and south of the Bumbeni Complex (modified after Duncan and Richards, 1991). (c) The Bouvet hot-spot track is situated in the Northern Natal Valley and it is adjacent to the onshore location of the Bumbeni Complex (modified after Morgan, 1981).

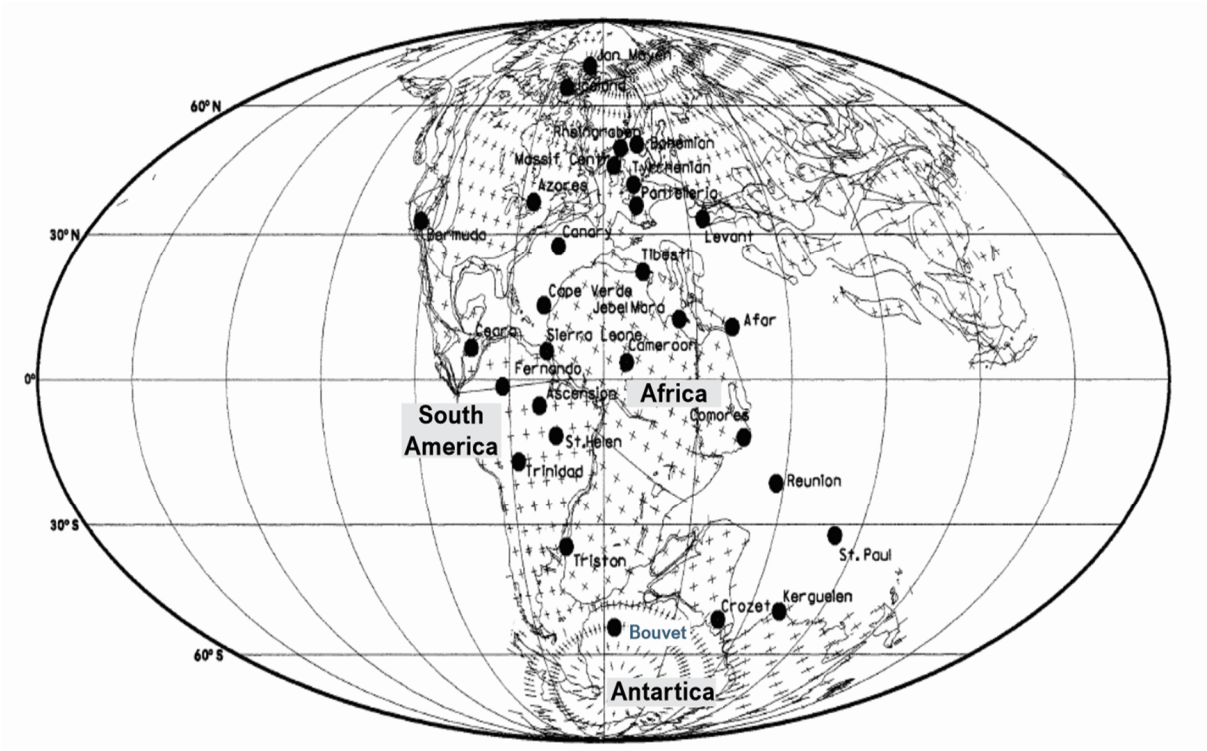

Figure 4.9: The Cretaceous (140 Ma) position of the major hot-spots associated with Pangea. Note the positions of the Bouvet (blue text) and Tristan da Cunha hot-spots. Modified after Golonka and Bocharova (2000) (Refer to Appendix 9 for the original map of the major hot-spots).

Although the Bouvet hot-spot hypothesis regarding the development of the Bumbeni Complex and Ridge is plausible, the presence of a hot-spot alone cannot account for the localised Bumbeni Complex volcanism and the orientation of the ridge. It follows that a second mechanism of formation requires investigating. The study region including the Lebombo mountains, the Maputaland Plain and the associated offshore region of the Northern Natal Valley, were affected by extensional stresses related to the Gondwana break-up event, about ~183–130 Ma (Cox, 1992; Watkeys, 2002; Hanyu et al., 2017). This period was associated with lithospheric thinning accompanied by extensional faulting and mafic intrusions associated with these faults (Cox, 1992; Hanyu et al., 2017). The Northern Natal Valley region adjacent to the Bumbeni Ridge is characterised by NE-SW and E-W oriented positive and negative magnetic anomalies on the Earth Magnetic Anomaly Grid data (Fig. 5a). Tikku et al. (2002) identified an extinct E-W oriented spreading centre, based on these magnetic anomalies, which was active ~133–125.3 Ma. When the orientation and extent of the Bumbeni Ridge is extrapolated offshore into the Northern Natal Valley, it correlates with an E-W oriented magnetic anomaly (Fig. 5a), which corresponds with the paleo-position of the extinct E-W oriented spreading centre proposed by Tikku et al. (2002) (Fig. 5b). The presence of this extinct spreading centre is likely associated with the Gondwana break-up related sea-floor spreading event in the Northern Natal Valley, which caused a north-south movement between the Mozambique Ridge and Africa, at ~160–125 Ma (Tikku et al., 2002).

Thus, the volcanism along the Bumbeni Ridge and the position of the Bumbeni Complex is attributed here to this extinct E-W oriented spreading centre, which is in contrast to Watkeys (2002) who attributed the formation of the complex to both the opening of the South Atlantic Ocean and the extraction of the Falkland Plateau from the Northern Natal Valley at ~133.5 Ma. The correlation of this extinct spreading centre with the Bumbeni Ridge is based on the extrapolation of its paleo-position and magnetic signatures, in the aeromagnetic data, with the position of the Bumbeni Ridge (Fig. 5a). Furthermore, the volcanism along the Bumbeni Ridge parallels deep crustal structures, associated with the Gondwana break-up event, developed in the offshore Northern Natal Valley (Fig. 5) (Tikku et al., 2002; Hanyu et al., 2017). This extinct E-W oriented spreading centre caused crustal weakness and localised extension in the Northern Natal Valley and most likely in the onshore region along the current position of the Bumbeni Ridge (Fig. 5a). This crustal extension would have influenced the upwelling of sublithospheric mantle and the inception of the Bumbeni volcanic activity and extension of the volcanism along the Bumbeni Ridge. Furthermore, the proposed NW-SE extension direction along the ridge is consistent with its NE orientation (Fig. 5a). This mechanism possibly eliminates the need of the Bouvet hot-spot activity. It is therefore suggested here, that the Bumbeni event formed along an onshore failed rift system attributed to the offshore extinct spreading centre. Furthermore, this failed

rift system, based on the NE-orientation of the Bumbeni Ridge, would have utilised a similarly oriented pre-existing weak zone, here attributed to the initial stages of Gondwana break-up (Cox, 1992; Watkeys, 2002). These interpretations corroborate with those of Hanyu et al. (2017) for the NE-SW and NW-SW oriented mafic intrusions in the Northern Natal Valley, which utilised zones of weakness, such as extensional faults, in the stretched continental crust. The stretching of the continental crust and the zones of weakness were attributed to the initial stages of Gondwana break-up at ~183 Ma (Hanyu et al., 2017). Furthermore, Leinweber and Jokat (2012) have suggested southeast movement of Antarctica relative to Africa between 159.1–124.8 Ma during Gondwana break-up. Therefore, the offshore extensional structures remnant from this process would be NE-SW oriented, similar to the orientation of the Bumbeni Ridge, and regions of weakness.

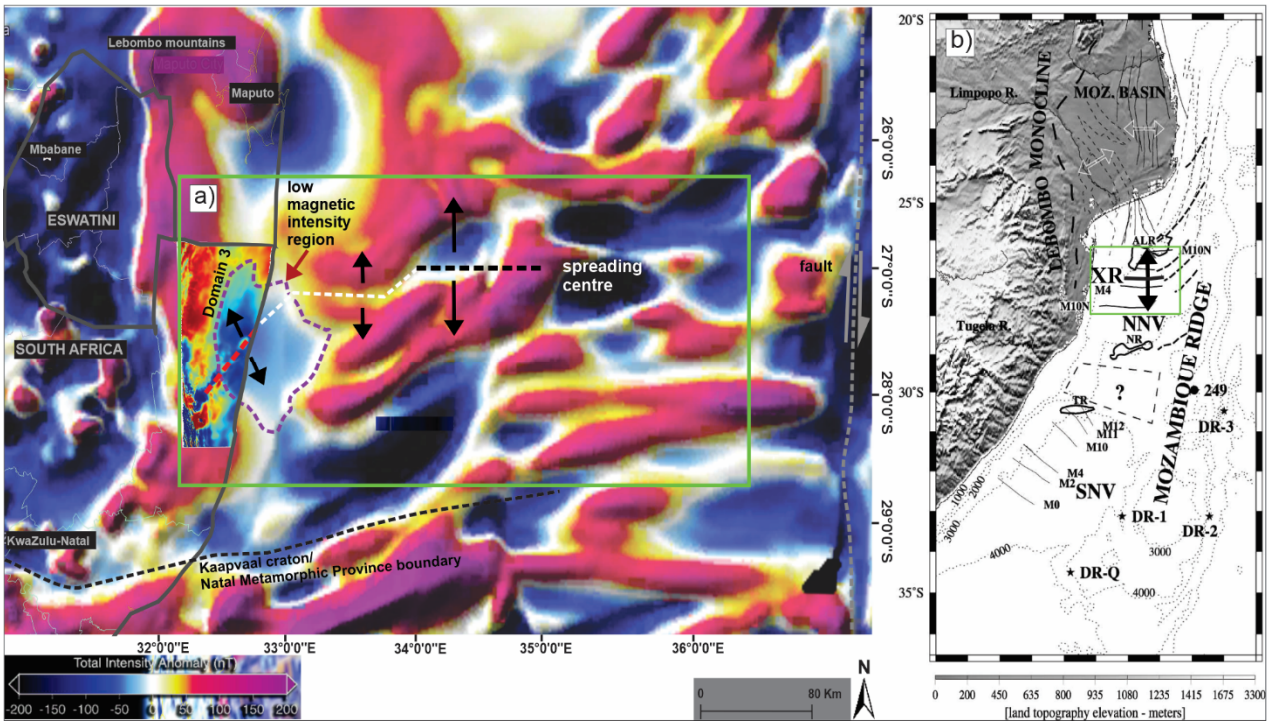

Figure 5: (a) The Total Magnetic Anomaly map, in this study, superimposed on the Earth Magnetic Anomaly Grid data (modified after Maus et al., 2009). The Earth Magnetic Anomaly Grid data reveals the NE-SW and E-W oriented positive and negative magnetic anomalies which are displaced by a transform fault towards the east. This figure shows the extrapolation of Domain 3 (purple polygon) and the Bumbeni Ridge (dashed red line) into the offshore region. The Bumbeni Ridge correlates well with the offshore intermediate magnetic anomalies (dashed white line) and the position of the E-W oriented extinct spreading centre proposed by Tikku et al. (2002). The paleo-position of the extinct spreading centre is highlighted with a dashed black line and the black arrows show the N-S extension related to the spreading centre. Note the grey arrows associated with the dashed white line and the Bumbeni Ridge show the localised extension directions consistent with the orientations of the associated structures as interpreted in the aeromagnetic data. (b) Topographic map showing the E-W oriented extinct spreading centre (XR) proposed by Tikku et al. (2002), in the Northern Natal Valley, highlighted with a green rectangle; the black arrows show a N-S spreading direction. Key: NNV (Northern Natal Valley), SNV (Southern Natal Valley) (from Tikku et al., 2002).

In summary, the Bumbeni Complex reveals bimodal volcanism, which is attributed here to localised extension of the continental crust associated with the upwelling of sublithospheric mantle. This scenario is attributed to both the presence of distal Bouvet hot-spot and the extinct E-W trending spreading centre located in the Northern Natal Valley at ~133–125.3 Ma, based on its paleo-position. It appears however that the Bouvet hot-spot contributed a minimal heat anomaly in the region occupied by the Bumbeni Complex and Ridge whereas it could have had more influence in the Northern Natal Valley, based on its paleo-position as shown in Figures 4.8 and 4.9. The localised extension associated with the upwelling of the sublithospheric mantle and the preferential ascension of the magma related to the plutonic bodies defining the Bumbeni Ridge proposed here, appear to have been more influenced by localised extension as a result of the presence of a once- active spreading centre. Thus, the formation of the Bumbeni event is interpreted here to be a combination of these processes, based on the known ages of the complex and the hot-spot tracks, and that the Bumbeni Complex represents a paleo-volcanic centre, which formed along a failed rift system.

4.5. Implications for the KwaZulu-Natal Province east edge and Gondwana break-up

The regional tectonic framework relevant to the study area includes the onshore and offshore events related to Gondwana break-up, which commenced in the Early Jurassic (Hawkesworth et al., 1999; Watkeys, 2002) and was responsible for the development of the southern African margin (Cox, 1992; Watkeys, 2002; Leinweber et al., 2013; Mueller and Jokat, 2019). The development of this margin including the Mozambique Coastal Plain and the Northern Natal Valley is a product of prolonged tectonic history related to the various stages of the Gondwana break-up event (Cox, 1992; Watkeys and Sokoutis, 1998; Jokat et al., 2003; Mueller and Jokat, 2019).

The Maputaland Plain forms part of the Mozambique Coastal Plain and occurs adjacent to the Northern Natal Valley. The crustal architecture of the crust underlying these regions is significant in understanding the effects the break-up of Gondwana had on the evolution of the study area. Previous studies have proposed either a continental crust (e.g., Dingle and Scruton, 1974; Moulin et al., 2020) or an oceanic crust for this region (e.g., Martin and Hartnady, 1986; Leinweber and Jokat, 2012). Hanyu et al. (2017) suggested that this basement consists of stretched continental crust littered with mafic volcanic intrusions. Mueller and Jokat (2019) have recently proposed an oceanic crust or crust transitional between continental and oceanic for the Mozambique Coastal Plain and the Northern Natal Valley and delineated the Continental-Oceanic Boundary.

In light of the still speculative nature of the basement crust in the Maputaland Plain and the Northern Natal Valley, the magnetic signature in Domain 3 has been interpreted here in combination with the

available Earth Magnetic Anomaly data (Figs. 3.45 and 5a) (Maus et al., 2009). This will allow conclusions to be made about the tectonic evolution and the nature of the crust in this region, particularly the Maputaland Plain and the adjacent offshore Northern Natal Valley region.

Domain 3, as previously mentioned, is defined by a broad zone of low magnetisation mainly in the Total Magnetic Anomaly and Reduced-to-Pole data sets (Figs. 3.43 and 3.45a). This zone correlates with a low magnetic region offshore, which is observed from the Earth Magnetic Anomaly Grid map (Fig. 5a). This offshore region is bound to the east by NE-SW and E-W oriented positive and negative magnetic anomalies, which are displaced by a transform fault towards the east (Fig. 5a). This study suggests that this onshore zone of magnetic low intensity in Domain 3 extends offshore in the Northern Natal Valley (Fig. 5a). Furthermore, the NE-SW and E-W oriented positive and negative magnetic anomalies do not show the classic sea-floor-spreading related (i.e., stripe-like) magnetic anomaly pattern caused by basaltic lavas erupting from mid-oceanic ridges during normal and reversed polarity periods (e.g., Florio et al., 2011; Bridges et al., 2012). Similarly, recent studies that utilised high-resolution magnetic and gravity data sets have not defined any well-expressed spreading anomalies for the study area and the adjacent Northern Natal Valley region (Leinweber and Jokat, 2011; Hanyu et al., 2017; Mueller et al., 2019). When this negative magnetic intensity zone is extrapolated offshore it indicates a region of low crustal magnetisation, combined with the absence of alternate reverse and normal polarity anomalies, which are representative of true seafloor spreading. Therefore, it is suggested here that this onshore and offshore region of magnetic low intensity extending from Domain 3 to the Northern Natal Valley is most likely a zone of thinned continental crust. This interpretation corroborates with the interpretation by Hanyu et al. (2017) who proposed thinning of the continental crust attributed to stretching, based on the distribution of magnetic intensity. Similarly, previous studies have also proposed a continental crust for the Northern Natal Valley (e.g., Dingle and Scruton, 1974; Moulin et al., 2020). The presence of the NE-SW and E-W oriented magnetic high and low structures in the adjacent offshore region of the Northern Natal Valley, are most likely related to mafic intrusions that intruded during positive and negative polarity periods (König and Jokat, 2010; Hanyu et al., 2017). Volcanic intrusions generally prefer regions of crustal weakness (Hastie et al., 2013; Tibaldi et al., 2017), therefore, it is inferred that these mafic intrusions may have exploited regions of weakness such as extensional fractures that were formed by paleo-extensional events most likely related to the initial stages of Gondwana break-up (Watkeys and Sokoutis, 1998; Watkeys, 2002). Furthermore, the southeast movement of Antarctica relative to Africa between 159.1–124.8 Ma during Gondwana break-up suggested by Leinweber and Jokat (2012) would have been associated with NE-SW oriented, remnant extensional structures likely representing regions of weakness. The normal magnetised plutonic bodies in Domain 3 would represent younger

plutonic bodies that intruded the onshore region of the stretched continental crust (Fig. 3.45a). The extensional stresses responsible for the stretching of the continental crust in the onshore and offshore regions are related to the formation of the passive continental margin during the break-up of Gondwana (~185–130 Ma) (Watkeys, 2002; Hanyu et al., 2017).

5. Conclusions

This study provides the most recent comprehensive interpretation of high-resolution aeromagnetic data, in conjunction with brittle deformation structures, over the Zululand Basin, with the aim of contributing towards understanding the tectonic framework of the basement geology and structural evolution of the Bumbeni Complex and Bumbeni Ridge.

The structural data obtained during field work has played an important role in defining the difference in the tectonic framework between the rhyolites of the Jurassic Lebombo Group, and the Early Cretaceous Bumbeni Complex. Furthermore, the analysis and interpretation of high-resolution aeromagnetic data also suggest markedly different tectonic events affecting the different lithological units. The deformation is defined by the difference in the tectonic framework, grouped into Domains 1–4, across the study region.

From this study the following conclusions can be drawn for tectonic deformation of the study area and the origin and structural evolution of the Bumbeni Complex and Bumbeni Ridge;

- The complex tectonic deformation of the Lebombo Group is related to the Gondwana break-up event, which commenced in the Early Jurassic (~180 Ma) and involved faulting and E-W oriented rifting along the Lebombo mountains. The evidence from this study is in accordance with three of the previously defined deformation events that affected the Lebombo Group, and can be related to the stages of Gondwana break-up, with the first event being constrained between ~180–175 Ma, and the second and the third episodes constrained between 175–155 Ma and 155–135 Ma, respectively.
- The NNE–SSW oriented faults that occur in the Sabie River Formation are consistent with E-W oriented tectonic extension. These faults are here ascribed to the E-W oriented paleo-extensional tectonic event of the initial stages of Gondwana break-up (~180–175 Ma).
- The majority of normal and strike-slip faults occur in the competent rhyolites of the Jozini Formation. Its is suggested here that the major normal fault is consistent with a regional E-W directed extensional event of stage one of Gondwana break-up at ~180–175 Ma. The NW-SE orientation of this normal fault most likely resulted from block rotation during subsequent tectonic tilting (eastward) of the Lebombo Group volcanics.
- The NW-SE orientation of this normal fault most likely resulted from block rotation during subsequent tectonic tilting (eastward) of the Lebombo Group volcanics.

- This study has shown that the N–S orientations of the dextral strike-slip faults and the systematic joint sets occurring in Jozini Formation rhyolites are representative of a dextral strike-slip regime, which can be interpreted on a dextral Riedel shear system. The formation of these dextral strike-slip faults suggests that a rotation in the paleo-stress regime from a vertical σ_1 to a horizontal NE-SW oriented σ_1 may have occurred during deformation. This second deformation event (175–155 Ma) is attributed here to the offshore, dextral strike-slip movement of the Gastre Fault-Agulhas Falklands Fracture Zone system related to stage two of Gondwana break-up.

- Lineament analysis of structures using aeromagnetic data has defined four distinct magnetic domains (Domains 1–4), which are defined by their structural framework. The N-S oriented low frequency, deep seated lineaments in the SW region of Domain 1, correlate well with the Lebombo Group. These linear structures are likely related to the N-S oriented faults occurring in the Jozini Formation rhyolites, which are associated with the E-W oriented spreading attributed to the initial stages of Gondwana break-up (~180–175 Ma).

- The cross-cutting relationships revealed by the E-W and NE-SW oriented shallow structures, most likely fractures, of Domains 2, 3 and 4 suggest that the shallow structures occurred at different times and post-date the occurrence of the deep structures and most likely the Bumbeni Lineament. These shallow structures are related to the second deformation event which is constrained between stages 2 and 3 (175–135 Ma) of Gondwana break-up.

- The structural framework of the Sabie River and Jozini Formations is different to that of the Bumbeni Complex and Ridge, suggesting the deformation in the Lebombo Group occurred prior and/or during the eruption and intrusion of the Bumbeni Complex.

- The field evidence of both basaltic and rhyolitic rocks of the Mpilo and Fenda Formations of the Bumbeni Complex reveals bimodal volcanism typical of rift related extension.

- The formation of the Bumbeni Complex and Ridge is attributed to both the presence of the distal Bouvet hot-spot and a now-extinct E-W trending spreading centre located in the Northern Natal Valley at ~133–125.3 Ma. The preferential ascension of the magma related to the NE-striking remanent and non-remanently magnetised plutonic bodies defining the Bumbeni Ridge, appear to have been more influenced by localised extension as a result of the presence of a now-extinct spreading centre, in the Northern Natal Valley. Thus, the Bumbeni event is attributed to a combination of these processes and was once a volcanic centre formed along a failed rift system.

- From the positional correlation of the exposed complex with the negative anomaly and the pyroclastic rocks of the Fenda Formation in the NZA borehole, this study has revealed that the

Bumbeni Complex extends below the subsurface and its extent is greater than previously understood.

The prolonged tectonic history related to the various stages of the Gondwana break-up event, also has implications for the tectonic evolution of the KwaZulu-Natal coastal margin including the Maputaland Plain and the Northern Natal Valley, and the nature of the crust in these regions.

This study has revealed a zone of thinned continental crust which extends from Domain 3, of the study region, to the offshore region in the Northern Natal Valley. Therefore, this study concludes that there is thinned continental crust underlying the Maputaland Plain and the Northern Natal Valley regions. This region of the crust hosts volcanic intrusions, intruded during positive and negative polarity periods, that exploited extensional fractures that were formed by paleo-extensional events related to Gondwana break-up. In conclusion, the crust underlying the Maputaland Plain and the offshore region of the Northern Natal Valley, in close-proximity to Domain 3, is not true oceanic crust.

6. References

Abdunaser, K., 2012. Structural style and tectonic evolution of the northwest Sirt Basin–Cretaceous-Tertiary Rift, Libya, PhD thesis (unpubl.). Department of Earth Sciences, University of Durham, 261 pp.

Abul Khair, H., Cooke, D., Hand, M. 2015. Paleo stress contribution to fault and natural fracture distribution in the Cooper Basin. Journal of Structural Geology, 79, 31–41.

Aerophysx, 2018. Magnetic and Radiometric field survey, Final Report, Council for Geoscience, Lung-2017-070 Zululand, 36 pp.

Ahlgren, S. 2001. The nucleation and evolution of Riedel shear zones as deformation bands in porous sandstone. Journal of Structural Geology, 23(8), 1203–1214.

Al Kadasi, A.N., 2014. Interpretation of aeromagnetic data in terms of surface and subsurface geological structures, southwestern Yemen. Arab J Geosci, 8, 1163–1179.

Allmendinger, R. W., Cardozo, N. C., Fisher, D., 2013, Structural Geology Algorithms: Vectors and Tensors: Cambridge, England, Cambridge University Press, 289 pp.

Allsopp, H.L., Manton, W.I., Bristow, J.W., Erlank, A.J., 1984. Rb-Sr geochronology of Karoo felsic volcanics. In: Erlank A.J., (Ed.) Petrogenesis of the volcanic rocks of the Karoo Province. Special Publication of the Geological Society of South Africa Special Publication, 13, 273–280.

Anderson, D. L., 1994. Superplumes or supercontinents?. Geology, 22(1), 39–42.

Anderson, E. M. 1905. The dynamics of faulting. Transactions of the Edinburgh Geological Society, 8(3), 387–402.

Angelier, J. 1989. From orientation to magnitudes in paleostress determinations using fault slip data. Journal of Structural Geology, 11(1-2), 37–50.

Angelier, J. 1984. Tectonic analysis of fault slip data sets. J. geophys. Res. 89, 5953–5848.

Ansari, A. H., Alamdar, K., 2009. Reduction to the Pole of Magnetic Anomalies Using Analytic Signal. World Applied Sciences Journal, 7(4), 405–409.

Armstrong, R.A., Bristow, J.W., Cox, K.G., 1984. The Rooi Rand dyke swarm, southern Lebombo. In: Erlank, A.J. (Ed.), Petrogenesis of the Volcanic Rocks of the Karoo Province. Geological Society of South Africa Special Publication, 13, 77–86.

Arlegui, L., Simón, J. L., 2001. Geometry and distribution of regional joint sets in a non-homogeneous stress field: case study in the Ebro basin (Spain). Journal of Structural Geology,23, 297–313.

Ashwell, P. A., Kennedy, B. M., Edwards, M., Cole, J. W., 2018. Characteristics and consequences of lava dome collapse at Ruawahia, Taupo Volcanic Zone, New Zealand. Bulletin of Volcanology, 80(43), 1–16.

Baby, G., Guillocheau, F., Boulogne, C., Robin, C., Dall'Asta, M., 2018. Uplift history of a transform continental margin revealed by the stratigraphic record: The case of the Agulhas transform margin along the Southern African Plateau. Tectonophysics, 731–732, 104–130.

Bahat, D., Rabinovitch, A., Frid, V., 2005. Tensile Fracturing in Rocks. First Edition. Springer-Verlag, Berlin, 570 pp.

Barkhuizen, J.G., 1989. The Bumbeni line-An Aligned Group of N.E. Trending Bodies in Northern Natal. In 1st South African Geophysical Association (SAGA) Biennial Conference and Exhibition.

Bartlett, W. L., Friedman, M., Logan, J. M., 1981. Experimental folding and faulting of rocks under confining pressure Part IX. Wrench faults in limestone layers. Tectonophysics, 79, 255–277.

Bates, R.L., Jackson, J.A. (Eds.)., 1987. Glossary of Geology. Third Edition. American Geological Institute, Alexandria, 788 pp.

Ben-Avraham, Z., Hartnady, C. J. H., Kitchin, K. A., 1997. Structure and tectonics of the Agulhas-Falkland fracture zone. Tectonophysics, 282, 83–98.

Billay, A., Havenga, M., Cole, J., Zadorozhnaya V., 2014. Preliminary report on high resolution airborne magnetics, electromagnetics and soil sampling in the Tugela terraine and surrounding areas, KwaZulu-Natal, South Africa. Unpublished Internal Report, Council for Geoscience, 2014-0161, 199 pp.

Blakely, R.J., Wells, R.E. Weaver, C.S., Johnson, S.Y., 2002. Location, structure, and seismicity of the Seattle fault zone, Washington: Evidence from aeromagnetic anomalies, geological mapping, and seismic-reflection data. Geological Society of America Bulletin, 114, 169–177.

Boger, S. D., Wilson, C. J. L., Fanning, C. M., 2001. Early Paleozoic tectonism within the East Antarctic craton: The final suture between east and west Gondwana?. Geology, 29(5), 463.

Bordy, E.M., Head, H., 2018. Lithostratigraphy of the Clarens Formation (Stormberg Group, Karoo Supergroup), South Africa. South African Journal of Geology, 121 (1), 119–130.

Botha, G., Porat, N., 2007. Soil chronosequence development in dunes on the southeast African coastal plain, Maputaland, South Africa. Quaternary International, 162–163, 111–132.

Bridges, D. L., Mickus, K., Gao, S. S., Abdelsalam, M. G., Alemu, A., 2012. Magnetic stripes of a transitional continental rift in Afar. Geology, 40(3), 203–206.

Bristow, J.W., 1980. The geochronology and geochemistry of Karoo volcanics in the Lebombo and adjacent areas, PhD thesis (unpubl.). Department of Geochemistry, University of Cape Town, 234 pp.

Bristow, J.W., Allsopp, H.L., Erlank, A.J., Marsh, J.S., Armstrong, R.A., 1984. Strontium isototpe characterization of Karoo volcanic rocks. In: Erlank, A.J., (Ed.) Petrogenesis of the volcanic rocks of the Karoo Province. Special Publication of the Geological Society of South Africa Special Publication, 13, 295–329.

Bristow, J.W., Duncan, A.R., 1983. Rhyolitic dome formation and plinian activity in the Bumbeni complex, Southern Lebombo. South African Journal of Geology, 86 (3), 273–279.

Bristow, J.W., Cleverly, R.W., 1983. A note on the volcanic stratigraphy and intrusive rocks of the Lebombo monocline and adjacent areas. Trans. geol. Soc. S. Afr., 86, 55–61.

Bristow, J. W., Saggerson, E. P., 1983a. A general account of Karoo vulcanicity in southern Africa. Geologische Rundschau, 72(3), 1015–1059.

Bristow, J. W., Saggerson, E. P., 1983b. A review of Karoo vulcanicity in Southern Africa. Bulletin Volcanologique, 46(2), 135–159.

Broad, D.S., Jungslager, E.H.A., McLachlan, I.R., Roux, J., 2006. Offshore Mesozoic Basins. In: Johnson, M.R., Anhaeusser, C.R., Thomas, R.J. (Eds.), The Geology of South Africa. Geological Society of South Africa, Johannesburg/Council for Geoscience, Pretoria, 553–571.

Bushan, S.K., 2000. Malani Rhyolites- A Review. Gondwana Research, 3, 65–77.

Catuneanu, O, Hancox, P.J., Rubidge, B.S., 1998. Reciprocal flexural behaviour and contrasting stratigraphies: a new basin development model for the Karoo retroarc foreland system, South Africa. Basin Research, 10 (4), 417–439.

Chabangu, N., Beck, B., Hicks, N., Botha, G., Viljoen, J., Davids, S., Cloete, M., 2014. The investigation of CO2 storage potential in the Zululand Basin in South Africa. Energy Procedia, 63, 2789–2799.

Chevallier, L., Woodford, A.C., 1999. Morpho-tectonics and mechanism of emplacement of the dolerite rings and sills of the western Karoo, South Africa. S.Afr.J .Geol., 102, 43–54.

Christie-Blick and Biddle, 1985. Deformation and basin formation along strike-slip faults. In: Christie-Blick, N., Biddle, K.T., (Ed.), Strike-slip deformation, basin formation, and sedimentation, Special Publications of SEPM (SP37), 1–34.

Cleverly, R.W., Bristow, J.W., 1979. Revised volcanic stratigraphy of the Lebombo Monocline, South African Journal of Geology, 82 (2), 227–230.

Cloete, H.C.C., Truter, J., 2001. Major and Trace Element Analysis by X-ray Fluorescence Spectrometry at the Council for Geoscience. Open File Report 2001-0074, Council for Geoscience, Pretoria, South Africa, unpublished internal report, 26 pp.

Cooper, M.R., 2018. Cretaceous Fossils of South-Central Africa: An Illustrated Guide. CRC Press/Balkema, The Netherlands. 1–51 pp.

Cooper, G. R. J., 2014. Reducing the dependence of the analytic signal amplitude of aeromagnetic data on the source vector direction. Geophysics, 79(4), J55–J60.

Council for Geoscience, 2019. 1: 1 000 000-scale geological map of South Africa.

Cox, K. G., 1992. Karoo igneous activity, and the early stages of the break-up of Gondwanaland. Geological Society, London, Special Publications, 68, 137–148.

Cox, K.G., Bristow, J.W., 1984. The Sabie River basalt Formation of the Lebombo monocline and south-east Zimbabwe. In: Erlank (Ed.), Petrogenesis of the volcanic rocks of the Karoo province: Geological Society of South Africa Special Publication 13, 1–26 pp.

Cox, K. G., Johnson, R. L., Monkman, L. J., Stillman, C. J., Vail, J. R., Wood, D. N., 1965. The Geology of the Nuanetsi Igneous Province. Philosophical Transactions of the Royal Society A: Mathematical, Physical and Engineering Sciences, 257(1078), 71–218.

Craill, C., Havenga, M., Chirenje, E., Nxantsiya, Z., Hicks, N., Botha, G., 2019. Interpretation of the Zululand high resolution airborne magnetic data. Unpublished Internal Report, Council for Geoscience, 2018–0272, 87 pp.

Curto, J.B., Vidotti, R.M., Fuck, R.A., Blakely, R.J., Alvarenga, C.J.S., Dantas, E.L., 2014. The tectonic evolution of the Transbrasiliano Lineament in northern Paraná Basin, Brazil, as inferred from aeromagnetic data. J. Geophys. Res. Solid Earth, 119, 1544–1562.

Davis, G. H., Bump, A. P., García, P. E., Ahlgren, S. G., 2000. Conjugate Riedel deformation band shear zones. Journal of Structural Geology, 22, 169–190.

De Castro, D. L., Fuck, R. A., Phillips, J. D., Vidotti, R. M., Bezerra, F. H. R., Dantas, E. L., 2014. Crustal structure beneath the Paleozoic Parnaíba Basin revealed by airborne gravity and magnetic data, Brazil. Tectonophysics, 614, 128–145.

Deino, A. L., Orsi, G., de Vita, S., Piochi, M., 2004. The age of the Neapolitan Yellow Tuff caldera-forming eruption (Campi Flegrei caldera Italy) assessed by $^{40}Ar/^{39}Ar$ dating method. Journal of Volcanology and Geothermal Research, 133(1–4), 157–170.

Delvaux, D., Moeys, R., Stapel, G., Melnikov, A., Ermikov, V., 1995. Palaeostress reconstructions and geodynamics of the Baikal region, Central Asia, Part I. Palaeozoic and Mesozoic pre-rift evolution. Tectonophysics, 252(1-4), 61–101.

Dingle, R. V., Scrutton, R. A., 1974. Continental Breakup and the Development of Post-Paleozoic Sedimentary Basins around Southern Africa. Geological Society of America Bulletin, 85(9), 1467–1474.

Duncan, A.R., Erlank, A.J., Marsh, J.S., 1984. Regional geochemistry of the Karoo igneous province. In: Erlank, A.J. (Ed.), Petrogenesis of the Volcanic Rocks of the Karoo Province. Geological Society of South Africa Special Publication, 13, 355–388.

Duncan, R. A., Hooper, P. R., Rehacek, J., Marsh, J. S., Duncan, A. R., 1997. The timing and duration of the Karoo igneous event, southern Gondwana. Journal of Geophysical Research: Solid Earth, 102, 18127–18138.

Duncan, A.R., Marsh, J.S., 2006. The Karoo Igneous Province. In: The Geology of South Africa, Johnson, M. R., Anhaeusser, C. R. and Thomas, R. J., Geological Society of South Africa/Council for Geoscience. 501–520.

Duncan, R. A., Richards, M. A., 1991. Hotspots, mantle plumes, flood basalts, and true polar wander. Reviews of Geophysics, 29(1), 31–50.

Dyer, R., 1988. Using joint interactions to estimate paleostress ratios. Journal of Structural Geology, Vol. 10 (7), 685—699.

Eagles, G., König, M., 2008. A model of plate kinematics in Gondwana breakup. Geophysical Journal International, 173(2), 703–717.

Eales, H. V., Marsh, J. S., Cox, K. G., 1984. The Karoo igneous province: An introduction. In: Erlank (Ed.), Petrogenesis of the volcanic rocks of the Karoo province: Geological Society of South Africa Special Publication 13, 1–26 pp.

Elburg, M., Goldberg, A., 2000. Age and geochemistry of Karoo dolerite dykes from northeast Botswana. Journal of African Earth Sciences, 31, 539–554.

Ellam, R.M., Cox, K.G., 1991. An interpretation of Karoo picrate basalts in terms of interaction between asthenospheric magmas and mantle lithosphere. Earth and Planetary Science Letters 105, 330–342.

Elliot, P., Laharia, P., 2008. The use of aeromagnetics and airborne gravity in Petroleum exploration. 7th International Conference and Exposition on Petroleum Geophysics, P-91, 1–2. Available online [https://www.spgindia.org/2008/091.pdf] (Accessed: 2/4/2018).

Encarnación, J., Fleming, T. H., Elliot, D. H., Eales, H. V., 1996. Synchronous emplacement of Ferrar and Karoo dolerites and the early breakup of Gondwana. Geology, 24(6), 535–538.

Engelder, T., 1985. Loading paths to joint propagation during a tectonic cycle: an example from the Appalachian Plateau, USA. Journal of Structural Geology 7, 459–476.

Engelder, T., Geiser, P., 1980. On the use of regional joint sets as trajectories of paleostress fields during the development of the Appalachian Plateau, New York. Journal of Geophysical Research: Solid Earth, 85(B11), 6319–6341.

Fisher, R.V., 1979. Models for pyroclastic surges and pyroclastic flows. J. Volcanol. Geotherm. Res., 6, 305–318.

Florio, G., Fedi, M., Cella, F., 2011. Insights on the spreading of the Tyrrhenian Sea from the magnetic anomaly pattern. Terra Nova, 23, 127–133.

Fossen, H., 2010. Structural Geology. First Edition. Cambridge University Press, Cambridge, New York, Melbourne, Madrid, Cape Town, Singapore, São Paulo, Delhi, Dubai, Tokyo, 463 pp.

Golonka, J., Bocharova, N. Y., 2000. Hot spot activity and the break-up of Pangea. Palaeogeography, Palaeoclimatology, Palaeoecology, 161, 49–69.

Goss, A. R., Kay, S. M., Mpodozis, C., Singer, B. S., 2009. The Incapillo Caldera and Dome Complex (~28° S, Central Andes): A stranded magma chamber over a dying arc. Journal of Volcanology and Geothermal Research, 184(3–4), 389–404.

Gradstein, F.M., Ogg, J.G., Schmitz, M.D., Ogg, G.M., 2012. The Geologic Time Scale 2012. First Edition, Elsevier, Oxford, United Kingdom, University of Oslo, Geological Museum, Oslo, Norway, 1144 pp.

Green, A., 2011. The late Cretaceous to Holocene sequence stratigraphy of a sheared passive upper continental margin, northern KwaZulu-Natal, South Africa. Marine Geology, 289,17–28.

Gunn, P.J., 1997. Application of aeromagnetic to sedimentary basin studies. AGSO Journal of Australian Geology and Geophysics, 17, 133–144.

Gunn, P.J., Dentith, M.C., 1997. Magnetic responses associated with mineral deposits. AGSO Journal of Australian Geology and Geophysics, 17, 145–158.

Gudmundsson, A., 1984. Formation of dykes, feeder-dykes, and the intrusion of dykes from magma Chambers. Bulletin Volcanologique, 47, 537–550.

Gunn, P.J. Maidment, D., Milligan, P., 1995. Interpreting aeromagnetic data in areas of limited outcrop: An example from the Arunta Block, Northern Territory Interpreting aeromagnetic data in areas of limited outcrop: An example from the Arunta Block, Northern Territory: Exploration Geophysics, 26, 227–232.

Hancock, P. L., 1991. Determining contemporary stress directions from neotectonic joint systems. Philosophical Transactions of the Royal Society of London. Series A: Physical and Engineering Sciences, 337(1645), 29–40.

Hancock, P. L., Engelder, T., 1989. Neotectonic joints. Geological Society of America Bulletin, 101(10), 1197–1208.

Hanyu, T., Nogi, Y., Fujii, M., 2017. Crustal formation and evolution processes in the Natal Valley and Mozambique Ridge, off South Africa: Polar Science, 13, 66–81.

Harris, A. J. L., Rowland, S. K., 2009. Effusion rate controls on lava flow length and the role of heat loss: a review. In: Thordarson, T., Self, S., Larsen, G., Rowland, S. K., Hoskuldsson, A. (Eds) Studies in Volcanology: The Legacy of George Walker. Special Publications of IAVCEI, 2, 33–51. Geological Society, London. 1750-8207/09/# IAVCEI 2009.

Hastie, W.W., Aubourg, C., Watkeys, M.K., 2011a. When an 'inverse' fabric is not inverse: an integrated AMS-SPO study in MORB-like dykes. Terra Nova, 23, 49–55.

Hastie, W. W., Watkeys, M.K., Aubourg, C., 2011b. Significance of magnetic and petrofabric in Karoo-feeder dykes, northern Lebombo. Tectonophysics, 513, 96–111.

Hastie, W. W., Watkeys, M. K., Aubourg, C., 2013. Characterisation of grain-size, shape and orientation of plagioclase in the Rooi Rand dyke swarm, South Africa. Tectonophysics, 583, 145–157.

Hastie, W. W., Watkeys, M. K., Aubourg, C., 2014. Magma flow in dyke swarms of the Karoo LIP: Implications for the mantle plume hypothesis. Gondwana Research, 25(2), 736–755.

Hawkesworth, C., Kelley, S., Turner, S., Le Roex, A., Storey, B., 1999. Mantle processes during Gondwana break-up and dispersal. Journal of African Earth Sciences, 28(1), 239–261.

Hemans, D.A., 1976. Geology of the igneous rocks of the St. Lucia 27 ½°32' Sheet from Mkuze in the north to the Hluhluwe River in the south. Unpublished Internal Report, Rep. Geol. Surv. S. Afr. 51 pp.

Hicks, N., 2017. The seismic stratigraphy, geological evolution and CO_2 storage potential of the offshore Durban Basin, South Africa, PhD thesis (unpubl.). University of KwaZulu-Natal, Durban, South Africa. 125 pp.

Hill, P., Bankey, V., Langenheim, V., 1997. Introduction to Potential Fields: Magnetics. U.S. Geological Survey, FS-236-95, 1–2.

Hinojosa-Prieto, H.R., Vidal-Solano, J.R., Kibler, K.W., Hinojosa-García, H.J., 2016. Geology of the Selene perlite deposit in the northern Sierra Madre Occidental, northeastern Sonora, Mexico. 68 (1), 129–163.

Hinze, W. J., Von Frese, R.B., Saad, A. H., 2012. Gravity and magnetic exploration: Principles, practices, andapplications. Cambridge University Press: New York. 1–515.

Hoyer, L., 2015. Rock fabric study of Karoo dolerite sills along the KwaZulu-Natal north coast, South Africa: Implications for the magma source. PhD thesis (unpubl.). University of KwaZulu-Natal, Durban, South Africa. 262 pp.

Hughes, G. R., Mahood, G. A., 2011. Silicic calderas in arc settings: Characteristics, distribution, and tectonic controls. Geological Society of America Bulletin, 123(7–8), 1577–1595.

Hunt, C.P., Moskowitz, B.M., Banerjee, S.K., 1995. Magnetic Properties of Rocks and Minerals. American Geophysical Union, 189–204. Available online [https://agupubs.onlinelibrary.wiley.com/doi/abs/10.1029/RF003p0189]. (Accessed 14/5/2018). doi:10.1029/rf003p0189.

Igwe, O., Okonkwo, I. A., 2016. Application of paleostress analysis for the identification of potential instability precursors within the Benue Trough Nigeria. Geoenvironmental Disasters, 3(1), 1–15.

Ito, G., Lin, J., 1995. Oceanic spreading center–hotspot interactions: Constraints from along-isochron bathymetric and gravity anomalies. Geology, 23 (7), 657–660.

Johnson, M.R., van Vuuren, C.J., Visser, J.N.J., Cole, D.I., de V. Wickens, H., Christie, A.D.M., Roberts, D.L., Brandl, G., 2006. Sedimentary rocks of the Karoo Supergroup. In: Johnson, M.R., Anhaeusser, C.R., Thomas, R.J. (Eds.), The Geology of South Africa. Geological Society of South Africa, Johannesburg/Council for Geoscience, Pretoria, 461–499.

Jokat, W., Boebel, T., König, M., Meyer, U., 2003. Timing and geometry of early Gondwana breakup. J. Geophys. Res. 108, 2428–2842.

Joubert, P., Johnson, M.R., 1998. Abridged Lexicon of South Africa Stratigraphy. South African Committee for Stratigraphy, Council for Geoscience. 160 pp.

Jourdan, F., Bertrand, H., Féraud, G., Le Gall, B., Watkeys, M. K., 2009. Lithospheric mantle evolution monitored by overlapping large igneous provinces: Case study in southern Africa. Lithos, 107, 257–268.

Jourdan, F., Féraud, G., Bertrand, H., Watkeys, M.K., 2007a. From flood basalts to the inception of oceanization: Example from the $^{40}Ar/^{39}Ar$ high-resolution picture of the Karoo large igneous province, Geochem. Geophys. Geosyst., 8, 1–20.

Jourdan, F., Bertrand, H., Schärer, U., Blichert-Toft, J., Féraud, G., Kampunzu, A. B., 2007b. Major and Trace Element and Sr, Nd, Hf, and Pb Isotope Compositions of the Karoo Large Igneous Province, Botswana–Zimbabwe: Lithosphere vs Mantle Plume Contribution. Journal of Petrology, 48, 1043–1077.

Jourdan, F., Féraud, G., Bertrand, H., Kampunzu, A.B., Tshoso, G., Le Gall, B., Tiercelin, J.J., Capiez, P., 2004. The Karoo triple junction questioned: evidence from Jurassic and Proterozoic $^{40}Ar/^{39}Ar$ ages and geochemistry of the giant Okavango dyke swarm (Botswana). Earth and Planetary Science Letters, 222, 989–1006.

Jourdan, F., Féraud, G., Bertrand, H., Kampunzu, A. B., Tshoso, G., Watkeys, M. K., Le Gall, B., 2005. Karoo large igneous province: Brevity, origin, and relation to mass extinction questioned by new $^{40}Ar/^{39}Ar$ age data. Geology, 33(9), 745–748.

Jourdan, F., Féraud, G., Bertrand, H., Watkeys, M. K., Kampunzu, A. B., Le Gall, B., 2006. Basement control on dyke distribution in Large Igneous Provinces: Case study of the Karoo triple junction. Earth and Planetary Science Letters, 241, 307–322.

Jourdan, F., Féraud, G., Bertrand, H., Watkeys, M. K., Renne, P. R., 2008. The $^{40}Ar/^{39}Ar$ ages of the sill complex of the Karoo large igneous province: Implications for the Pliensbachian-Toarcian climate change. Geochemistry, Geophysics, Geosystems, 9(6), 1–20.

Katz, Y., Weinberger, R., Aydin, A., 2004. Geometry and kinematic evolution of Riedel shear structures, Capitol Reef National Park, Utah, 26(3), 491–501.

Killick, A. M., Thwaites, A. M., Germs, G. J. B., Schoch, A. E., 1988. Pseudotachylite associated with a bedding-parallel fault zone between the Witwatersrand and Ventersdorp Supergroups, South Africa. Geologische Rundschau, 77(1), 329–344.

König, M., Jokat, W., 2010. Advanced insights into magmatism and volcanism of the Mozambique Ridge and Mozambique Basin in the view of new potential field data. Geophys. J. Int.Geophysical Journal International, 180, 158–180.

Korringa, M. K., 1973. Linear Vent Area of the Soldier Meadow Tuff, an Ash-Flow Sheet in Northwestern Nevada. Geological Society of America Bulletin, 84(12), 3849–3866.

Kennedey, W.J., Klinger, H.C., 1975. Cretaceous faunas from Zululand and Natal, South Africa. Introduction, Stratigraphy. Bulletin British Museum of Natural History, Geology, 25, 265–315.

Klausen, M. B., 2009. The Lebombo monocline and associated feeder dyke swarm: Diagnostic of a successful and highly volcanic rifted margin?. Tectonophysics, 468(1–4), 42–62.

Lacombe, O., Angelier, J., Laurent, P., Bergerat, F., Tourneret, C., 1990. Joint analyses of calcite twins and fault slips as a key for deciphering polyphase tectonics: Burgundy as a case study. Tectonophysics, 182(3-4), 279–300.

Landman, B.E., 2017. Petrography, mineralogy and geochemistry of the rock formations of the Zululand Basin based on borehole NZA. MSc thesis (unpubl.). University of Pretoria, Pretoria, South Africa. 126 pp.

Le Bas, M. J., Le Maitre, R. W., Streckeisen, A., Zanettin, B., 1986. A Chemical Classification of Volcanic Rocks Based on the Total Alkali-Silica Diagram. Journal of Petrology, 27(3), 745–750.

Le Gall, B., Tshoso, G., Jourdan, F., Féraud, G., Bertrand, H., Tiercelin, J. J., Maia, M., 2002. $^{40}Ar/^{39}Ar$ geochronology and structural data from the giant Okavango and related mafic dyke swarms,

Karoo igneous province, northern Botswana. Earth and Planetary Science Letters, 202, 595–606.

Leinweber, V. T., Jokat, W., 2011. Is there continental crust underneath the northern Natal Valley and the Mozambique Coastal Plains? Geophysical Research Letters, L14303, 38, 1–7.

Leinweber, V.T., Jokat, W., 2012. The Jurassic history of the Africa-Antarctica corridor-new constraints from magnetic data on the conjugate continental margins. Tectonophysics 530–531, 87–101.

Leinweber, V. T., Klingelhoefer, F., Neben, S., Reichert, C., Aslanian, D., Matias, L., Jokat, W. 2013. The crustal structure of the Central Mozambique continental margin — Wide-angle seismic, gravity and magnetic study in the Mozambique Channel, Eastern Africa. Tectonophysics, 599, 170–196.

Le Maitre, R. W. (Editor), Streckeisen, A., Zanettin, B., Le Bas, M.J., Bonin, B., Bateman, P., Bellieni, G., Dudek, A., Efremova, S., Keller, J., Lameyre, J., Sabine, P.A., Schmid, R., Sørensen, H., Woolley, A.R., 2002. Igneous Rocks: A classification and Glossary of Terms. Second Edition, Cambridge University Press, United Kingdom and New York, 236 pp.

MacLeod, I. N., Jones, K., Dai, T. F., 1993. 3-D analytic signal in the interpretation of total magnetic field data at low magnetic latitudes. Exploration Geophysics, 24(4), 679–688.

MacLeod, N. S., Sherrod, D. R., 1988. Geologic evidence for a magma chamber beneath Newberry Volcano, Oregon. Journal of Geophysical Research: Solid Earth, 93(B9), 10067–10079.

Magnall, N., James, M. R., Tuffen, H., Vye-Brown, C., 2017. Emplacing a Cooling-Limited Rhyolite Lava Flow: Similarities with Basaltic Lava Flows. Frontiers in Earth Science, 5:44, 1–19.

Marsh, J. S., Eales, H. V., 1984. The chemistry and Petrogenesis of igneous rocks of the Karoo central area, Southern Africa. In: Erlank A.J., (Ed.) Petrogenesis of the volcanic rocks of the Karoo Province. Special Publication of the Geological Society of South Africa Special Publication, 13, 27–67.

Martin, A. K., 1987. Plate reorganisations around Southern Africa, hot-spots and extinctions. Tectonophysics, 142, 309–316.

Martin, A. K., Hartnady, C.J.H., 1986. Plate tectonic development of the southwest Indian Ocean: A revised reconstruction of East Antarctica and Africa, J. Geophys. Res, 91, 4767–4786.

Marsh, J. S., Hooper, P.R., Rehacek, J., R., Duncan, R.A., Duncan. A.R., 1997. Stratigraphy and Age of Karoo Basalts of Lesotho and Implications for Correlations Within the Karoo Igneous Province. In: Mahoney, J.J., Coffin, M.F., (Eds.), Large Igneous Provinces: Continental, Oceanic, and

Planetary Flood Volcanism. Geophysical Monograph 100. American Geophysical Union, Washington, 438 pp.

Maus, S., Macmillan, S., Chernova, T., Choi, S., Dater, D., Golovkov, V., Lesur, V., Lowes, F., Lühr, H., Mai, W., McLean, S., Olsen, N., Rother, M., Sabaka, T., Thomson, A., Zvereva, T., 2005. The 10th-Generation International Geomagnetic Reference Field. International Association of Geomagnetism and Aeronomy (IAGA), Division V, Working Group VMOD: Geomagnetic Field Modelling: Geophysical Journal International 161, 561–565.

Maus, S., Barckhausen, U., Berkenbosch, H., Bournas, N., Brozena, J., Childers, V., Dostaler, F., Fairhead, J.D., Finn, C., Von Frese, R.R.B., Gaina, C., Golynsky, S., Kucks, R., Lühr, H., Milligan, P., Mogren, S., Müller, R.D., Olesen, O., Pilkington, M., Saltus, R., Schreckenberger, B., Thébault, E., Tontini, F.C., 2009. EMAG2: A 2-arc min resolution Earth Magnetic Anomaly Grid compiled from satellite, airborne, and marine magnetic measurements. Geochemistry, Geophys. Geosystems 10, 1–12.

McEnroe, S.A., Fabian, K., Robinson, P., Gaina, C., Brown, L.L., 2009. Crustal Magnetism, Lamellar Magnetism and Rocks That Remember. Elements, 5, 241–246.

McMillan, I.K., 2003. Foraminiferally defined biostratigraphic episodes and sedimentation pattern of the Cretaceous drift succession (Early Barremian to Late Maastrichtian) in seven basins on the South African and southern Namibian continental margin. South African Journal of Science, 99, 537–576.

Meth, D.L., 1996. The Geology and Geochemistry of the Rooi Rand Dyke Swarm. MSc thesis (unpubl.). University of Natal, Durban, South Africa. 189 pp.

Mohriak, W.U., Rosendahl, B.R., Turner, J.P., and Valente, S.C., 2002. Crustal architecture of South Atlantic volcanic margins. In: Menzies, M.A., Klemperer, S.L., Ebinger, C.J., and Baker, J., (Eds), Volcanic Rifted Margins: Boulder, Colorado, Geological Society of America Special Paper 362, 159-202 pp.

Morgan, W. J., 1981. Hotspot tracks and the early rifting of the Atlantic. Processes of Planetary Rifting, 1–4.

Morgan, W.J., 1983. Hotspot tracks and the early rifting of the Atlantic. In: Morgan, P., Baker, B.H., (Eds), Processes of Continental Rifting. Tectonophysics, 94, 123–139.

Morris, A., Ferrill, D. A., Brent Henderson, D. B., 1996. Slip-tendency analysis and fault reactivation. Geology, 24(3), 275–278.

Mothes, P. A., Hall, M. L., 2008. The plinian fallout associated with Quilotoa's 800 yr BP eruption, Ecuadorian Andes. Journal of Volcanology and Geothermal Research, 176(1), 56–69.

Moulin, M., Aslanian, D., Evain, M., Leprêtre, A., Schnurle, P., Verrier, F., Thompson, J., De Clarens, P., Leroy, S., Dias, N., the PAMELA-MOZ35 Team., 2020. Gondwana breakup: Messages from the North Natal Valley. Terra Nova, 32, 205–214.

Mueller, C. O., Jokat, W., 2019. The initial Gondwana break-up: A synthesis based on new potential field data of the Africa-Antarctica Corridor. Tectonophysics, 750, 301–328.

Muirhead, J. D., Airoldi, G., White, J. D. L., Rowland, J. V., 2014. Cracking the lid: Sill-fed dikes are the likely feeders of flood basalt eruptions. Earth and Planetary Science Letters, 406, 187–197.

Nxantsiya, Z., 2017. A study of the southwestern Karoo Basin in South Africa using magnetic and gravity data, MSc thesis (unpubl.). Department of Geology, Faculty of Science and Agriculture University of Fort Hare, South Africa, 210 pp.

Ogg, J. G., Ogg, G., Gradstein, F. M., 2016. A Concise Geologic Time Scale. First Edition, Elsevier, 234 pp.

Oladunjoye, M. A., Olayinka, A. I., Alaba, M., and Adabanija, M. A., 2016. Interpretation of high resolution aeromagnetic data for lineaments study and occurrence of Banded Iron Formation in Ogbomoso area, Southwestern Nigeria. Journal of African Earth Sciences, 114, 43–53.

Orife, T., Arlegui, L., Lisle, R. J., 2002. DIPSLIP: a QuickBasic stress inversion program for analysing sets of faults without slip lineations. Computers & Geosciences, 28(6), 775–781.

Paterson, N.R., Reeves, C.V., 1985. Applications of gravity and magnetic surveys: The state-of-the-art in 1985. Geophysics, 50, 2558–2594.

Porat, N., Botha, G., 2008. The luminescence chronology of dune development on the Maputaland coastal plain, southeast Africa. Quaternary Science Reviews, 27, 1024–1046.

Price, N. J., 1966. Fault and Joint Development in Brittle and Semi-brittle Rock. First Edition. Pergamon Press, Oxford, London, Edinburg, New York, Toronto, Sydney, Paris, Braunschweig, 176 pp.

Ramsay, J.G., Lisle, R.J., 2000. The Techniques of Modern Structural Geology. Vol. 3: Application of 693 continuous mechanics in structural geology. Academic Press, London, 374 pp.

Reeves, C. V., 1978. A failed Gondwana spreading axis in southern Africa. Nature, 273, 222–223.

Reeves, C., 2005. Aeromagnetic Surveys Principles, Practice & Interpretation. Geosoft, 1-1–10-9, 1–155.

Rogers, M. A., Budding, K.E., Christie, V.L., 1996. Distinguishing tectonic joints from cooling joints. In: the Bandelier Tuff (Pleistocene), Pajarito Plateau, Los Alamos County, New Mexico Margaret Anne Rogers, Karin E. Budding, and V. L. Christie, 293–301. In: Goff, F., Kues, B. S., Rogers, M. A., McFadden, L. S., Gardner, J. N., (Eds.), Jemez Mountains Region, New Mexico Geological Society 47th Annual Fall Field Conference Guidebook, 484 pp.

Reimold, W. U., 1995. Pseudotachylite in impact structures - generation by friction melting and shock brecciation?: A review and discussion. Earth-Science Reviews 39, 247–265.

Reynolds, J.M., 2011. An Introduction to Applied and Environmental Geophysics. Second Edition, Reynolds International Ltd, 696 pp.

Reynolds International, 2011. Aeromagnetic surveys. Technical summary sheet no. 21. Available online [http://www.reynolds-international.co.uk/uploads/files/21tssaero-magnetic.pdf] (Accessed: 2/4/2018).

Riley, T. R., Millar, I. L., Watkeys, M. K., Curtis, M. L., Leat, P. T., Klausen, M. B., and Fanning, C. M., 2004. U-Pb zircon (SHRIMP) ages for the Lebombo rhyolites, South Africa: refining the duration of Karoo volcanism. Journal of the Geological Society, 161(4), 547–550.

Sa'ad, Z. K., Al-Mashaikie, A.K., Ali M., Al-Hawbanie., 2010. Petrography and Geochemical Study of the Perlite Rocks from Bait Al-Qeyarie, Kawlan Area, Yemen.

Saggerson, E. P., Bristow, J. W., 1983. The geology and structural relationships of the southern Lebombo volcanic and intrusive rocks, South Africa. Bulletin Volcanologique, 46(2), 161–181.

Saintot, A., Stephens, M. B., Viola, G., Nordgulen, Ø., 2011. Brittle tectonic evolution and paleostress field reconstruction in the southwestern part of the Fennoscandian Shield, Forsmark, Sweden. Tectonics, 30(4), 1–36.

Scutter, C. R., Cas, R. A. F., Moore, C. L., de Rita, D., 1998. Facies architecture and origin of a submarine rhyolitic lava flow-dome complex, Ponza, Italy. Journal of Geophysical Research: Solid Earth, 103(B11), 27551–27566.

Self, S., Goff, F., Gardner, J. N., Wright, J. V., Kite, W. M., 1986. Explosive rhyolitic volcanism in the Jemez Mountains: Vent locations, caldera development and relation to regional structure. Journal of Geophysical Research, 91(B2), 1779–1798.

Shackleton, R. M., 1996. The final collision zone between East and West Gondwana: where is it? Journal of African Earth Sciences, 23(3), 271–287.

Shone, R.W., 2006. Onshore Post-Karoo Mesozoic Deposits. In: Johnson, M.R., Anhaeusser, C.R., Thomas, R.J. (Eds.), The Geology of South Africa. Geological Society of South Africa, Johannesburg/Council for Geoscience, Pretoria, 541–552.

Smith, R.M.H., 1990. A review of stratigraphy and sedimentary environments of the Karoo Basin of South Africa. Journal of African Earth Sciences, 10, 117–13.

Smith, R.M.H., Eriksson, P.G., Botha, W.J., 1993. A review of the stratigraphy and sedimentary environments of the Karoo-aged basins of Southern Africa. Journal of African Earth Sciences (and the Middle East), 16(1–2), 143–169.

Smith, A.G., Hallam, A., 1970. The fit of the southern continents. Nature, 225, 139–144.

South African Committee for Stratigraphy (SACS)., 1980. Stratigraphy of South Africa. Part 1 (Comp. L.E. Kent). Lithostratigraphy of the Republic of South Africa, South West Africa/Namibia, and the Republics of Bophuthatswana, Transkei and Venda. Handbook 8, Geological Survey of South Africa, 569–574 pp.

Sparks, R. S. J., 1976. Grain size variations in ignimbrites and implications for the transport of pyroclastic flows. Sedimentology, 23, 147–188.

Sparks, R. S. J., Tait, S. R., Yanev, Y., 1999. Dense welding caused by volatile resorption. Journal of the Geological Society, 156(2), 217–225.

Storey, B. C., 1995. The role of mantle plumes in continental breakup: case histories from Gondwanaland. Nature, 377(6547), 301–308.

Storey, B.C., Kyle, P.R., 1997. An active mantle mechanism for Gondwana break-up. South African Journal of Geology 100, 283–290.

Stratten, T., 1964. Interim Report on the Bumbeni Suite of Rocks. Unpublished Internal Report, Council for Geoscience, Pietermaritzburg, 1–32 pp.

Svensen, H. H., Polteau, S., Cawthorn, G., Planke, S., 2014. Sub-volcanic Intrusions in the Karoo Basin, South Africa. Advances in Volcanology, 349–362.

Sweeney, R.J., Falloon, T.J., Green, D.H., Tatsumi, Y., 1991. The mantle origins of Karoo picrites. Earth and Planetary Science Letters 107, 256–271.

Tankard, A.J., Jackson, M.P.A., Eriksson, K.A., Hobday, D.K., Hunter, D.R., Minter, W.E.L., 1982. Crustal Evolution of Southern Africa: 3.8 Billion Years of Earth History. Springer-Verlag, 523 pp.

Telford, W. M., Geldart, L.P., Sheriff, R. E., 1990. Applied Geophysics. Second Edition, Cambridge University Press, Cambridge, New York, Port Cheste, Melbourne and Sydney, 744 pp.

Tibaldi, A., Bonali, F. L., Corazzato, C., 2017. Structural control on volcanoes and magma paths from local- to orogen-scale: The central Andes case. Tectonophysics, 699, 16–41.

Tikku, A. A., Marks, K. M., Kovacs, L. C., 2002. An Early Cretaceous extinct spreading center in the northern Natal valley. Tectonophysics, 347, 87–108.

Toschek, P., 1972. Geological Well completion report of Borehole ZG 1/72. Internal Report, Southern Oil Exploration Corporation (PTY) Limited. PSV 903, 52 pp.

Verma, S. P., 2001. Geochemical Evidence for a Rift-Related Origin of Bimodal Volcanism at Meseta Rio San Juan, North-Central Mexican Volcanic Belt. International Geology Review, 43(6), 475–493.

Viljoen, J.H.A., Hicks, N., Botha, G.A., Davids, S., Musekiwa, C., Singh, R.G., Stapelberg, F.D.J., Cloete, M. 2011. Towards an effective CO_2 storage capacity assessment of the Zululand basin, South Africa. Unpublished Internal Report, Council for Geoscience, 1–115.

Walker, G. P. L., Huntingdon, A. T., Sanders, A. T., Dinsdale, J. L., 1973. Lengths of Lava Flows [and Discussion]. Philosophical Transactions of the Royal Society A: Mathematical, Physical and Engineering Sciences, 274(1238), 107–118.

Walker, G. P. L., 1981. Plinian eruptions and their products. Bulletin Volcanologique, 44(3), 223–240.

Watkeys, M.K., 2002. Development of the Lebombo rifted volcanic margin of southeast Africa. In: Menzies, M.A., Klemperer, S.L., Ebinger, C.J., and Baker, J., (Eds.): Volcanic Rifted Margins: Boulder, Colorado, Geological Society of America Special Paper, 362, 27–46.

Watkeys, M.K., 2006. Gondwana break-up: a South African perspective. In: Johnson, M.R., Anhaeusser, C.R., Thomas, R.J. (Eds.), The Geology of South Africa. Geological Society of South Africa. Johannesburg/Council for Geoscience, Pretoria, 531–539 pp.

Watkeys, M. K., Mason, T. R., Goodman, P. S., 1993. The rôle of geology in the development of Maputaland, South Africa. Journal of African Earth Sciences, 16(1–2), 205–221.

Watkeys, M, K., Sokoutis, D., 1998. Transtension in southeastern Africa associated with Gondwana break-up. In: Holdsworth, R. E., Starchan, R. A., and Dewey, J. E. (Eds.), Continental

Transpressional and Transtensional Tectonics: Geological Society, London, Special Publications, 135, 203–214.

Weinberger, R., Eyal, Y., Mortimer, N., 2010. Formation of systematic joints in metamorphic rocks due to release of residual elastic strain energy, Otago Schist, New Zealand. Journal of Structural Geology, 32(3), 288–305.

Wemegah, D.D., Preko, K., Noye, R.M., Boadi, B., Menyeh, A., Danuor, K., Amenyoh, T., 2015. Geophysical interpretation of possible gold mineralization zones in Kyerano, south-western Ghana using aeromagnetic and radiometric datasets. Journal of Geosciences and Environmental Protections, 3, 67–82.

Wijns, C., Perez, C., Kowalczyk, P., 2005. Theta map: Edge detection in magnetic data. Geophysics, 70(4), L39–L43.

Woodcock, N. H., Fischer, M., 1986. Strike-slip duplexes. Journal of Structural Geology, 8, 725–735.

Wolmarans, L. G., Du Preez, J. W. 1986. The geology of the St. Lucia area. Explanation of Sheet $27^{1/2}32$. Geol. Surv. S. Afr. 42 pp.

Wolmarans, L.G., Saggerson, E.P., 1988. Geology of the Volcanic and Intrusive Rocks of the Southern Lebombo Mountains. Geocongress. University of Natal, Durban. 37 pp.

Žalohar, J., Vrabec, M., 2007. Paleostress analysis of heterogeneous fault-slip data: The Gauss method. Journal of Structural Geology, 29(11), 1798–1810.

Appendices

Appendix 1

Geochemistry data from samples in this study (Nxwala Member in the Pratley Perlite Mine area). Results of major elements oxides (in wt%) and trace elements (in ppm) are presented.

Rock type	tuff	perlite flow	tuff	perlitic pitchstone
Sample	**NH-Z-18-001**	**NH-Z-18-002**	**NH-Z-18-004**	**NH-Z-18-006**
SiO_2	71,5	71,73	71,85	72,47
TiO_2	0,22	0,16	0,13	0,22
Al_2O_3	13,94	13,33	12,02	13,16
Fe_2O_3 (t)	1,69	1,56	0,95	1,63
MnO	0,026	0,033	0,015	0,022
MgO	0,62	0,07	0,74	0,05
CaO	0,76	0,64	1,41	0,67
Na_2O	2,57	3,11	1,53	3,67
K_2O	3,72	4,62	3,48	4,19
P_2O_5	0,014	0,013	0,014	0,035
Cr_2O_3	0,006	0,013	0,006	0,007
LOI	4,68	4,35	7,53	3,56
Total	**99,75**	**99,63**	**99,67**	**99,69**
Ag	<3	<3	<3	<3
As	3,2	<3	<3	3,2
Ba	250	301	245	510
Bi	<3	<3	<3	<3
Br	2	<2	<2	2
Cd	<3	<3	<3	<3
Ce	84	103	66	188
Co	<3	<3	<3	<3

Cr	3,4	<3	<3	3,1
Cu	11	9,1	6,1	6
Ga	18	18	15	17
Ge	<2	<2	<2	<2
Hf	10	9,4	7,1	6,9
La	50	56	41	143
Mo	3,9	4,3	<2	4,9
Nb	36	35	32	29
Nd	35	35	25	70
Ni	3,6	<3	<3	<3
Pb	11	13	9,2	13
Rb	143	183	97	173
Sb	<3	<3	<3	<3
Sc	3,1	<3	<3	<3
Se	<3	<3	<3	<3
Sm	5,9	5,9	<5	12
Sn	5,5	6,2	4,8	6,3
Sr	64	53	534	77
Ta	4	3	3,1	<3
Th	20	21	16	22
U	3,3	4,5	3,4	3,7
V	4,4	<3	<3	3,1
W	4,6	3,6	<3	4
Y	37	30	21	49
Yb	<3	<3	<3	<3
Zn	37	30	24	26
Zr	205	190	146	205

Appendix 2

Geochemistry data from Bristow and Duncan (1983) for the Nxwala Member in the Pratley Perlite Mine area. The major element oxides are presented in wt% and trace elements in ppm.

	1		2		3		4	
%	L507		NP		78/41a		78/41b	
SiO_2	77,31	78,29	72,16	75,87	70,79	76,53	69,73	74,40
TiO_2	0,15	0,15	0,15	0,16	0,15	0,16	0,14	0,15
Al_2O_3	11,74	11,89	12,80	13,46	13,22	14,29	12,74	13,60
Fe_2O_3	1,51	1,54	1,37	1,44	1,35	1,46	1,78	1,90
MnO	0,01	0,01	0,02	0,02	0,03	0,03	0,03	0,03
MgO	0,18	0,19	0,12	0,13	0,61	0,66	0,70	0,75
CaO	0,55	0,56	0,66	0,69	0,61	0,66	0,64	0,68
Na_2O	3,15	3,19	2,96	3,11	2,42	2,62	3,24	3,46
K_2O	4,12	4,17	4,85	5,10	3,31	3,58	4,72	5,03
P_2O_5	0,02	0,02	0,01	0,01				
H_2O^+	0,70		4,70		6,15		4,80	
H_2O^-	0,73		0,24		0,92		0,82	
Total	100,17		100,04		99,56		99,34	
ppm								
Rb	145	147	188	198	59	64	75	80
Ba	327	331	331	348	343	373	309	330
Sr	50	51	52	55	221	241	187	200
Zr	170	172	187	197	185	201	167	178
Nb	38	39	43	45	41	45	37	40
Cr	<1	<1	<1	<1	3,5	3,8	5,6	6
V	3,0	3,0	<1	<1	5,4	5,9	7,5	8
Sc	2,0	2,0	2,5	2,6	<1	<1	2,4	2,6
Zn	21	21	32	34	34	37	38	40
Cu	4,7	4,8	8,8	9	6,8	7	8	9
Y	27	27	28	29	27	29	26	28
Zr/Nb	4,5		4,3		4,5		4,5	

1. Glassy rhyolite from zone within perlitic pitchstone.
2. Perlitic pitchstone.
3. Composite sample from basal part of Nxwala air-fall deposit.
4. Composite sample from uppermost part of Nxwala air-fall deposit.

Appendix 3

Geochemistry data from Landman (2017) from samples collected in the NZA drill core. The major element oxides (in wt%) of samples N35, N36, N37, N38 and N40 were plotted on the TAS classification diagram.

Sample	Lithofacies	SiO_2	TiO_2	Al_2O_3	Fe_2O_3	MnO	MgO	CaO	Na_2O	K_2O	P_2O_5	Cr_2O_3	LOI	Total
N33	Lapilli-tuff	81.56	0.25	10.09	0.80	0.01	0.29	0.63	2.53	3.48	0.04	0.01	0.31	100
N34	Lapilli-tuff	57.54	0.23	12.29	8.51	0.33	0.84	1.51	3.90	2.65	0.07	<0.001	12.13	100
N35	Lapilli-stone	75.34	0.33	13.42	1.90	0.01	0.56	0.91	3.92	3.27	0.04	0.00	0.31	100
N36	Tuff-breccia	73.40	0.78	12.66	2.75	0.01	0.37	1.61	3.23	4.75	0.13	0.00	0.31	100
N37	Lapilli-stone	75.12	0.24	13.82	1.24	0.01	0.62	1.00	4.69	2.90	0.06	0.00	0.31	100
N38	Lapilli-stone	75.06	0.33	13.46	1.64	0.02	0.61	0.93	4.25	3.34	0.05	0.00	0.31	100
N39	Lapilli-stone	66.75	0.30	12.19	2.41	0.07	0.80	1.44	4.36	3.31	0.06	<0.001	8.31	100
N40	Tuff	79.91	0.35	11.04	1.19	0.00	0.41	0.60	3.05	3.10	0.05	0.00	0.31	100

Appendix 4

Lithological descriptions of the Nxwala Member pyroclastic rocks (PPM-Locality 1) based on field observations. The thicknesses are recorded from the youngest to the oldest lithological unit (i.e., the youngest unit is found at the top of the table).

Lithology	**Thickness (cm)**	**Description**
Pyroclastic breccia	120	Very poorly sorted pyroclastic breccia, displaying multiple weathering colours of blocks, bombs and lapilli-sized pyroclasts. The pyroclasts constitute perlite, rhyolite and tuff in ash matrix and are in places banded. The thickness of individual bands is 1 to 5 cm-thick.
Tuff	10	Poorly-sorted, moderate red tuff comprising predominantly lapilli-sized, angular to sub-rounded, rhyolite and perlite pyroclasts embedded in ash matrix. Dominant pyroclasts are on average 2 cm in diameter. Larger pyroclasts of up to 4 cm are locally present towards the top. The tuff grades upward into the pyroclastic breccia
Lapillistone	3	Poorly-sorted, whitish-cream lapilli stone composed of lapilli-sized, angular to sub-rounded, rhyolite and perlite pyroclasts, and glass fragments in tuff matrix. Scattered pyroclasts and glass fragments are on average 2 cm in diameter. The lapillistone grades into the overlying thick lapilli tuff unit.
Tuff	5	Blocky textured and clast-poor medium grey tuff consisting of randomly distributed angular rhyolitic and perlitic pyroclasts of up to 2 mm in diameter.
Tuff	2	Thin, lens-shaped, clast-poor and structureless white tuff comprising sporadic angular rhyolite and glass fragments of up to 0.3 cm in diameter. The locally developed tuff shows a sharp contact with the overlying grey tuff.
Tuff	11	Homogeneous light to moderate red tuff composed of angular to sub-rounded lapilli-sized rhyolite, perlite and tuff pyroclasts set in ash matrix. The dominant pyroclasts are 0.1 to 0.5 cm in diameter. Localised, elongated pyroclasts of up to 2.5 cm in diameter are present towards the top. The tuff displays a sharp contact with the overlying white coloured tuff.
Lapillistone	7	Coarsening-upward, whitish-cream lapillistone consisting of angular to sub-rounded perlite, rhyolite and tuff pyroclasts set in fine-grained ash matrix. The dominant pyroclasts vary in size from 1 to 2 cm in diameter. In places, rhyolite pyroclasts display small-scale (0.1-0.2 cm thick) flow banding. Sharp contact.
Tuff	4	Poorly-sorted, moderate red tuff comprising angular to sub-angular perlite, rhyolite and tuff pyroclasts. The pyroclasts range in size from 0.5 to 1 cm in diameter. The tuff shows a gradational contact with the overlying lapillistone.

Appendix 5

Lithological descriptions of the Nxwala Member perlite overlying the tuff unit (PPM-Locality 2) based on field observation.

Lithology	**Thickness (cm)**	**Description**
Perlite	100	Grey-black perlite unit separated from the underlying tuff by an alteration zone (contact).
Tuff	1000	Fine-grained, white-cream basal tuff unit.

Appendix 6

Descriptions of the Bumbeni Complex lithologies intersected by the NZA borehole (521.21–571 m- depth).

Depth		Thickness (m)	Lithology	Description
From	To			
		1740		Sandstone, calcareous sandstone, and siltstone of the Zululand Group overlie the pyroclastic rocks of the Bumbeni Complex. A weathering surface is developed above the lapillistone and forms the nonconformable contact with the sandstone of the Zululand Group
521.21	522.21	1	Lapillistone	Poorly-sorted, coarsening-upward grey-black lapillistone comprising angular to sub-rounded, lapilli-sized, cream and green tuff and pumice pyroclasts, as well as glass fragments set in ash-sized matrix. A weathering surface is developed above this unit and is unconformably overlain by the calcareous sandstone unit comprising the Zululand Group.
522.21	528.30	6.09	Lapillistone	Poorly-sorted, cream to grey lapillistone mainly comprising angular to sub-angular, multiple-coloured (white, red, black, green) pyroclasts of rhyolite, tuff and glass fragments in a cream-coloured, fine-grained ash matrix. Top contact: gradational
528.30	543.01	14.71	Lapillistone	Poorly-sorted, coarsening-upward, cream lapillistone consisting of angular to sub-angular tuff and rhyolite pyroclasts as well as dark glass fragments embedded in a cream-coloured ash matrix. Top contact: gradational
543.01	549.56	6.55	Lapillistone	Poorly-sorted, brown-cream lapillistone comprising lapilli-sized angular pumice and glass fragments set in green (chloritic) to reddish-brown matrix.
549.56	549.86	0.3	Tuff	Fine-grained, grey-brown coloured ash tuff. Top contact: gradational
549.86	550.01	0.15	Lapillistone	Poorly-sorted, cream lapillistone consisting of angular pumice, tuff and glass fragments in ash matrix. Top contact: gradational
550.01	550.41	0.40	Tuff	Fine-grained grey to light red ash tuff. Top contact: gradational
550.41	550.91	0.5	Lapillistone	Poorly-sorted, grey-cream lapillistone composed of tuff, rhyolite and pumice pyroclasts in a coarse-grained ash matrix. Top contact: gradational
550.91	551.21	0.3	Lapilli tuff	Poorly-sorted, coarse-grained, grey-black lapilli tuff comprising lapilli-sized angular pumice and tuff-like (cream) pyroclasts as well as glass fragments set in a fine-grained glassy matrix. Top contact: gradational
551.21	555.79	4.58	Lapillistone	The fining upward, mainly cream and greenish-coloured lapillistone, comprises angular to sub-angular lapilli sized tuff, rhyolite and pumice pyroclasts in ash matrix. Top contact: gradational

555.79	556.79	1	Lapilli tuff	Fining-upward, cream lapilli tuff comprising rhyolite pyroclasts and glass fragments (black to grey). The lapilli tuff grades into a thin (2-8 mm thick), laminated ash tuff developed at the top of the unit which forms a gradational contact with the overlying lapillistone unit.
556.79	561.04	4.25	Lapillistone	Upward-fining succession of lapillistone and fine-grained tuff. The lapillistone is a poorly-sorted and cream-coloured with angular to sub-angular tuff, rhyolite and glass pyroclasts. Top contact: gradational
561.04	561.44	0.40	Tuff	Fine-grained cream ash tuff. Top contact: sharp
561.44	561.65	0.21	Lapilli tuff	Poorly-sorted, cream lapilli tuff composed of lapilli-sized tuff, and glass fragments in a cream to greenish (chloritised) matrix. Top contact: gradational
561.65	567.75	6.1	Lapillistone	Poorly-sorted, whitish-cream lapillistone comprising angular pumice and tuff pyroclasts set in ash matrix which is mainly cream and greenish in places. Top contact: gradational
567.75	568.15	0.4	Tuff	Fine-grained, cream-grey ash tuff. Top contact: sharp
568.15	570.65	15.5	Lapilli tuff	Poorly-sorted, cream lapilli tuff with lapilli-sized pyroclasts comprising tuff, pumice and glass fragments embedded in ash matrix. Top contact: gradational
570.65	571	0.35	Tuff	Upward fining, cream-coloured welded and ash tuff. Top contact: gradational

Appendix 7

Descriptions of the lithologies intersected by the ZB borehole (1427.57–1545.75 m-depth)

Depth (m)	Thickness (m)	Lithology	Lithology type	Description
From	To			
1427.57	1428.57	1	Rhyolite breccia	Light grey rhyolite breccia. The breccia comprises angular to sub-rounded (reddish-brown, green, grey and cream) clasts and are 1-4 cm in diameter. This unit grades into a grey homogeneous flow unit with a poorly developed flow banding. The top of the rhyolite is overlain by the Cretaceous rocks comprising the Zululand Group.
1428.57	1429.57	1	Rhyolite breccia	Light grey rhyolite breccia. The breccia forms a sharp lower contact with underlying rhyolite flow. The breccia comprises angular to sub-rounded clasts (reddish-brown, green, grey and cream) and are 1-4 cm in diameter. This unit grades into a grey homogeneous flow unit with a poorly developed flow banding.
1429.57	1437.57	8	Rhyolite	Light to dark grey porphyritic rhyolite flows.
1437.57	1440.12	2.55	Rhyolite	Light to dark grey porphyritic rhyolite flows.
1440.12	1443.92	3.8	Rhyolite	Dark grey porphyritic rhyolite grades upward into the light grey porphyritic rhyolite flow with an autobrecciated flow top.
1443.92	1447.92	4	Rhyolite	Dark grey porphyritic rhyolite grades upward into the light grey porphyritic rhyolite flow. The top of the rhyolite flow is not autobrecciated.
1447.92	1450.82	2.9	Tuff	grey-brown tuff.
1450.82	1450.92	0.1	Rhyolite	Light to dark grey porphyritic rhyolite flow with an autobrecciated flow top.
1450.92	1451.92	1	Rhyolite	Light to dark grey porphyritic rhyolite flow with an autobrecciated flow top.
1451.92	1452.32	0.4	Tuff	grey-brown tuff.
1452.32	1452.72	0.4	Rhyolite	Light to dark grey porphyritic rhyolite flow with an autobrecciated flow top.
1452.72	1452.82	0.1	Tuff	grey-brown tuff.
1452.82	1453.78	0.96	Rhyolite	Light to dark grey porphyritic rhyolite flow with an autobrecciated flow top.
1453.78	1453.81	0.03	Tuff	grey-brown tuff.
1453.81	1455.17	1.36	Rhyolite	Light to dark grey porphyritic rhyolite flow with an autobrecciated flow top.
1455.17	1455.25	0.08	Tuff	grey-brown tuff.
1455.25	1455.34	0.09	Rhyolite	Light to dark grey porphyritic rhyolite flow with an autobrecciated flow top.
1455.34	1455.45	0.11	Tuff	grey-brown tuff.
1455.45	1455.90	0.45	Rhyolite	Light to dark grey porphyritic rhyolite flow with an autobrecciated flow top.
1455.90	1456.10	0.2	Tuff	grey-brown tuff.
1456.10	1456.50	0.4	Rhyolite	Light to dark grey porphyritic rhyolite flow with an autobrecciated flow top.
1456.50	1456.70	0.2	Tuff	

1456.70	1461.20	4.5	Rhyolite	Light to dark grey porphyritic rhyolite flow with an autobrecciated flow top.
1461.20	1462.45	1.25	Rhyolite	Light to dark grey porphyritic rhyolite flow with an autobrecciated flow top.
1462.45	1463.10	0.65	Rhyolite	Light to dark grey porphyritic rhyolite flow with an autobrecciated flow top.
1463.10	1464.06	0.96	Rhyolite	Light to dark grey porphyritic rhyolite flow with an autobrecciated flow top.
1464.06	1465.11	1.05	Rhyolite	Light to dark grey porphyritic rhyolite flow with an autobrecciated flow top.
1465.11	1466.11	1	Rhyolite	Light to dark grey porphyritic rhyolite flow with an autobrecciated flow top.
1466.11	1467.25	1.14	Rhyolite	Light to dark grey porphyritic rhyolite flow with an autobrecciated flow top.
1467.25	1467.65	0.4	Rhyolite	Grey porphyritic rhyolite flow with an autobrecciated flow top. The joints developed in the rhyolite are filled with red jasper.
1467.65	1477.45	9.8	Tuff	grey-brown tuff.
1477.45	1477.62	0.17	Pumice	grey pumiceous zone.
1477.62	1477.78	0.16	Tuff	grey-brown tuff.
1477.78	1477.94	0.16	Pumice	grey pumiceous zone.
1477.94	1478.10	0.16	Tuff	grey-brown tuff.
1478.10	1478.20	0.1	Pumice	grey pumiceous zone.
1478.20	1543.40	65.2	Rhyolite	grey-coloured, porphyritic rhyolite.
1543.40	1543.51	0.11	Tuff	grey-brown tuff.
1543.51	1545.68	2.17	Rhyolite	grey-coloured, porphyritic rhyolite.
1545.68	1545.75	0.07	Tuff	grey-brown tuff.

Appendix 8

Descriptions of the mafic lava and tuff intersected by the ZD borehole (1054–1080 m-depth)

Depth (m)		**Thickness (m)**	**Lithology**	**Description**
From	To			
0	1054	1054		sandstone, siltstone and shale of the Zululand Group overlie the rhyolite
1054	1061	7	Tuff	fine-grained, brown tuff
1061	1068.5	7.5	Mafic lava	dark-grey, coarse-grained mafic lava comprising angular to sub-angular, dark, pale green and reddish-brown mafic minerals set in fine crystalline matrix.
1068.5	1080	11.5	Tuff	fine-grained, brown tuff